

De-black boxing of reactive blending : an experimental and computational approach

Citation for published version (APA):

Prusty, M. (2006). *De-black boxing of reactive blending : an experimental and computational approach*. [Phd Thesis 1 (Research TU/e / Graduation TU/e), Chemical Engineering and Chemistry]. Technische Universiteit Eindhoven. <https://doi.org/10.6100/IR612788>

DOI:

[10.6100/IR612788](https://doi.org/10.6100/IR612788)

Document status and date:

Published: 01/01/2006

Document Version:

Publisher's PDF, also known as Version of Record (includes final page, issue and volume numbers)

Please check the document version of this publication:

- A submitted manuscript is the version of the article upon submission and before peer-review. There can be important differences between the submitted version and the official published version of record. People interested in the research are advised to contact the author for the final version of the publication, or visit the DOI to the publisher's website.
- The final author version and the galley proof are versions of the publication after peer review.
- The final published version features the final layout of the paper including the volume, issue and page numbers.

[Link to publication](#)

General rights

Copyright and moral rights for the publications made accessible in the public portal are retained by the authors and/or other copyright owners and it is a condition of accessing publications that users recognise and abide by the legal requirements associated with these rights.

- Users may download and print one copy of any publication from the public portal for the purpose of private study or research.
- You may not further distribute the material or use it for any profit-making activity or commercial gain
- You may freely distribute the URL identifying the publication in the public portal.

If the publication is distributed under the terms of Article 25fa of the Dutch Copyright Act, indicated by the "Taverne" license above, please follow below link for the End User Agreement:

www.tue.nl/taverne

Take down policy

If you believe that this document breaches copyright please contact us at:

openaccess@tue.nl

providing details and we will investigate your claim.

De-black boxing of reactive blending: an experimental and computational approach

PROEFSCHRIFT

ter verkrijging van de graad van doctor aan de
Technische Universiteit Eindhoven, op gezag van de
Rector Magnificus, prof.dr.ir. C.J. van Duijn, voor een
commissie aangewezen door het College voor
Promoties in het openbaar te verdedigen
op dinsdag 19 september 2006 om 16.00 uur

door

Manoranjan Prusty

geboren te Chauliaganj, India

Dit proefschrift is goedgekeurd door de promotor:

prof.dr. P.J. Lemstra

Copromotoren:

dr.ir. J.G.P. Goossens

en

dr.ir. P.D. Anderson

Prusty, Manoranjan

A catalogue record is available from the Library Eindhoven University of Technology

ISBN-10: 90-386-2818-8

ISBN-13: 978-90-386-2818-9

NUR 913

Copyright © 2006 by Manoranjan Prusty.

The work described in this thesis has been carried out at Polymer Technology (SKT) within the Department of Chemical Engineering and Chemistry, Eindhoven University of Technology, The Netherlands. Financial support has been supplied by the Dutch Polymer Institute (DPI; project #266).

Design Cover: M. Prusty and Paul Verspaget (Grafische Vormgeving-Communicatie)

Printed at the Universiteitsdrukkerij, Eindhoven University of Technology.

Dedicated to my parents and my family

Contents

Summary	xi
1 General Introduction	1
1.1 Introduction	1
1.2 Polymer blends	2
1.3 Reactive blending of an immiscible blend	6
1.4 Reactive blending of a partially miscible blend	7
1.5 Objective of the thesis	9
1.6 Outline of the thesis	9
2 Mechanism and kinetics of formation of oxazolines from styrene acrylonitrile and aminoethanol	11
2.1 Introduction	11
2.2 Experimental	12
2.2.1 Materials	12
2.2.2 Synthesis of SAN-oxazoline in melt	12
2.2.3 Synthesis of SAN-oxazoline in solution	13
2.2.4 Synthesis of 2-isopropyl-1,3-oxazoline	13
2.2.5 Analysis	13
2.2.6 Design of experiments	13
2.3 Results and Discussion	14
2.3.1 Mechanism	14
2.3.2 Effect of catalyst	16
2.3.3 Kinetics	19
2.3.4 Design of experiments	22
2.4 Conclusions	24
3 Interfacial reaction between random oxazoline functionalized and random acid functionalized polymers	25
3.1 Introduction	25
3.2 Experimental	27
3.2.1 Materials	27
3.2.2 Preparation of random oxazoline-modified SAN (ran-SAN-oxaz)	28
3.2.3 Preparation of multilayer samples	28
3.2.4 ATR-FTIR spectroscopy	29
3.2.5 Variable-Angle Spectroscopic Ellipsometry	30

3.2.6	Elongational flow	31
3.3	Results	31
3.3.1	Model reaction between acid and oxazoline	32
3.3.2	Interfacial reaction between acid- and oxazoline-containing polymers	33
3.3.3	Effect of oxazoline concentration on the interfacial reaction	34
3.3.4	Effect of temperature on the kinetics of interfacial reaction	35
3.3.5	Effect of thickness of oxazoline layer on the interfacial reaction	36
3.3.6	Effect of diffusion of reactive chains through nonreactive SAN	36
3.3.7	Development of interface thickness	38
3.3.8	Effect of interface renewal on the late stage of the interfacial reaction	41
3.4	Discussion	42
3.5	Conclusions	43
4	Interfacial reaction between random acid functionalized and end oxazoline functionalized polymers	47
4.1	Introduction	47
4.2	Experimental	48
4.2.1	Materials	48
4.2.2	Synthesis of end acid-functionalized SAN (end-SAN-acid)	48
4.2.3	Synthesis of end oxazoline-functionalized SAN (end-SAN-oxaz)	49
4.2.4	Preparation of bilayer samples	50
4.2.5	MALDI-TOF-MS	50
4.2.6	Nuclear Magnetic Resonance Spectroscopy (NMR)	50
4.2.7	LC-MS	50
4.2.8	Triple-SEC	51
4.2.9	ATR-FTIR spectroscopy	51
4.3	Results	51
4.3.1	Preparation of end acid-functionalized SAN (end-SAN-acid) via RAFT	51
4.3.2	End oxazoline-functionalized SAN (end-SAN-oxaz)	53
4.3.3	Interfacial reaction between a bilayer sample of PEMA and end-SAN-oxaz	56
4.4	Discussion	57
4.5	Conclusions	59
5	Phase behavior of PMMA/SAN systems with reactive groups	61
5.1	Introduction	61
5.2	Experimental	62
5.2.1	Materials	62
5.2.2	Sample preparation	62
5.2.3	Cloud point measurements	63
5.2.4	Fourier-Transform Infrared Spectroscopy (FTIR)	63
5.2.5	Size Exclusion Chromatography	63
5.3	Results and Discussion	63
5.3.1	Phase diagram of PMMA/SAN	64
5.3.2	Effect of acid groups on the phase behaviour of PMMA/SAN blends	65
5.3.3	Effect of oxazoline groups on the phase behaviour of PMMA/SAN blends	66

5.3.4	Effect of reaction between acid and oxazoline group in the phase behaviour of PMMA/SAN	66
5.4	Conclusions	67
6	Experimental and computational study on structure development of PMMA/SAN blends	69
6.1	Introduction	69
6.2	Model equations	71
6.2.1	Non-dimensionalization of the equations	72
6.3	Numerical methods	73
6.4	Experimental	73
6.4.1	Materials	73
6.4.2	Sample preparation	74
6.4.3	Cloud point measurements	74
6.4.4	Small-Angle Light Scattering (SALS)	74
6.5	Results and discussion	74
6.5.1	Phase diagram	74
6.5.2	Different stages of phase separation	75
6.5.3	Analysis of early stage of phase separation	77
6.5.4	Analysis of intermediate and late stage of phase separation	79
6.6	Numerical results	82
6.6.1	System definition	82
6.6.2	Effect of hydrodynamics	82
6.7	Quantitative comparison between numerical and experimental results	85
6.8	Conclusions	87
7	Computational study on the initial stage of phase separation in ternary blends of homopolymers and block copolymers	89
7.1	Introduction	89
7.2	Free energy of the system	93
7.2.1	System definition	93
7.2.2	Homogeneous part	93
7.2.3	The long range contribution	96
7.2.4	The gradient contribution	96
7.2.5	The total Helmholtz energy density	97
7.3	The evolution equations	97
7.3.1	For a ternary system without reaction	97
7.3.2	For a ternary system with reaction	99
7.4	Balance equation of mass and momentum	99
7.5	Numerical methods	100
7.6	Results and Discussion	100
7.6.1	Validation of the result	100
7.6.2	Monomer system	104
7.6.3	Polymer system	104
7.7	Concluding remarks	107
	Bibliography	109

Technology Assessment	121
Samenvatting	123
Acknowledgements	127
Curriculum Vitae	129

Summary

Polymers are often blended/mixed with each other to tailor the final properties. Due to the long chain nature, mixing of polymers on a molecular scale is very difficult and, therefore, most polymer pairs are immiscible and usually display poor mechanical properties upon blending, due to a high interfacial tension and concomitantly an unstable morphology. This can be overcome by the addition of compatibilizers, viz. block copolymer, which are active at the interface and reduce the interfacial tension and stabilize the dispersed phase by suppressing coalescence. Generally, block copolymers of the A-B type are used to stabilize A/B mixtures, but these can also be generated in-situ, known as reactive blending. This process is currently a black box process involving diffusion of reactive chains to the interface, fast reactions between the reactive groups, with a superimposed complex flow, i.e. shear and elongational, all occurring at the same time.

The objective of the research described in the thesis was to gain more insight into the fundamental processes that occur during reactive blending of immiscible and partially miscible blends by combining both experiments and computations. Experimentally, a model system of polymers with oxazoline and acid functionalities was studied, which react relatively slow compared to the commonly used anhydride/amine systems. The computational approach of the complex reactive blending process with a diffuse-interface modeling was split into a number of steps with increasing complexity. Starting from the phase separation process of a homopolymer mixture without reaction, the approach was extended from pure block copolymers to ternary mixtures of two homopolymers and the corresponding block copolymer.

For the experimental study, oxazoline-modified polymers with random distribution of oxazolines were obtained from poly(styrene-*co*-acrylonitrile) (SAN) by reaction with 2-amino ethanol, both in solution and in melt. The conversion of the nitrile functionality into oxazoline was monitored by FTIR and NMR spectroscopy. The melt modification gave a higher conversion than the solution modification. The reaction mechanism was investigated with a model system of 2-isopropyl-1,3-oxazoline, which was prepared by the reaction of 2-aminoethanol with isobutyronitrile in presence of Lewis acid catalysts. The reaction products were analyzed with ^1H NMR spectroscopy and GC-MS. Along with reaction mechanism the reaction kinetics and the effect of different catalysts were investigated and showed that zinc- and cadmium-based systems were the most active and selective catalysts.

Generally, reactive blending is carried out on large-scale extruders, in which a complex flow field is superimposed on the system components with the interfacial reaction. To avoid the complicating effect of flow on the interfacial reaction, all experiments described in this thesis were carried out on simple bilayer systems. For the immiscible system with the oxazoline and acid functionalities, the effect of the position of the oxazoline functional group along the SAN copolymer chain on the interfacial reaction kinetics and interface thickness was studied using

FTIR spectroscopy and ellipsometry respectively. First, a random oxazoline-functionalized SAN was used with a random acid-functionalized poly(ethylene) (*random-random system*). The interfacial reaction was found to be first order with respect to the initial oxazoline concentration. In the early stage, the interfacial reaction followed an Arrhenius behavior, indicative for a reaction-controlled regime. The time scale of the reaction was compared with the time scale of diffusion of reactive chains using a trilayer sample, by using an additional non-reactive SAN-layer in between the two reactive layers, and it was observed that the time scale of diffusion is much faster compared to the time scale of reaction. Next, the actual development of interface thickness as measured with ellipsometry revealed that there was a sharp increase in interface thickness in the early times of the reaction up to a plateau value, whereas the interfacial reaction continued to increase. Refreshment of the interface was established by applying an elongational flow, facilitating the migration of new reactive chains from the bulk to the interfacial region, and showed that the extent of the interfacial reaction can be further increased. Based on the obtained results, a model for the interfacial reaction was proposed with three reaction stages. In the initial stage, both the extent of the interfacial reaction and the interface thickness increase because of migration of reactive chain segments from the bulk to the interface leading to the formation of H-shaped graft copolymers at the interface. In the intermediate stage, the migration of reactive chain segments slows down because of the presence of branched graft copolymers at the interface. In the late stage, no migration of reactive chains from the bulk to the interface takes place, because the interface is saturated with the branched graft copolymers and only intra-chain copolymerization reactions can occur. Second, an end oxazoline-functionalized SAN instead of the random oxazoline-functionalized SAN was used in the bilayer systems with acid-functionalized poly(ethylene) to study the interfacial reaction kinetics (*end-random system*). The initial stage is similar to the random-random system except that Y-shaped copolymers are formed in end-random systems. The interfacial tension is known to be lower for Y-shaped copolymer than the H-shaped copolymer leading to the spontaneous formation of a corrugated interface in the intermediate stage of reaction. At the late stage, the undulation grows leading to micelles formation at the poly(ethylene) phase, which facilitates further migration of new reactive chain segments from the bulk to the interface and the interfacial reaction continues to increase for longer times, thus interface refreshing might not be needed to drive the reaction further.

For reactive blending of partially miscible blends, the phase separation process was studied experimentally with small-angle light scattering (SALS) and was confronted with modeling results using a diffuse-interface modeling (DIM) approach. To investigate the effect of reaction between oxazoline and acid groups on the phase separation of partially miscible blends, a systematic study was set up. First, the phase separation was studied with a model system of two non-reactive polymers: poly(methyl methacrylate) (PMMA) and SAN. The SALS-study showed a lower critical solution temperature (LCST) of 203 °C for a mixture with a weight ratio 70/30 PMMA/SAN28 (28 wt% AN). Second, the effect of acid end-groups on the phase separation was studied with SAN/end-PMMA-acid system, for which a critical temperature of 250 °C was observed due to the enhanced interaction between the nitrile and acid groups. Next, the effect of oxazoline functionalities on the phase separation was studied with ran-SAN-oxaz/PMMA systems and it was observed that the LCST shifts to even higher temperatures for the SAN/end-PMMA-acid system, due to the additional repulsion between styrene, acrylonitrile and oxazoline segments in ran-SAN-oxaz copolymer. The critical temperature was not observed within the experimental temperature window (max. 300 °C), for the reactive system of ran-SAN-oxaz/end-PMMA-acid, because of the formation of

additional copolymers.

Finally, the phase separation process of reactive systems was studied numerically by first starting with the phase separation of homopolymer mixtures. The coarsening dynamics showed only macrophase separation with three different stages of phase separation, viz. initial, intermediate and late stage. The power-law scaling coefficient (α) may vary from 0.33 (diffusion controlled) to 1.0 (hydrodynamics controlled). In the investigated PMMA/SAN28 system, this coefficient varied from 0.55 in the intermediate stage to 0.86 in the late stage, indicating that the system becomes more dominated by hydrodynamics in the late stage of phase separation. The computational analysis showed that the power-law coefficient changed from 0.38 to 0.69 when the capillary number (Ca) was reduced from 10 to 0.5. Next, the critical parameters, such as the interfacial thickness and diffusion constants, were obtained from the small-angle light scattering (SALS)-study and used in the calculations to predict the phase separation kinetics with the Cahn-Hilliard model. The experimental time scale for the onset of phase separation was slower than the numerically predicted time scale, which might be due to the lower random noise level used in the simulations. For the diblock copolymers, the coarsening dynamics was found to be only related to microphase separation. Next, the phase separation of the ternary system of homopolymer and block copolymer containing 20 vol% of block copolymer was studied. Only the initial stage of the phase separation process was observed, whereas the intermediate and late stages were not observed, which might be due to the evolution of two different length scales during the phase separation. Both micro- and macrophase separation were observed when the length of the block copolymer is smaller than the homopolymer. After simulating the ternary mixture containing a fixed percentage of block copolymer, the model can be extended to study the reactive system where the block copolymer is formed with time from the reaction of the homopolymers containing reactive groups.

Chapter 1

General Introduction

1.1 Introduction

Polymers have played an important role since the beginning of life. Well-known natural polymers, such as DNA, RNA, proteins and polysaccharides, play a crucial role in plant and animal life. Natural polymers have been exploited as materials for providing clothing, weapons, shelter, writing materials and other requirements. In the nineteenth century, natural polymers were modified to meet technical requirements and classical examples are nitrocellulose, cellophane and natural rubber. The fact that natural rubber (cis-poly(isoprene)) could be cross-linked (vulcanized) with sulphur (Goodyear 1847) stimulated the development of the rubber industry with useful products such as tires for cars.

The first fully synthetic polymer was found by Baekeland at the University of Gent in the beginning of the 20th century by reacting phenol and formaldehyde resulting in a black insoluble resin. In 1907 Baekeland started his Bakelite company in the USA and Bakelite as a (thermoset) polymer became a commercial success. Baekeland, however, never realized in his life that he had made a polymer! The concept of the polymer chain was postulated in the 1920s by Staudinger (Freiburg), but his views were not accepted in the scientific community at that point in time. In the 1930s the experimental evidence for long chain molecules consisting of repeating units became evident by the discovery of poly(ethylene) at ICI but more notably by the systematic approach by Carothers at Du Pont in synthesizing poly(amides) (nylons). The lack of supply of natural rubber during World War II from Asian countries to USA and Europe triggered the start of the synthetic rubber industry. The synthetic polymer (plastic) industry took really off the ground in the 1950s when Ziegler and Natta invented a catalyst system to produce stereoregular polymers such as (isotactic) poly(propylene) (i-PP) and (linear) poly(ethylenes) (PE).

In the 1960s and 1970s, the production of engineering plastics, such as polyesters (poly(ethylene terephthalate) (PET) and poly(butylene terephthalate) (PBT)), polycarbonate (PC), poly(phenylene ether) (PPE), catered the market with useful products. The 1980s, in retrospect, was probably the most successful decade and expectations were running high concerning the growth and development of synthetic polymers. The control over polymerization processes was boosted by the new metallocene-based catalyst systems (Kaminsky, Sinn, Brintzinger in Europe, Ewen in the USA) enabling the production of novel polymer structures such as syndiotactic-poly(styrene) (s-PS) and s-PP and extending the range into low(er) density

poly(ethylenes), matching the properties of elastomers. Polymer superfibers were introduced (aramids, PE) with mechanical properties exceeding steel and glass fibers (based on weight comparison). The border between synthetic and natural polymers was crossed by using bacteria to produce linear polyesters such as the polyhydroxyalkanoates (ICI/Zeneca).

Next to polymers for engineering applications, a whole new class of functional polymers was envisaged with special properties such as intrinsic conductivity and emitting light, the so-called poly-LEDs for flexible displays (Friend c.s. in Cambridge). Corporate R&D programs were initiated in industry to open new fields, e.g. advanced composites (BASF) and novel engineering plastics (Shell with polyketones). Synthetic polymers, originally introduced as substitutes for classical inorganic construction materials, viz. plastics with the appeal of cheap and poor quality, were matured in the 1980s into materials with often a unique property profile. The term "polymere werkstoffe" was coined in the German literature to replace "Kunststoffe" with the connotation of "ersatz".

At the turn of the century, however, the enthusiasm in industry to develop new polymers became close to zero. Major development programs were terminated such as the aliphatic polyketones (Carilon[®], Shell) and s-PS by Dow. The introduction of new polymers on a commercial scale needs too much effort in terms of production cost and marketing and probably there will be no new polymers on the market the coming decades. In fact, the majority of polymers we use today have been invented in the 1950s and 1960s, even in advanced applications such as in medical technology (Warzelhan, 2004).

The focus is now on post-reactor modification rather than on making novel polymer structures in the reactor. If one can produce improved materials by blending existing polymers, the costs as well as the development time can be reduced. Today, polymer blends constitute about 30 volume percent of the total polymer consumption.

1.2 Polymer blends

Polymer blending is a convenient route for developing new polymeric materials, as it combines properties of both blend components to obtain materials with synergistic properties. The blending process is generally carried out on standard industrial equipment, such as twin-screw extruders. An additional advantage of polymer blending is that a wide range of material properties can be obtained by merely changing the blend composition and concomitantly the properties can be fine-tuned for a particular application.

Polymer blends can be classified into three categories depending on the miscibility on molecular scale. The first category is called a miscible blend, in which the polymers are miscible over a wide range of temperatures and at all compositions due to specific interactions. A well-known example is poly(styrene)/poly(phenylene ether) (PS/PPO). The second category is called a partially miscible blend, for which miscibility is only observed in a specific temperature and/or concentration window. The third category is called immiscible blend, in which the polymers are not thermodynamically miscible (at molecular scale) at any temperature nor concentration.

Since the majority of the polymer pairs are immiscible, dispersion of one polymer into another polymer is typically achieved by intense mechanical mixing at high temperatures at which all components are in the molten state. The main feature of polymer mixtures, compared with immiscible mixtures of low molecular weight fluids such as oil and water, is the high viscous, non-Newtonian behavior combined with a relatively low interfacial ten-

sion. Mechanical mixing is thus very effective to produce fine (micrometer sized) dispersions through droplet breakup, which is governed by the capillary number, Ca , i.e. the ratio of the deforming shear stress τ exerted on the drop by the external flow field and the shape-conserving, interfacial stress σ/R (with σ the interfacial tension and R the local radius), $Ca = \frac{\tau}{(\sigma/R)}$ (Taylor, 1934). For small capillary numbers, the interfacial stress withstands the shear stress and an ellipsoid drops shape persists. Above a critical value, typically in the initial stage of mixing when the dispersed domains are large, the shear stress dominates the interfacial stress, and the dispersed drops are stretched affinely with the matrix into long thin threads (see Figure 1.1). If the local radius of the thread becomes sufficiently small, interfacial Rayleigh disturbances grow on the thread and result in a breakup of the liquid threads into small drops.

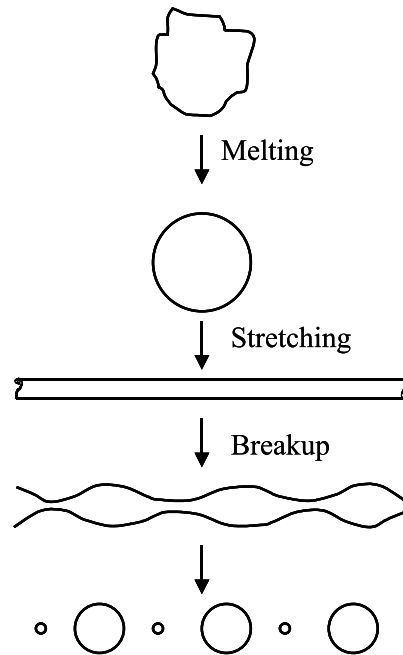


Figure 1.1: Schematics representation of the breakup process occur during melt blending of immiscible polymers.

Apart from a tendency towards finer morphologies resulting from stretching and breakup, coarsening of the morphology may occur due to coalescence of the dispersed droplets, especially in the low shear rate regions. Elmendorp (1986) experimentally showed that already at a low volume fraction of the dispersed phase the morphology can significantly coarsen by coalescence. Chesters (1991) showed that coalescence of droplets in simple shear flow is governed by two processes; collision probability, i.e. whether the droplets collide within a given process time, and film drainage, i.e. whether the film between the droplets drains sufficiently during the available interaction time. The ratio between the required collision time, t_{coll} , and the available process time, t_{proc} , indicates whether a collision is to be expected. The collision probability was found to increase with the applied shear rate and the volume frac-

tion of dispersed phase, whereas it was independent of the droplet size (Abid, 1993; Abid and Chesters, 1994; Chesters, 1991). For film drainage, various regimes were distinguished by Chesters (1991) depending on the rigidity and mobility of the interfaces. For rigid-particle drainage, when two solids approach each other at a velocity v , the fluid between them must be squeezed out of the narrow gap, which is difficult because the fluid cannot slip against the surface of the spheres (see Figure 1.2a). The pressure required to force the fluid out of the gap acts on the sphere and is felt as a hydrodynamic interaction a repulsive "lubrication force". This lubrication force scales inversely with the width of the gap (h) between the spheres and hence is so singular (diverging for small h) that a finite external force is not sufficient to bring two spheres into contact in a finite time. This results in reducing the collision rate to essentially zero.

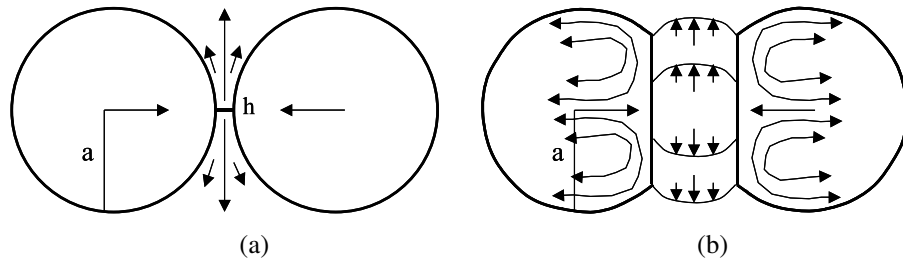


Figure 1.2: (a) Two hard solid spheres (b) two deformable drops approaching towards each other in shear flow.

For deformed-particle drainage, when two droplets approach each other in a matrix, instead of a stick boundary condition on the surface of the droplets, the escaping radially outward velocity v_p may set up a recirculating "fountain flow" inside the approaching droplets (Figure 1.2b). This results in a resistance that slows down the particle approach. The coalescence efficiency due to this resistance depends on the interfacial mobility of the particles. Assuming that the particles approach along the line of the centers, the relationship between the forces and approaching velocity of the particles was calculated using a lubrication approximation (Chesters, 1991). It was assumed that coalescence occurs when the gap between the two particles reaches a critical value h_c at which the matrix film between particles automatically ruptures. It was theoretically shown that $h_c = (A\bar{D}/16\pi\Gamma)^{1/3}$, where A is the Hamaker constant (Vrij, 1966; Vrij and Overbeek, 1968; Chesters, 1991) and \bar{D} is an average particle diameter. The typical value of h_c for micron-sized polymer particles is about 5 nm (Janssen and Meijer, 1995). The coalescence efficiency was then calculated for three ranges of viscosity ratio ("mobile", "partially mobile", and "rigid interfaces" in the original work of Chesters (1991)). For example, in the case where the viscosity ratio is near unity the coalescence efficiency is (Janssen and Meijer, 1995)

$$E_{ij} = \exp\left(-0.077 \left(\frac{\eta_m \bar{D} \dot{\gamma}}{\Gamma}\right) \left(\frac{\bar{D}}{h_c}\right) \left(\frac{\eta_d}{\eta_m}\right)\right) \quad (1.1)$$

where η , Γ and $\dot{\gamma}$ are viscosity, interfacial tension, and shear rate respectively. Subscripts m and n indicate the continuous and dispersed phase, respectively. Equation (1.1) predicts that the coalescence efficiency decreases with viscosity ratio ($\frac{\eta_d}{\eta_m}$), capillary number, and the ratio of the average particle size to the minimum film thickness.

The final morphology of immiscible polymer blends is the result of the dynamic equilibrium between these two opposing phenomena, i.e. droplet breakup and droplet coalescence and is frozen-in in the solid state. Moreover, in a subsequent processing step, the morphology may alter due to the typical processing conditions. Therefore, interfacial agents, often called compatibilizers, are required to refine and stabilize the morphology. Preformed block or graft copolymers have been traditionally added to polymer blends as compatibilizers. There is a long standing debate regarding the role of copolymers as compatibilizer. One is the conventional view in promoting mixing of immiscible homopolymers by reducing the interfacial tension and so promoting droplet breakup (Paul and Newman, 1997). However, some experimental investigations suggest that this explanation is not correct (Sundararaj and Macosko, 1995; Macosko *et al.*, 1996). Recent experiments by Tan *et al.* (1996) strongly suggest that copolymers inhibit coalescence of droplets in shear-induced collisions giving rise to repulsive forces between droplets.

Based on the experimental evidence of Tan *et al.* (1996), Milner and Xi (1996) and Milner (1997) tried to explain the role of copolymer compatibilizer formed by grafting reaction during reactive blending by first analyzing the static properties of copolymer layers followed by the dynamic properties in the mixer. At static conditions, the presence of the copolymer chains at the interface leads to an increase in hydrostatic pressure. This pressure is just sufficient to drive away enough homopolymers against the osmotic pressure to maintain a constant density in the layer and favors an increase of the interfacial area, which decreases the interfacial tension. Second, a static repulsive force results when two droplets containing copolymers approach each other closely enough that their copolymer layers begin to overlap (see Figure 1.3a). This repulsive force prevents coalescence when the droplets approach each other as a result of Brownian motion.

However, the situation changes completely when polymer droplets with copolymers attached to it approach each other in a shear flow where the hydrodynamics forces are large (see Figure 1.3b). A repulsive force exist between the droplets because of the work done by the fountain flow to sweep the copolymers to the back of the droplets. These repulsive forces suppress the coalescence of the polymer droplets.

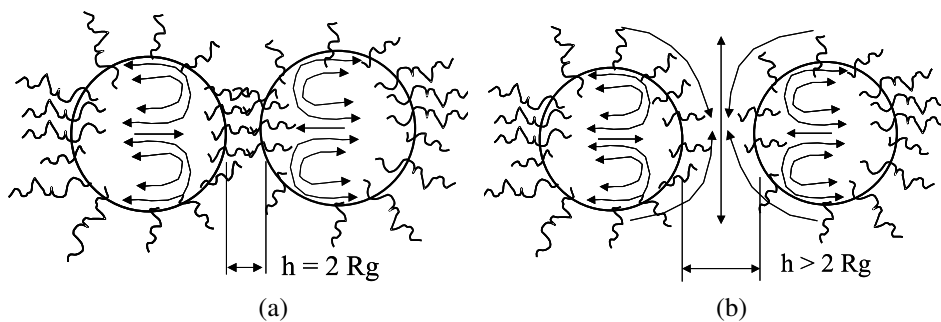


Figure 1.3: Mechanism for block copolymer suppression of coalescence: (a) static condition and (b) dynamic condition in shear flow.

Although block copolymers can be effectively used as compatibilizers in polymer blends, due to the lack of economic viable routes for the synthesis of such copolymers and the high probability of formation of micelles (Fayt *et al.*, 1981), compatibilization by preformed copolymers has not been used as extensively as the potential utility suggests. A good alternative

is to generate the compatibilizing copolymers in-situ by a chemical reaction between suitable functionalized polymers during the extrusion process. This process is known as reactive blending/compatibilization.

1.3 Reactive blending of an immiscible blend

Generally, reactive blending is carried out in an extruder, where the residence time is very short. Thus, it is necessary to have either a relatively high concentration of reactive groups on the two polymers or highly reactive functional groups to get high conversion to copolymers. The majority of polymers used in blends are polycondensates with nucleophilic end groups, such as carboxylic acids, amines and hydroxyls, which can form covalent bonds with suitable electrophilic functionalities, such as cyclic anhydrides, epoxides, oxazolines and isocyanates attached to the second polymer. Orr *et al.* (2001) studied the kinetics of homogeneous coupling reactions using poly(styrene) samples with different terminal groups. It was found that the reactivity increases in the following order: acid/amine, epoxy/amine, acid/oxazoline, acid/epoxy and amine/anhydride. The most common reactive pair is amine/anhydride, which has been used for many commercial blends, e.g. poly(amide)/poly(phenylene ether)/styrene-butadiene copolymer (Noryl, GTX, GE) (Hobbs *et al.*, 1989) and poly(amide)/ethylene-propylene rubber (Zytel ST, DuPont) (Epstein, 1979). Carboxylic acid/epoxy (Olivier, 1986; Pratt *et al.*, 1986) and acid/oxazoline (Baker and Saleem, 1987a,b) have also been considered potential reactive pairs for reactive blending. Saleem and Baker (1990) used acid-functionalized poly(ethylene) with oxazoline-functionalized poly(styrene) to produce compatible blends. Recently, oxazoline-modified poly(styrene-*co*-acrylonitrile) was used for the blending of acrylonitrile butadiene styrene with poly(amide) (Hu *et al.*, 1998).

Although reactive blending is common practice in a large number of industrial processes, studies on the fundamental processes such as the interfacial reaction and the related kinetics, diffusion and the effect of flow on the morphology development during processing are scarce. First of all, the interfacial reaction during blending is difficult to follow because of the low concentration of in-situ formed copolymer during reaction. Secondly, the complicated flow-fields in batch-mixers and continuous mixers, such as twin-screw extruders, introduce a number of difficulties in studying the interfacial reaction in-situ. All the above reasons prevent direct monitoring of the interfacial reaction during blending. In the past, several studies were performed to follow the interfacial kinetics with indirect methods, such as torque measurement (Mori *et al.*, 1984; Baker and Saleem, 1987b, 1988), and off-line techniques, such as NMR spectroscopy (Pillion and Utracki, 1984; Pillion *et al.*, 1987) and extraction techniques (Ide and Hasegawa, 1974; Borggreve and Gaymans, 1989; Baker and Saleem, 1987a). Since then, Scott and Macosko (1994) developed a new technique for direct monitoring the interfacial reaction with Fourier transform infrared (FTIR) spectroscopy. To avoid the complicating effect of flow on the interfacial reaction kinetics, they designed a bilayer film approach using poly(styrene-*co*-maleic anhydride) (SMA) copolymers and low-molecular-weight poly(amide-11), in which the interfacial reaction was studied with FTIR spectroscopy. The reaction between primary aliphatic amines and anhydrides in this system is very fast. In order to understand the influence of the reaction kinetics on the morphology development in more detail, Schafer *et al.* (1996) studied a system of a high molecular weight acid-containing copolymer of ethylene and a low molecular weight oxazoline-containing polymer. Note that all these studies were performed for a combination of a high molecular weight polymer with

a low molecular weight polymer. Studies on reaction between two high molecular weight polymers are still lacking.

In addition to the interfacial reaction, flow plays a major role in the reactive blending process (Jeon *et al.*, 2004; Macosko *et al.*, 2005; Orr *et al.*, 1997; Lyu *et al.*, 1999). Generally, during reactive blending, the kinetics and the extent of the interfacial reaction depend upon both the interfacial area generation due to elongation and the convection due to flow. The influence of the interfacial area generation could be separated from the influence of flow by shearing pre-made multi-layered samples, as shown by Zhao and Macosko (2002). They studied the effect of dynamic and steady shear flow on the interfacial reaction kinetics on samples of amine-terminated polystyrene (PS-NH₂) and anhydride-terminated poly(methyl methacrylate) system consisting of 640 layers. Both steady- and dynamic-shear flow increase the anhydride conversion by approximately 10 % in 5 minutes. To our knowledge, the influence of only interface generation on the interfacial reaction kinetics without flow has not been studied yet. Apart from experimental investigations, a few theoretical analyses of polymer-polymer interfacial reactions have been explored for simple cases, such as the irreversible reaction between end-functionalized polymers at a planar interface. Fredrickson (Fredrickson, 1996; Fredrickson and Milner, 1996) and O'Shaughnessy and co-workers (O'Shaughnessy and Sawhney, 1996; O'Shaughnessy and Vavlynois, 1999) independently treated interfacial reactions in the absence of flow with only a small fraction of the polymer chains in each phase being end-functionalized. They showed that with increasing time, the interface becomes saturated with the in-situ formed copolymers and the reaction rate decreases markedly and hence the reaction becomes diffusion-controlled.

1.4 Reactive blending of a partially miscible blend

For a partially miscible blend, the morphology is generally controlled by the phase separation kinetics (Utracki, 1998). It is well known that the phase separation in partially miscible blends may occur via two different mechanisms: binodal decomposition, for which the system is thermodynamically metastable, and spinodal decomposition, for which the system is thermodynamically unstable. In literature, a large number of comprehensive experimental and theoretical studies on spinodal decomposition have been reported. Many researchers (Olabisi *et al.*, 1979; Paul, 1978; Gunton *et al.*, 1983) studied experimentally the spinodal decomposition behavior of polymer blends having either a lower critical solution temperature (LCST), for which phase separation occurs by increasing the temperature, or an upper critical solution temperature (UCST), for which phase separation occurs by decreasing the temperature. UCST-systems containing poly(butadiene) (PB)/poly(isoprene) (PI) and poly(isoprene) (PI) and poly(ethylene-co-propylene) (PEP) were studied by Hashimoto *et al.* (1991) and Cumming *et al.* (1992), respectively. Hashimoto *et al.* (1991) distinguished three stages of spinodal decomposition, i.e. early, intermediate and late stage. Similar studies were reported on the spinodal decomposition of poly(carbonate) (PC)/poly(styrene-co-acrylonitrile)(SAN), poly(vinyl methyl ether) (PVME)/PS and poly(methyl methacrylate) (PMMA)/SAN, having a LCST behavior. From all these blends, the combination of PMMA and SAN is most suitable for experimentation. The refractive index difference between PMMA and SAN is large enough to yield enough contrast for small-angle light scattering measurements, the primary technique to study phase separation kinetics and both polymers have similar glass transition temperatures, meaning that differences in mobility cancel out. Furthermore, by varying the

acrylonitrile (AN) content of the SAN-copolymer, the miscibility of SAN with PMMA can be systematically adjusted (Suess *et al.*, 1987; Cowie and Lath, 1988).

Apart from the experimental investigations cited above, several computational methods have also been applied to study the spinodal decomposition process. Microscopic numerical approaches, such as Monte Carlo simulations (Petschek and Metiu, 1983; Meakin and Deutch, 1983) and molecular dynamics (Mruzik *et al.*, 1978), have been used to study the spinodal decomposition in polymer blends, but also mesoscopic approaches, such as the density particle dynamic approach (Vliet *et al.*, 2000), have been adopted. Similar results have also been reported with macroscopic models using the Cahn-Hilliard model (Tran *et al.*, 2005).

The literature is very rich with respect to the phase behavior of partial miscible blends under quiescent conditions. However, only few data are available regarding phase separation under flow. Flow such as shear may induce mixing or de-mixing depending on the flow condition (Wolf, 1984; Fernandez *et al.*, 1995; Clarke and McLeish, 1998; Yuan and Jupp, 2002). Hindawi *et al.* (1992), Fernandez *et al.* (1995) and El Malbrouk and Bousmina (2005) observed both mixing and demixing of PS/PVME mixture depending upon the amplitude of the imposed shear rate. Whereas, Papathanasiou *et al.* (1999) observed only shear-induced miscibility of 7 °C at moderately low shear rates (0.1 s^{-1}) for SAN/PMMA mixture, however their observations were based only on TEM analysis. Similar observations were made by Lyngaae-Jorgenson and Sondergaard (1987), Madbouly *et al.* (1999), Madbouly (2003) and Kammer *et al.* (1991). However pronounced shear-induced demixing was never observed in SAN/PMMA system in contrast to the PS/PVME system.

The role of added block copolymers or block copolymers formed in-situ in suppressing the spinodal decomposition was studied both experimentally and numerically. Park and Roe (1991) studied the late-stage coarsening behavior of PS/PB blends in the presence of PS-b-PB block copolymers. The block copolymer retarded the coarsening rate and the extent of retardation increased with increasing amounts of block copolymer and upon increasing the molecular weight of the copolymer. These results were consistent with the light scattering results obtained by Roe and Kuo (1990) on similar blend systems. Hashimoto and Izumitani (1993, 1994) found that the coarsening rate decreased significantly with increasing amounts of block copolymer up to 6% in a ternary system containing PB, SBR and SBR-b-PB block copolymers. Although there are a number of studies in the literature focusing on the effect of addition of pre-made block copolymers on the phase behavior of binary blends, studies concerning the effect of in-situ reaction on the phase behaviour of binary blends are scarce.

The phase behavior of binary blends is not only affected by the graft copolymer, but also by the nature of the end group (Schacht and Koberstein, 2002; Van Durme *et al.*, 2006; Lee *et al.*, 2001). Schacht and Koberstein (2002) demonstrated that the incorporation of a fluorosilane group at the end of polystyrene chains enhances the miscibility with poly(vinyl methyl ether) (PVME). An increase of the LCST of approx. 10 °C was observed. Van Durme *et al.* (2006) also showed that different hydrophilic/hydrophobic end groups have a large influence on the LCST behavior of PVME in water. Hydroxy-terminated PVME shifts the miscibility gap to higher temperatures, whereas a hydrophobic Br-containing end group causes PVME to be insoluble at room temperature. Lee *et al.* (2001) also showed that by varying the end group from methyl to amide attached to poly(dimethylsiloxane) (PDMS), the UCST of poly(isoprene)/PDMS decreases by 165 °C.

Apart from the experimental investigations, theoretical studies were also performed for ternary blends of homopolymers/block copolymer systems using a time-dependent Ginzburg-Landau equation (Cahn and Hilliard, 1959; Cahn, 1964; Cook, 1970). Kawakatsu (1994) and Kawakatsu

et al. (1993, 1994) studied ternary mixtures for the monomer system in two dimensions without hydrodynamic interaction where the polymerization index was taken as one. The domain growth was observed to slow down by the presence of surfactants/block copolymers. Kawakatsu (1994) observed that the phase separation of the ternary system was dominated by macroscopic phase separation of the homopolymers with shorter block copolymers. The phase separation kinetics was governed by microphase separation when longer block copolymers were used in the system. Kielhorn and Muthukumar (1999) studied the ternary symmetric homopolymer/diblock copolymer system with a time-dependent Ginzburg-Landau equation for the time evolution of the order parameter. They observed for the polymer system the accumulation of the diblock copolymer at the interface of the domains through expulsion from the interior of the domains.

Next, the effect of reaction on spinodal decomposition was modeled based on reversible reactions with Monte Carlo methods (Glotzer *et al.*, 1994, 1995) and with finite difference methods (Puri and Frisch, 1994; Motoyama, 1996). The evolution of the morphology seems to critically depend on the relative time scales of segregation (diffusion) and reaction. Schulz and Frisch (1994) and Schulz and Paul (1998) studied the reaction-diffusion systems with irreversible reactions in the context of interpenetrating polymer networks (IPN's) and found that the spinodal decomposition was frozen by the irreversible reaction. Recently, Maurits *et al.* (1999) studied the reactive blending process of a system containing two homopolymers that can form a diblock copolymer. They showed that both macro- and microphase separation can occur using a dynamic mean field density functional theory.

1.5 Objective of the thesis

The main objective of the thesis is to de-blackbox the reactive blending process with the model system of oxazoline-functionalized polymers with carboxylic acid-functionalized polymers by combining both experiments and computations. The experimental study is divided into two parts. First, the reactive blending in immiscible blend is studied to understand the effect of distribution of oxazoline and acid groups along the polymer chains on the interfacial reaction kinetics of immiscible blends. Second, for the partial miscible blends, the investigation is aimed on the effect of oxazoline end groups and acid end groups and finally the effect of the reaction between the two groups on the phase behavior of the PMMA/SAN system. The computation with diffuse-interface modeling is performed to understand different stages of phase separation in homopolymer blends of PMMA/SAN. Finally, the computation is aimed on the effect of block copolymers on the phase separation of partially miscible system, which will extend to study reactive systems in future.

1.6 Outline of the thesis

In Chapter 2, the modification of the nitrile group of SAN to oxazoline is discussed with special focus on the reaction mechanism. The effect of cations, such as zinc and cadmium, and anions, such as acetate, stearate and iodide, on the reaction is studied. The oxazoline yield has been optimized with a design of experiments approach. The reaction kinetics is studied both for the model and the polymer system.

In Chapter 3, the interfacial reaction kinetics between bilayer films of poly(ethylene-co-methacrylic acid) (PEMA) with random oxazoline functionalized SAN (ran-SAN-oxaz) is

studied. Along with the interfacial reaction kinetics, the growth of the interfacial thickness is also studied with ellipsometry. The effect of interface regeneration on the interfacial reaction is studied using elongational flow. Finally, a schematic model for different stages of the interfacial reaction is proposed for the bilayer system.

In Chapter 4, the synthesis and characterization of end acid functionalized SAN (end-SAN-acid) followed by end oxazoline functionalized SAN (end-SAN-oxaz) is described. The interfacial reaction kinetics of end-SAN-oxaz with PEMA is studied with FTIR spectroscopy. Finally, a similar reaction model is proposed and compared with the model obtained system from Chapter 3.

The phase behavior of the partial miscible system containing two complementary groups, i.e. carboxylic acid and oxazoline, is studied in Chapter 5. First, the effect of carboxylic end group is investigated with SAN/end-PMMA-acid system followed by the effect of oxazoline group in ran-SAN-oxaz/PMMA system. Finally, the effect of reaction on the phase behavior is studied with ran-SAN-oxaz/end-PMMA-acid system.

The structure development for PMMA/SAN homopolymers is studied with diffuse-interface modeling and compared with the experimental results in Chapter 6. The effect of hydrodynamics is studied numerically by varying the capillary number and different stages of phase separation is studied experimentally with SALS.

In Chapter 7 the structure development for a mixture of homopolymers and block copolymers is studied numerically. The effect of block length and hydrodynamics is studied for the ternary blend. Finally, the effect of the reaction on the phase separation kinetics of the reactive blend is investigated.

Chapter 2

Mechanism and kinetics of formation of oxazolines from styrene acrylonitrile and aminoethanol

2.1 Introduction

Blending of polymers offers attractive opportunities for developing new materials. Most polymer pairs used in blends are thermodynamically immiscible. Compatibilization is therefore a pre-requisite to obtain the desired properties. Both pre-synthesized or in-situ formed block or graft copolymers can be used as compatibilizers. In-situ formed compatibilizers have a lower tendency to form micelles, which reduce the compatibilization efficiency, and are also more attractive from an economic point of view. These in-situ compatibilizers are prepared by blending polymers with suitable functional groups. During the blending process the functional groups react with each other and create a copolymer that can act as a compatibilizer (Utracki, 1989; Brown, 1992).

The effectiveness of in-situ compatibilization of immiscible polymer blends depends, amongst other parameters, on the type of the functional groups involved. Oxazolines are known to be reactive towards numerous other functionalities bearing labile hydrogen atoms, such as carboxylic acids, amines, hydroxyls, phenolics and mercaptans (Frump, 1971; Culberston, 2002), which explains their usefulness for compatibilization of immiscible blends (Baker and Saleem, 1987b; Fujitsu *et al.*, 1989; Vainio *et al.*, 1996). 1,3-Oxazoline (2-oxazoline) is the most used of all possible isomers. There are many methods described for its synthesis starting from carboxylic acids at high temperatures and more acidic conditions (Meyers and Mihelich, 1976; Wenker, 1935), carboxylic esters (Lowenthal *et al.*, 1990; Corey and Wang, 1993), aldehydes (Badiang and Aube, 1996) and nitriles (Witte and Seelinger, 1974). The last decade has brought a growing interest in oxazolines among polymer chemists. Until now, two routes have been explored to obtain oxazoline-modified polymers. One method comprises the copolymerization of an oxazoline-bearing vinyl monomer with a second monomer of interest.

This method was originally developed and commercialized by the Dow Chemical Company to obtain so-called "Reactive polystyrene"(RPS). A second method involves the grafting of an oxazoline-containing monomer onto an existing polymer chain via a free-radical mechanism. More recently a third method, where chemical conversion of a nitrile group, as present in for instance styrene acrylonitrile (SAN) copolymers, into an oxazoline functionality with an amino-alcohol was reported (Hseih and Pfeiffer, 1995; Hseih *et al.*, 1995). In a similar fashion, oxazoline-modified nitrile butadiene rubber (NBR) (Piglowski *et al.*, 2000; Scaffaro *et al.*, 2000) was prepared. The reaction mechanism, reaction kinetics and the effect of the catalyst on the above mentioned system has not been studied in detail to our knowledge. In this paper, we report on a detailed investigation on the reaction mechanism and the reaction kinetics for the metal catalyzed and un-catalyzed formation of oxazolines. A model system of isobutyronitrile and 2-aminoethanol was used for the mechanistic study. Further, the activity and selectivity of various catalysts on the reaction were examined for both the model and polymer system. The conditions for the optimum production of oxazoline from the reactants were explored using a design of experiments approach.

2.2 Experimental

2.2.1 Materials

The styrene acrylonitrile copolymer (SAN) used in this study contained 28 wt% acrylonitrile and was obtained from the DOW Chemical Company. The number-average and weight-average molar masses were 41 kg/mol and 91 kg/mol respectively. Reactive polystyrene (RPS-1005) containing 1 wt% oxazoline was obtained from EPOCROS. 1,2-Dichlorobenzene (DCB), chloroform, methanol and dichloromethane were obtained from Aldrich Chemicals. 2-Aminoethanol, isobutyronitrile and 1,4-dioxane were obtained from Sigma Aldrich. The various catalysts, i.e. zinc acetate dihydrate, cadmium acetate dihydrate, manganese (III) acetate dihydrate, nickel (II) acetate tetrahydrate, lanthanum acetate hydrate, tin (II) acetate, tin(IV) acetate, sodium acetate trihydrate, calcium acetate monohydrate, magnesium acetate tetrahydrate, lithium acetate dihydrate, zinc trifluoroacetate hydrate, zinc p-toluenesulfonate hydrate, zinc acetylacetonate hydrate, zinc bromide, zinc iodide, zinc chloride, zinc diethylthiocarbamate, zinc hexafluorosilicate hydrate and zinc stearate, were purchased from Sigma Aldrich. Isobutyroamide (Aldrich Chemicals) and N-acetyethanolamine were obtained from Acros Chemicals. All chemicals, solvents and polymers were used as purchased.

2.2.2 Synthesis of SAN-oxazoline in melt

A Banbury batch mixer was used for the oxazoline functionalization of SAN in the melt. The capacity of the mixer was 60 ml. SAN was first molten at 130 °C and a rotation speed of 35 rpm was employed. Then, the pre-made mixture of aminoethanol and catalyst was added. Samples were taken after regular time intervals and quenched immediately with liquid nitrogen. The quenched samples were purified by dissolving in chloroform (5 wt% solution) and precipitated with 10-fold amounts of methanol. The procedure was repeated twice to ensure complete removal of unreacted aminoethanol. The purified samples were dried in a vacuum oven at 45 °C for 2 days before subjecting to FTIR analysis.

2.2.3 Synthesis of SAN-oxazoline in solution

The SAN was first dissolved in dichlorobenzene. Then, a specified amount of catalyst was added. Subsequently, 2-aminoethanol was introduced into the mixture. The reaction temperature was kept constant. Samples were taken after regular time intervals and purified in order to determine the conversion as a function of time. For purification, an equal volume of chloroform was added to the sample for dissolution and the samples were precipitated twice with a 10-fold amount of methanol for complete removal of unreacted aminoethanol. The purified samples were dried at 45 °C under vacuum for 2 days before further analysis.

2.2.4 Synthesis of 2-isopropyl-1,3-oxazoline

2-Aminoethanol (1.03 g, 0.015 mol) and isobutyronitrile (0.92 g, 0.015 mol) were mixed in a Wheaton vial provided with a screw-cap mininert valve, which can withstand pressures up to 10 bar. Since the components were not fully miscible 1,4-dioxane (0.40 g) was added to obtain a homogeneous solution. The catalyst concentration was 3 mol% based on isobutyronitrile. All reactions were carried out at 150 °C. To follow the reaction kinetics, aliquots of approximately 10 mg were taken after different time intervals and analyzed with ¹H NMR spectroscopy using chloroform-d1 as solvent.

2.2.5 Analysis

For FTIR analysis of polymer samples, 15 mg of the modified polymer was dissolved in 1 ml dichloromethane. Spectra were recorded on a BioRad Excalibur 3000 infrared spectrometer. The intensity of the stretching vibration of C=N of the oxazoline group at 1664 cm⁻¹ was used to quantify the oxazoline formation. A calibration curve was obtained by measuring the area under the 1664 cm⁻¹ peak for different concentrations of RPS-1005 in dichloromethane. The phenyl stretching vibration at 1494 cm⁻¹ from styrene was used as reference. For the model reaction, the products were analyzed by ¹H NMR (Varian Mercury-400, 400 MHz, chloroform-d1), GC-FID and GC-MS. For GC-MS, methanol was used as the solvent carrier with a 30 m × 0.25 mm internal diameter CPSIL 8CB column. The temperature program used for GC was from 30 to 275 °C. For MS detection a HP 5973 MSD was used.

2.2.6 Design of experiments

The Design-Expert software from Stat-Ease was used for the design of the experiments and the analysis of the obtained results. The design used for the analysis was Response Surface D-optimal with a 2-factorial model. The response factor design is a method in which multi-variable experiments are used and the results are analyzed to establish the effect of the factors on the response parameter, i.e. oxazoline concentration. Using analysis of variance (ANOVA), the significant factors were identified and by a multiple regression analysis the relationship between the response and the significant factors was established and expressed in the form of a mathematical equation (in coded and uncoded form, so with actual factor values) (Myers and Montgomery, 2001).

For the model system, the effect of catalyst and temperature on the oxazoline yield was separately studied. To establish possible interaction of these parameters on the yield, a design of experiment (DOE) approach with a five-factor analysis was done. The factors are time (t in hr) (2-6 hrs), temperature (T in °C) (130 – 160 °C), IBN amount (7.3-16 mmol), AE amount

(7.3-16.2 mmol) and catalyst (in this case zinc acetate dihydrate) amount (0.22-0.45 mmol). A response factor design with a 2-factorial model was used with a total of 22 experiments. The DOE approach with a five-factor analysis was also followed for the SAN modification in solution. The factors investigated are amount of AE (4.7-48 mmol), amount of catalyst (0.15-0.65 mmol), temperature (T in °C) (130 – 160 °C), time (t in hr) (6-12 hrs), type of catalyst (zinc and cadmium acetate) with a constant amount of SAN at 15.8 mmol. In this case also a response factor design with a 2-factorial model was used with 24 experiments in total.

2.3 Results and Discussion

2.3.1 Mechanism

For the mechanistic study, 2-aminoethanol (AE) and isobutyronitrile (IBN) were chosen as model system. In preliminary experiments, the reaction between AE and IBN was carried out both in the absence and in the presence of zinc acetate dihydrate as catalyst. In the absence of the catalyst, only a small amount (3 mol%) of 2-isopropyl-1,3-oxazoline (OXAZ) was found. In principle, OXAZ can be formed via two different routes: a direct reaction of IBN with AE and via hydrolysis of the nitrile (Figure 2.1).

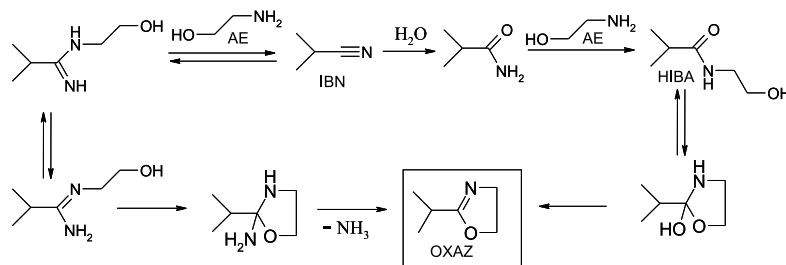


Figure 2.1: Schematic presentation of the two possible uncatalyzed routes to 2-isopropyl-1,3-oxazoline. The direct reaction of IBN with AE is most probable (see text).

Although slow, the overall reaction is selective and no other products than OXAZ could be detected. For the direct reaction of IBN with AE, both the hydroxide and the amine functionality of AE can undergo a reversible nucleophilic addition over the nitrile bond forming an alkoxy-imine or an amino-imine, respectively. However, only the latter can undergo a second nucleophilic addition over the imine double bond to form the 1,3-oxazolidin-2-amine. Finally, elimination of ammonia affords the formation of OXAZ. The second plausible route to OXAZ consists of a nitrile hydrolysis followed by an intramolecular nucleophilic substitution at the carbonyl group, finally followed by dehydration. To study whether this route was indeed viable, isobutyramide (IBA) was reacted with water or AE. Although amides are known to undergo hydrolysis to form the corresponding carboxylic acid (Vaughn and Robbins, 1975), IBA did not react with water [1:1 (molar)] under the reaction conditions applied (entry 6; Table 2.1). On the other hand, IBA reacts with AE to form N-(2-hydroxyethyl)isobutyramide (HIBA) in 19 % yield (entry 4, Table 2.1). As a model for HIBA, N-(2-hydroxyethyl)acetamide (NAEA) was heated under the same conditions (entry

8; Table 2.1). The reactant was recovered unchanged, indicating that intramolecular nucleophilic addition to the carbonyl bonds and/or the subsequent dehydration is difficult under these conditions. Therefore, it can be concluded that the uncatalyzed formation of OXAZ most probably proceeds via a direct nucleophilic addition of AE to IBN.

Table 2.1: Obtained products and their corresponding amounts after 7 hrs of reaction of isobutyronitrile and 2-aminoethanol (with and without zinc acetate dihydrate catalyst)

Expt.	Reactants			Products (mol%)					
				OXAZ	IBA	HIBA	IBN	AE	NAEA
1	AE	IBN	Cat	74	0.5	2.5	23	26	0
2	AE	IBN	No Cat	3	0	0	97	97	0
3	AE	IBA	Cat	0	48	52	0	48	0
4	AE	IBA	No Cat	0	81	19	0	81	0
5	Water	IBA	Cat	0	99	0	0	0	0
6	Water	IBA	No Cat	0	99	0	0	0	0
7		NAEA	Cat	0	0	0	0	0	99
8		NAEA	No Cat	0	0	0	0	0	99

AE: 2-Aminoethanol ; IBN: Isobutyronitrile ; IBA: Isobutyroamide ; OXAZ: 2-Propyl-1,3-oxazoline ; HIBA: N-(2-hydroxyethyl)-isobutyramide ; NAEA: N-acetyethanolamine

Table 2.2: GC and NMR data of the reactants and products (for abbreviations, see Table 2.1, DO: Dioxane)

	AE	IN	IBA	OXAZ	HIBA	DO
¹ H NMR (chemical shift, ppm)	3.63,2.87	2.73,1.36	2.4,1.2	3.82,4.23	3.42,1.2	3.72
GC-MS (retention time, min)	7.1	5.1	17.9	17.0	27.1	9.6

In the presence of zinc acetate, the reaction is considerably faster. The products and their corresponding amounts formed after 7 hours of reaction were analyzed by ¹H NMR spectroscopy and GC-MS and are listed in Table 2.1. ¹H NMR and GC-MS data are given in Table 2.2. OXAZ was selectively formed with a conversion of 74 % after 7 hours at 150 °C, whereas the uncatalyzed reaction only gave 3 % conversion. The only side products detected were IBA and HIBA, present at levels equivalent to the amount of catalyst used, suggesting that IBA may be formed via a catalytic hydrolysis of the nitrile group (Kopylovich *et al.*, 2002; Kukushkin and Pombeiro, 2002). HIBA is formed upon nucleophilic substitution of AE with IBA. Figure 2.2 displays the schematic representation of the catalytic cycle for the zinc-mediated coupling of IBN and AE yielding OXAZ. Partial replacement of acetate by AE leads to a zinc-2-aminoethanoate complex containing a pendant amine-functionality in equilibrium with the corresponding zinc N-(2-hydroxyethyl)amido complex. Coordination

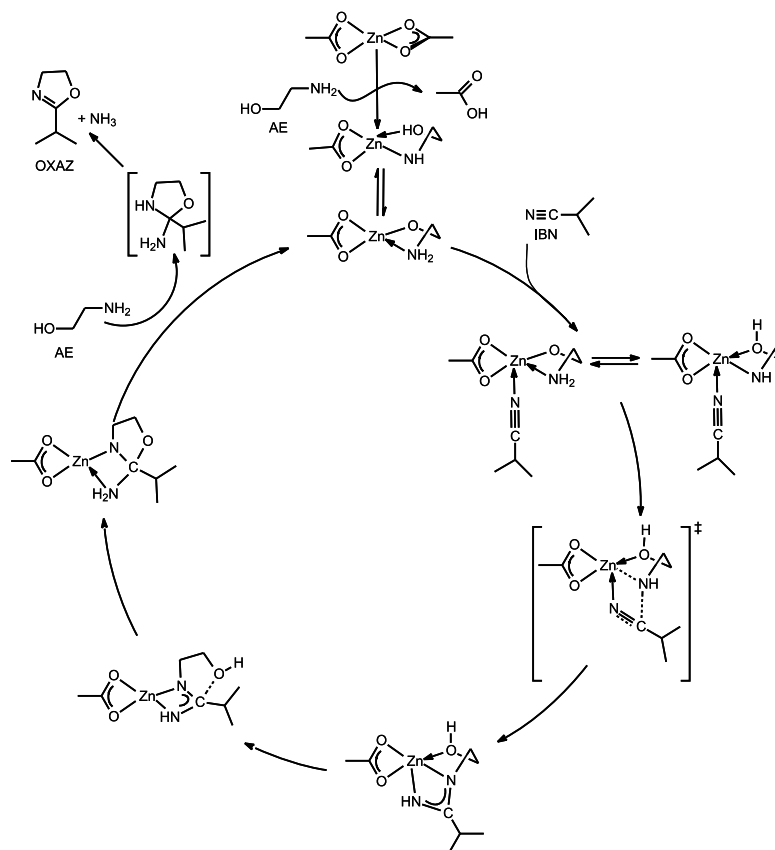


Figure 2.2: Schematic presentation of the catalytic cycle for the zinc-mediated production of 2-isopropyl-1,3-oxazoline.

of IBN to this complex leads to polarization of the nitrile functionality, which facilitates a nucleophilic attack from the adjacent amine to form a zinc N-(2-hydroxyethyl)-diazallyl complex. A similar reactivity has been observed for various main-group and transition metal amido complexes and results from the effective charge delocalization within the diazaallyl moiety of the amidinato complexes formed (Boere *et al.*, 1987; Chen *et al.*, 2001). Although delocalized, amidinato ligands are strongly polarized and the amidinate-carbon is prone to nucleophilic attack. For example, the pendant hydroxyl functionality can undergo nucleophilic addition over the formal imine bond, affording the corresponding zinc 1,3-oxazolidino-2-amine complex. Finally, protonolysis affords the free 1,3-oxazolidine-2-amine that readily loses ammonia to yield the corresponding OXAZ.

2.3.2 Effect of catalyst

The effect of various catalysts on the model system and the polymer system was studied for both the melt- and solution-modification route. For the model system, both the metal ion and

the ligands were varied, whereas for the polymer system only the metal ions were varied.

Model system

For the model system, the amount of OXAZ formed after 5 hours is given in Table 2.3. First, the effect of the Lewis acidity of the different metals was investigated. From Table 2.3, it is evident that zinc- and cadmium-based catalysts are by far the most effective, while nickel and manganese acetates are only moderately active. Alkaline metals (Li, Na, K) give low conversions (20 %), whereas alkaline earth metal, aluminum, lanthanide and tin acetates yield negligible amounts of OXAZ. To be an active catalyst, a moderately Lewis acidic metal center with vacant coordination sites is required. Alkaline earth metals, aluminum and lanthanum are most probably too Lewis acidic to allow a facile substitution of bidentately bonded substituents such as the acetate and the amino-oxazolidino groups. For the somewhat less Lewis acidic alkaline metals this is a lesser problem as they lead to some conversion. Lowering the Lewis acidity of the metal to some extent indeed has a positive effect on the activity of the catalyst. Zinc and cadmium give the highest yields, i.e. approximately 75 % conversion of oxazoline after 5 hours at 150 °C. Lowering the Lewis acidity even further, as in the case of the low-valent transition metals (manganese and nickel) and the divalent tin, leads to a decrease in activity.

Table 2.3: Effect of cation on the oxazoline formation at 150 °C and reaction time of 5 hrs with 3 mol% catalyst

Catalyst	Oxazoline (% conversion)
Lanthanum (III) acetate hydrate	< 1
Tin (II) acetate	< 1
Tin (IV) acetate	< 1
Aluminum acetate	< 1
Calcium acetate monohydrate	< 1
Magnesium acetate tetrahydrate	< 1
Lithium acetate dihydrate	20
Sodium acetate trihydrate	22
Potassium acetate	21
Nickel (II) acetate tetrahydrate	35
Manganese (III) acetate dihydrate	40
Zinc acetate dihydrate	73
Cadmium acetate dihydrate	78

Since cadmium is an environmentally unfriendly catalyst, zinc complexes were chosen to study the effect of the ligand. The results presented in Table 2.4 indicate that zinc trifluoroacetate hydrate, zinc acetate hydrate and zinc iodide give the highest conversions (70-75 %), followed by zinc p-toluene sulfonate (57 %) and zinc bromide (62 %). This is not surprising, since the corresponding ligands are all known to be good leaving groups. The bidentate acetylacetonate ligand generally binds strongly to Lewis acidic metals and is not displaced as readily as carboxylates and sulfonates. The halide series follow the expected trend, where the best leaving group (iodide) gives the highest conversion. The low activity of zinc di-

Table 2.4: Effect of anions on the oxazoline formation at 150 °C and reaction time of 5 hrs

Catalyst	Oxazoline (% conversion)		Solubility ^a	
	3 % cat	0.3 % cat	3 % cat	0.3 % cat
Zinc trifluoroacetate hydrate	75		++	
Zinc acetate dihydrate	73	42	++	++
Zinc p-toluenesulfonate hydrate	57		++	
Zinc acetylacetonate hydrate	36		+	
Zinc diethyldithiocarbamate	9		-	
Zinc hexafluorosilicate hydrate	8		-	
Zinc chloride	40		+	
Zinc bromide	62		+	
Zinc iodide	71	48	+	++
Zinc stearate		40		++

^a++ soluble; + less soluble; - insoluble

ethyldithiocarbamate and zinc hexafluorosilicate hydrate is most probably due to the fact that these compounds are not soluble in the reaction mixture.

Further studies using a ten-fold lower catalyst concentration using zinc acetate, zinc stearate and zinc iodide gave some interesting results. As can be seen from Table 2.4, the conversions are comparable for all three catalysts, which is in agreement with the initial catalytic runs using zinc iodide (71 %) and zinc acetate (70 %). Interesting, though, is the fact that with 0.3 mol% of catalyst the conversion is only 40 % lower than when 3 mol% of catalyst is used. This suggests that at higher catalyst concentrations a smaller fraction of the catalyst is active, which may be related to limited solubility of the catalyst.

Polymer system

For the polymer system, one catalyst from each group of the periodic table was chosen and examined for its effect on the conversion of reaction from SAN into SAN-oxazoline (SAN-OXAZ). Figure 2.3a and 2.3b show the effects of various catalysts on the melt- and solution-modification reaction of SAN respectively. It was found that cadmium and zinc acetate gave a better yield than the other tested catalysts. This result is similar to the results obtained for the model system. The alkaline earth metal magnesium gave negligible amounts of SAN-OXAZ even after 90 min of reaction. The alkaline metal sodium acetate gave about 3 % yield for melt modification after 90 min and 1 % yield for solution modification after 360 min, which is similar to the result obtained for the nickel acetate.

The effect of catalyst concentration for the melt modification on the SAN-OXAZ yield after 60 min of reaction is presented in Figure 2.4 and shows that the yield of SAN-OXAZ increases with increasing catalyst concentration up to 1 mol% and after which it decreases with increasing catalyst concentration. The lower yield at high Zn-acetate levels might be ascribed to the formation of a catalyst-oxazoline complex that was not detected by FTIR.

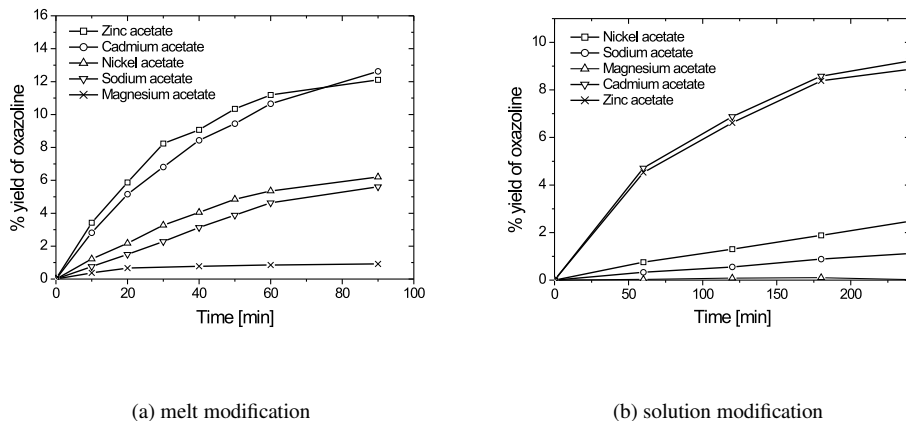


Figure 2.3: Effect of catalysts on (a) the melt modification and (b) the solution modification of SAN.

2.3.3 Kinetics

Model system

In the experimental section, the reactants, catalyst and solvents were reported in grams. For our kinetics study, the concentration is expressed in mol/g instead of the usual mol/liter. The mechanistic studies showed that OXAZ is formed as the major component in the catalytic coupling of IBN and AE. Neglecting the side products that contribute to approximately 2 %, the reaction can be expressed as



The rate of formation of oxazoline can then be expressed as (Levenspiel, 1972):

$$\frac{C_{OXAZ}}{C_{AE,0}(C_{AE,0} - C_{OXAZ})} = kt \quad (2.2)$$

where C_{OXAZ} is the concentration of OXAZ at any time. $C_{AE,0}$ is the initial concentration of AE. Equation (2.2) is used to calculate the kinetic parameters. The OXAZ concentration as a function of time for different temperatures was determined using $^1\text{H-NMR}$ spectroscopy. The OXAZ concentration increases smoothly with time as shown in Figure 2.5. Increasing the reaction temperature results in an increase in the rate of OXAZ formation, which seems to level off at 80 % yield of OXAZ at 160 °C. The good fit of the kinetics equation justifies the concentration expression in mol/gram, indicating that the density of the system does not change during the reaction. The curves shown in Figure 2.5 are further evaluated using Eq. (2.2). The reaction rate constant k is computed using the experimentally determined C_{OXAZ} at each temperature. The results are given in Table 2.5. Next, the activation energy of the reaction according to the Arrhenius equation was determined with a R^2 of 0.97. The frequency factor $k_0 = 1.17 \times 10^{11}$ g/(mol.s) and the activation energy $E_A = 103.5$ kJ/mol are also reported in Table 2.5.

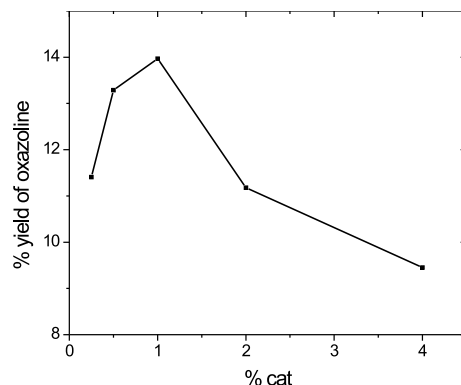


Figure 2.4: Effect of catalyst concentration on the melt modification of SAN.

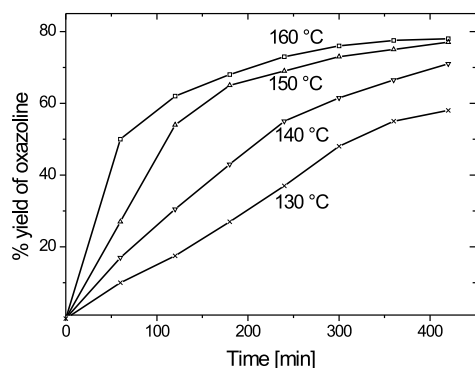


Figure 2.5: Production of isopropyl-2-oxazoline at different temperatures.

Polymer system

For the melt modification of SAN, only the oxazoline production at different temperatures is shown in Figure 2.6. A detailed kinetic study of the reaction in the melt was not possible because of the evaporation of AE during the reaction. For the polymer system, the kinetics was therefore only studied for the solution modification. The reaction was monitored by recording FTIR spectra of samples taken as a function of time. In Figure 2.7, the spectrum for pure SAN is compared with the modified SAN. A new peak appeared at 1664 cm^{-1} , which is characteristic for the C=N stretching vibration in the oxazoline ring. The peak at 2239 cm^{-1} , characteristic of the C \equiv N stretching vibration from nitrile group, decreased upon reaction. The extinction coefficient for the nitrile group is found to be much smaller than that of the oxazoline group. All kinetic data were based on the oxazoline conversion. The amount of oxazoline was calculated by comparing the 1664 cm^{-1} peak area in the modified sample against the calibration curve obtained from the RPS-1005. From Figure 2.7, it was found that only oxazoline was formed during the reaction with no side products. The kinetics equation

Table 2.5: Kinetic parameters for formation of 2-propyl-1,3-oxazoline from isobutyronitrile and aminoethanol in dioxane with zinc acetate dihydrate as catalyst

Temperature [K]	k [g/(mol.s)]
403	0.0045
413	0.0095
423	0.0255
433	0.0355

$$E_A = 103.43 \text{ kJ/mol}, k_0 = 1.17 \times 10^{11} \text{ g/(mol.s)}, R^2 = 0.97$$

can be written as



The rate of formation of SAN-OXAZ can then be expressed as (Levenspiel, 1972):

$$\frac{C_{\text{SAN-OXAZ}}}{C_{\text{AE},0}(C_{\text{AE},0} - C_{\text{SAN-OXAZ}})} = kt \quad (2.4)$$

where $C_{\text{SAN-OXAZ}}$ is the concentration of SAN-OXAZ at any time and $C_{\text{AE},0}$ is the initial concentration of AE. Equation (2.4) is used for the calculation of the kinetic parameters. The SAN-OXAZ concentration as a function of time for different temperatures was determined by FTIR spectroscopy. Figure 2.8 shows the yield of SAN-OXAZ as a function of time for different temperatures. It was found that the yield of oxazoline increases with temperature up to 150 °C and then decreases because of the evaporation of AE near to its boiling temperature. The curves shown in Figure 2.8 are further evaluated using Equation (2.4). The reaction rate constant k is computed using the experimentally determined $C_{\text{SAN-OXAZ}}$ values at each temperature. The results are given in Table 2.6. Next, the activation energy of the reaction according to the Arrhenius equation was determined with a R^2 of 0.98. The frequency factor $k_0 = 3.33 \times 10^4 \text{ g/(mmol.s)}$ and the activation energy $E_A = 66.8 \text{ kJ/mol}$ are also reported in Table 2.6. The reaction rate of model system is higher than that of the polymer system, which is probably due to the steric hindrance as is often observed in polymer analogous reactions (Ledwith *et al.*, 1989; Odian, 1994).

Table 2.6: Kinetic parameters for formation of SAN-OXAZ from SAN and aminoethanol in solution

Temperature [K]	k [g/(mol.s)]
403	1×10^{-8}
413	1.6×10^{-8}
423	3.3×10^{-8}

$$E_A = 66.8 \text{ kJ/mol}, k_0 = 3.33 \times 10^4 \text{ g/(mol.s)}, R^2 = 0.98$$

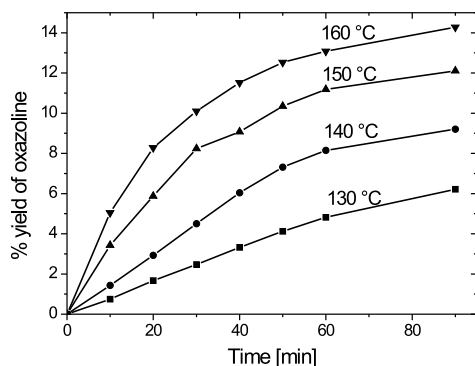


Figure 2.6: Production of SAN-oxazoline at different temperatures in the melt.

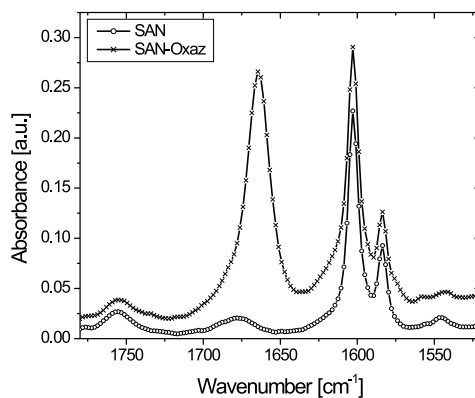


Figure 2.7: Infrared spectra of pure SAN and SAN-oxazoline.

2.3.4 Design of experiments

Model system

For the analysis of the results, a response factor design with a 2-factorial model was used. Using ANOVA, the significant factors were identified and by multiple regression analysis the relationship between the response and the significant factors can be presented in coded form as:

$$\log [OXAZ] = 0.74 + 0.10 t + 0.12 T + 0.05 [IBN] + 0.072 [AE] \quad (2.5)$$

with a standard deviation in [OXAZ] of 0.10 and a R^2 of 0.79. The adjusted and predicted R^2 values indicate that Equation (2.5) is a good model for describing the [OXAZ] response surface. The coefficients for IBN and AE are rather similar, because both IBN and AE are required to produce OXAZ. Optimizing the fit model showed that increasing the reaction time and temperature enhances the conversion as expected. [OXAZ] does not depend upon

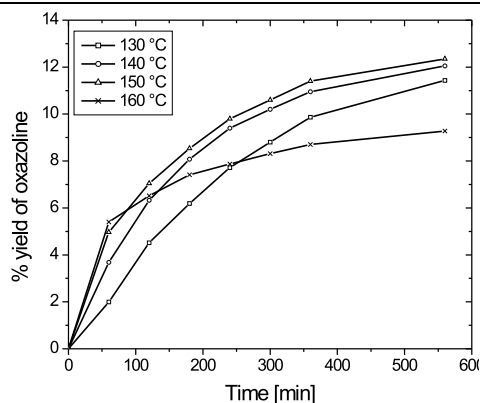


Figure 2.8: Production of SAN-oxazoline at different temperatures in solution.

the catalyst concentration in the range tested (1.5-3 mol%) and there is no inter-factorial influence on the [OXAZ].

Polymer system

For the analysis of the polymer system also the response factor design with a 2-factorial model was used. Using ANOVA, the significant factors were identified. Then, the relationship between the response and the significant factors was obtained by following the multiple regression analysis. The relationship can be represented in coded form by:

$$\log [\text{SAN} - \text{OXAZ}] = -2.17 + 0.37 [\text{AE}] + 0.11 \text{ cat} - 0.097 T + 0.038 t - 0.06 \text{ cat} - \text{type} \quad (2.6)$$

with a standard deviation in [SAN-OXAZ] of 0.11 and a R^2 of 0.94. The adjusted and predicted R^2 values indicate that Equation (2.6) is a good model for describing the [SAN-OXAZ] response surface. The [SAN-OXAZ] increases with increasing [AE] and time as also observed for the model system. In the polymer system, the acrylonitrile concentration is kept constant. The [SAN-OXAZ] decreases with increasing temperature and catalyst type, which is not in agreement with the model system. When we performed the analysis only for the zinc acetate, we found (with a standard deviation of 0.13 and R^2 of 0.9)

$$\log [\text{SAN} - \text{OXAZ}] = -2.08 + 0.4 [\text{AE}] \quad (2.7)$$

SAN-OXAZ now does not depend on the temperature in the time (6-12 h) and temperature range tested. Based on Equation (2.6), Figure 2.9 shows that for cadmium acetate the [SAN-OXAZ] decreases with temperature. The reason is not known, but it might be due to complex formation of AE with cadmium not detected by FTIR spectroscopy.

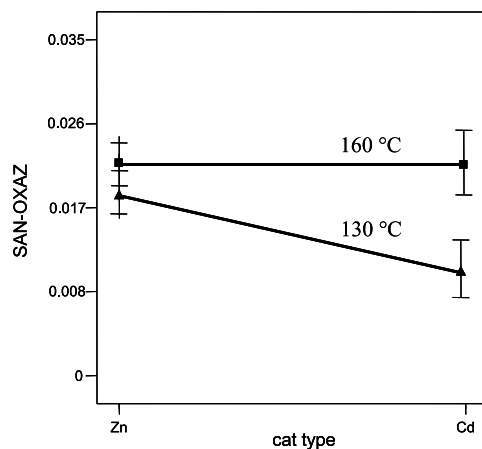


Figure 2.9: Production of SAN-oxazoline as a function of catalyst type and temperature (aminoethanol = 47.75 mmol, time = 12 hrs, catalyst concentration = 0.41 mmol) based on DOE-analysis.

2.4 Conclusions

For the low molecular weight model system, 2-propyl-1,3-oxazoline was selectively obtained when 2-aminoethanol was reacted with isobutyronitrile in the presence of a catalyst, probably via a direct attack of aminoethanol to isobutyronitrile. Traces of isobutyramide and N-(2-hydroxyethyl)-isobutyramide were formed, most probably as a result of catalytic nitrile hydrolysis or catalyst decomposition upon working-up the sample prior to analysis. From the broad range of metal acetates studied, zinc and cadmium acetates showed the best catalytic activity. Zinc catalysts with good leaving groups, such as zinc carboxylate and zinc iodide, showed the highest catalytic activity. Further, the solubility of the catalyst may play an important role, since for most reactions a ten-fold reduction in catalyst concentration yielded only a 40 % reduction of the overall observed activity. The study on the reaction kinetics showed that the reaction rate increases with temperature. The reaction rate of model system is higher than that of the polymer system, which is probably due to the steric hindrance as is often observed in polymer analogous reactions. Finally, from the design of experiments it was found that for the model system, the reaction time and temperature enhances the conversion of 2-isopropyl-1,3-oxazoline, whereas no dependency on catalyst concentration was found in the range tested. For the polymer system, the yield of SAN-oxazoline increases with increasing [AE] and time as also observed for the model system. SAN-oxazoline can also be produced in the melt with a maximum acrylonitrile conversion of 14 %, which is larger than in solution.

Chapter 3

Interfacial reaction between random oxazoline functionalized and random acid functionalized polymers

3.1 Introduction

Blending of polymers is a common route to get materials with properties that are superior to those of the constituents (Utracki, 2002; Janssen, 1993). Most polymer pairs are thermodynamically immiscible in the molten state. Hence, the blending process yields a product with a heterogeneous morphology that is characterized by the shape, size and distribution of the constituting domains. This morphology results from a complex interplay between the viscosity ratio, the interfacial properties and the processing conditions. On an industrial scale melt blending is generally carried out on twin-screw extruders in which complex flow fields, i.e. shear and elongational flow, are present. The elongational flow mainly accounts for stretching and break-up process of the dispersed droplets in the continuous matrix, whereas the shear flow accounts for both stretching and folding of the droplets (Janssen, 1993). The stretching (deformation) process during blending generally increases the interfacial area and hence the local dimensions decrease perpendicular to the flow direction. In the case of two viscous polymers, this drop deformation is mainly governed by the capillary number, Ca , i.e. the ratio of the deforming shear stress τ exerted on the drop by the external flow field and the shape-conserving, interfacial stress σ/R (with σ the interfacial tension and R the local radius), i.e. $Ca = \frac{\tau}{(\sigma/R)}$. For small capillary numbers, the interfacial stress withstands the shear stress and an ellipsoid drops shape persists (Koning *et al.*, 1998). Above a critical value, typically in the initial stage of mixing when the dispersed domains are large, the shear stress dominates the interfacial stress, and the dispersed drops are stretched affinely with the matrix into long thin threads. If the local radius of the thread becomes sufficiently small, interfacial Rayleigh disturbances grow on the thread and result in a breakup of these liquid threads into small drops. Apart from a tendency towards finer morphologies resulting from stretching and

breakup, a coarsening of the morphology occurs during processing due to coalescence of the dispersed droplets, especially in the low shear rate regions. Hence, the final morphology is the result of the dynamic equilibrium between these two opposing phenomena and is frozen-in in the solid state. Moreover, in a subsequent processing step, such as injection molding or film blowing, the morphology achieved may alter due to the typical processing conditions. This is why fixation of morphology is essential. One of the possible routes is the addition of copolymers as compatibilizer to the blend components. The compatibilizer generally decreases the interfacial tension and hence during processing, the deformation stresses can exceed the interfacial stresses for longer times resulting in smaller droplets. In addition, the compatibilizer molecules stabilize the finer morphology by inhibiting the coalescence process. However, these copolymers may form micelles during processing because of thermodynamic or kinetic reasons, thereby reducing the copolymer concentration at the interface and concomitantly their efficiency (Nakayama *et al.*, 1993). To suppress the micelle formation, reactive compatibilization between functional groups of the two polymers has been developed. During this process, the complementary functional groups first diffuse through the bulk to the interface, where they react in-situ to form copolymers and then reduce the interfacial tension. So, the reactive blending involves a complex process of diffusion, reaction and mixing all at the same time.

Although polymer blending by reactive compatibilization is a common practice in a large number of industrial processes, studies on the fundamental processes such as the interfacial reaction and the related kinetics, diffusion and the effect of flow on the morphology development during processing are scarce. First of all, the interfacial reaction during blending is difficult to follow because of the low concentration of in-situ formed copolymer during reaction. Secondly, the complicated flow-fields in batch-mixers and continuous mixers, such as twin-screw extruders, introduce a number of difficulties in studying the interfacial reaction in-situ. All the above reasons prevent the direct monitoring of the interfacial reaction during blending. In the past, several studies were performed to follow the interfacial kinetics with indirect methods such as torque measurement (Mori *et al.*, 1984; Baker and Saleem, 1987b, 1988), and off-line techniques such as NMR spectroscopy (Pillion and Utracki, 1984; Pillion *et al.*, 1987) and extraction techniques (Ide and Hasegawa, 1974; Borggreve and Gaymans, 1989; Baker and Saleem, 1987a). Since then, Scott and Macosko (Scott and Macosko, 1994) developed a new technique for direct monitoring the interfacial reaction with Fourier transform infrared (FTIR) spectroscopy. To avoid the complicating effect of flow on the interfacial reaction kinetics, they designed a bilayer film approach using poly(styrene-*co*-maleic anhydride) (SMA) copolymers and low-molecular-weight poly(amide-11), in which the interfacial reaction was studied with FTIR spectroscopy. The reaction between primary aliphatic amines and anhydrides in this system is very fast. In order to understand the influence of the reaction kinetics on the morphology development in more detail, Schafer *et al.* (1996) studied a system of a high molecular weight acid-containing copolymer of ethylene and a low molecular weight oxazoline-containing polymer. Note that all these studies were performed for a combination of a high molecular weight polymer with a low molecular weight polymer. Studies on reaction between two high molecular weight polymers are still lacking.

Along with the interfacial reaction kinetics, the actual development of the interfacial thickness is also of importance. There are a few studies related to the in-situ characterization of the interfacial thickness using ellipsometry (Yukioka and Inoue, 1994; Dedecker *et al.*, 1998). Yukioka and Inoue (1994) studied the development of the interfacial thickness in a reactive bilayer system, where one layer consisted of an amorphous polyamide (aPA) and the other

layer of a miscible blend of poly(styrene-*co*-acrylonitrile) (SAN) and SMA or pure SMA. For the aPA/SMA system, a maximum of the interfacial thickness was found as a function of MA content at 20 wt% MA. For aPA/(SAN25/SMA23) system, the interface thickness increased with increasing SMA23 content in the SAN25/SMA23 mixture. The maximum interface thickness attained in the above system was about 30 nm. Similarly, Dedecker *et al.* (1998) observed a maximum interface thickness of about 40 nm for a system of PA-12 and PS/SMA mixtures.

In addition to the interfacial reaction and the development of the interfacial thickness, flow plays a major role in the reactive compatibilization process (Jeon *et al.*, 2004; Macosko *et al.*, 2005; Orr *et al.*, 1997; Lyu *et al.*, 1999). Generally, during reactive compatibilization process, the kinetics and the extent of the interfacial reaction depend upon both the interfacial area generation due to elongation and the convection due to flow. The influence of the interfacial area generation could be separated from the influence of flow by shearing pre-made multi-layered samples, as shown by Zhao and Macosko (2002). They studied the effect of dynamic and steady shear flow on the interfacial kinetics on samples of amine-terminated polystyrene (PS-NH₂) and anhydride-terminated poly(methylmethacrylate) consisting of 640 layers. Both steady- and dynamic-shear flow increase the anhydride conversion by approximately 10 % in 5 minutes compared to non-sheared samples. To our knowledge, the influence of only interface generation on the interfacial reaction kinetics without flow has not been studied yet. The main objective of this work is to develop a model for different stages of the interfacial reaction in a bilayer system containing two high molecular weight polymers and then to study the effect of interfacial regeneration on the corresponding interfacial reaction. Attenuated Total Reflection FTIR (ATR-FTIR) is used for direct monitoring the interfacial reaction between poly(ethylene-*co*-methacrylic acid) (PEMA) and oxazoline-modified SAN (ran-SAN-oxaz). The development of the interface thickness during the reaction is studied with ellipsometry. The ellipsometry data are then correlated with the infrared data to get more insight in the migration of graft copolymers from the interface to the bulk during the reaction. The effect of migration of reactive chains from the bulk towards the interface on the interfacial reaction is studied with a novel trilayer system at the initial stage. Finally, the effect of interfacial regeneration on the interfacial reaction is studied by applying elongational flow on a bilayer sample.

3.2 Experimental

3.2.1 Materials

Poly(styrene-*co*-acrylonitrile) (SAN), containing 28 wt% acrylonitrile (AN), was obtained from the DOW Chemical Company (M_n of 41 kg/mol and M_w of 91 kg/mol, as measured by Size Exclusion Chromatography). The glass transition temperature as measured by DSC was 110 °C. Poly(ethylene-*co*-methacrylic acid) with 15 wt% methacrylic acid (PEMA-15) was obtained from Sigma Aldrich (M_n = 11 kg/mol and M_w = 51 kg/mol) and a melting temperature of 76 °C. Poly(ethylene-*co*-methacrylic acid) with 9 wt% methacrylic acid (PEMA-9) was provided by DuPont (Nucrel 0903HC, High-Clarity, M_n = 17 kg/mol and M_w = 82 kg/mol) and a melting temperature of 102 °C. 2-Aminoethanol (AE), 1,2-dichlorobenzene (DCB), zinc acetate (ZnAc), isopropanol, chlorobenzene (CB), phenylpropionic acid and ethyloxazoline were purchased from Sigma Aldrich and used without further purification.

3.2.2 Preparation of random oxazoline-modified SAN (ran-SAN-oxaz)

Ran-SAN-oxaz copolymers with different oxazoline concentrations (1.9, 3.5 and 5.4 wt%) were synthesized in solution. SAN was first dissolved in DCB at 150 °C followed by addition of 4 wt% (based on weight of SAN) of ZnAc catalyst and different wt% of 2-AE. Ammonia was removed continuously using a nitrogen flow. For purification, equal volumes of chloroform were added to the sample mixtures to obtain a homogeneous solution; the samples were then precipitated with a 10-fold of methanol. This procedure was repeated for complete removal of unreacted 2-AE. The purified samples were dried at 45 °C under vacuum for 2 days.

3.2.3 Preparation of multilayer samples

Bilayer samples

Ran-SAN-oxaz was dissolved in CB and thin films were prepared by spin coating using a KarlSus, RC8-apparatus. Different thicknesses of the ran-SAN-oxaz films were obtained with different concentration and different spin coating speed. Spin coating of thin films of PEMA-15 at room temperature was impossible due to lack of a proper solvent. Thus, 0.5 mm-thick films of PEMA-15 were prepared by compression molding at 180 °C for 30 min in a Collin compression press.

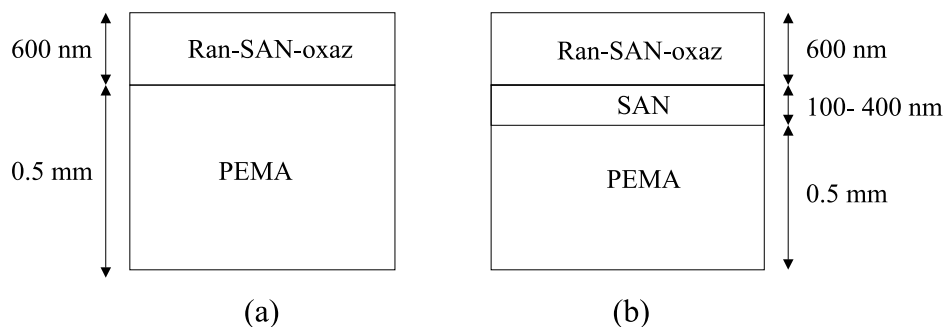


Figure 3.1: Dimensions of the (a) bilayer and (b) trilayer samples.

For the ATR-FTIR-measurements on the bilayer systems (see Figure 3.1a), a thin film (500-900 nm) of ran-SAN-oxaz was spin-coated on the top of the PEMA-15 film. Samples were transferred to an oven set at 50 °C for 2 hrs to remove residual solvent. For the ellipsometry measurements, the interface between the two layers should be very smooth. Therefore, both sides of the PEMA-15 films were first smoothed by sandwiching them between two fluorinated silicon wafers at 130 °C on a heating plate (Eurotherm) for 20 min. Thinner films (approximately 400 nm) of ran-SAN-oxaz-5.4 were spin-coated on a clean glass-slide using a 10 wt% solution of ran-SAN-oxaz-5.4 in CB. Subsequently, the thin films were mounted on the thick PEMA substrate by the floating-on-water and pick-up technique (Yukioka and Inoue, 1991; Yukioka *et al.*, 1992). The thus-prepared bilayer samples were dried under vacuum at 60 °C for 24 hrs to remove residual water. The bilayer samples were finally put onto the backside of the silicon wafer to reduce back reflection.

Trilayer samples

To measure the diffusion of ran-SAN-oxaz through a SAN layer, trilayer samples were prepared as schematically shown in Figure 3.1b. The ran-SAN-oxaz layer was positioned onto the PEMA-15-layer by floating-on-water and pick-up technique. The samples were put into an oven at 60 °C for 24 hrs after each fishing operation to remove the water and the residual solvent. The thickness of the ran-SAN-oxaz-5.4-layer was 600 nm, while the thickness of the intermediate SAN-layer was varied from 100 nm to 400 nm.

3.2.4 ATR-FTIR spectroscopy

The bilayer (shown in Figure 3.2) and trilayer samples were put upside down onto a temperature-controlled Golden-Gate ATR top-plate. The thinner ran-SAN-oxaz-layer was positioned in contact with the ATR-crystal, while the thicker PEMA-layer was positioned at the top. The bilayer sample was covered with a steel plate flushed with a continuous nitrogen gas-flow. The temperature of the ATR top-plate was adjusted from ambient temperature to 200 °C by a Eurotherm 3000 series temperature controller. The angle of incidence of the ATR was set at 45° with diamond as the ATR crystal material. The penetration depth was 1.0-1.5 μm for the spectral range of interest (1000-2000 cm^{-1}). A maximum thickness of approx. 600 nm was used for the ran-SAN-oxaz-layer to get information from the interfacial region. It was assumed that the evanescent wave was constant for different thicknesses of the thinner sample. The spectra were recorded using a BioRad Excalibur 3000 FTIR apparatus coupled with a MCT-detector cooled with liquid nitrogen. A spectral resolution of 4 cm^{-1} was used for all measurements in order to minimize the spectra accumulation time. The time resolutions and the numbers of scans can be found in Table 3.1. Peak integrations were carried out with the BioRad Win-IR Pro software. Two kinds of reaction processes were used, as listed in Table 3.1. Process I and II were used for the bilayer and trilayer samples respectively.

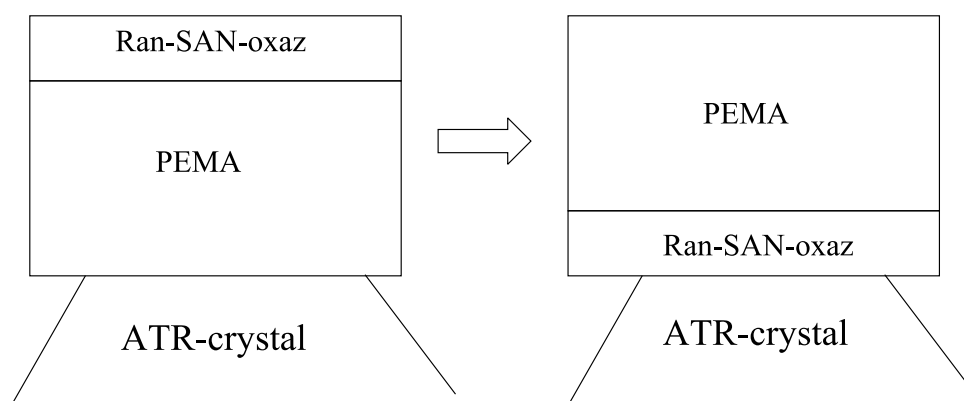


Figure 3.2: Schematics of bilayer sample on ATR crystal.

First, spectra of pure PEMA-15 and pure ran-SAN-oxaz were recorded as shown in Figure 3.3a and 3.3b respectively. For PEMA-15, the most interesting spectral range is related to the carbonyl stretching vibration of the carboxylic acid at approximately 1700 cm^{-1} and

Table 3.1: Annealing processes for the in-situ ATR-FTIR measurements

	Temperature profile	Time resolution [sec]	No. of scans
Process I	120 °C (30 min) → T_h (2 hr)	30	100
Process II	25 °C (10 min) → T_h (30 min)	10	33

T_h is between 140 and 190 °C

the in-plane bending vibration of $-\text{CH}_2-$ at 1457 cm^{-1} . These absorption bands were not used for the quantitative evaluation, because the PEMA-15-layer was only partly detected. For PEMA, an absorption band at 1740 cm^{-1} developed at higher temperatures, which is assigned to single carboxylic acid. These are formed at elevated temperature because of dissociation of intermolecular carboxylic acid dimers formed in the solid state (Earnest and MacKnight, 1980; Lee *et al.*, 1988). Close to the carbonyl stretching vibration of the PEMA, ran-SAN-oxaz shows the characteristic oxazoline $\text{C}=\text{N}$ stretching vibration at 1664 cm^{-1} .

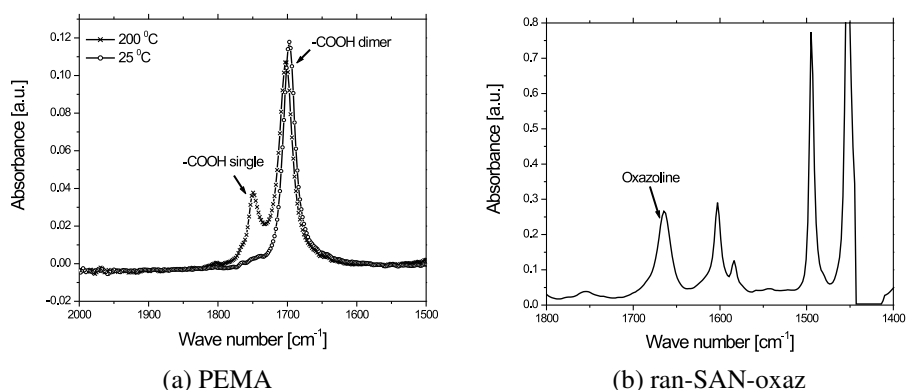


Figure 3.3: IR spectra of the starting components: a) PEMA and b) ran-SAN-oxaz.

3.2.5 Variable-Angle Spectroscopic Ellipsometry

Ellipsometric measurements were carried out by Variable-Angle Spectroscopic Ellipsometry (VASE) using a VASE[®] Research Spectroscopic Ellipsometer (J. A. Woollam Co., Inc., USA), equipped with an automated computer-controlled goniometer, a vertically mounted sample heating stage and a HS-190[™] monochromator. After reflection from the sample and passing through the analyzer, the light was dispersed onto the detector, which permits to perform fast measurements simultaneously at wavelengths between 300 and 800 nm. The retardation Δ and the reflection ratio $\tan\Psi$ of the reflected light were measured at three angles of incidence (60° , 70° and 80°) and at different temperatures. The results were analyzed with VASE Manager[™] Software.

For data analysis, a 3-layer model (see Figure 3.4) was used as described by Yukioka and Inoue (1991). With this model, the best set of values for the ran-SAN-oxaz layer (d_1) and the interface layer (d_3) can be estimated by fitting the experimental obtained Δ and $\tan\Psi$.

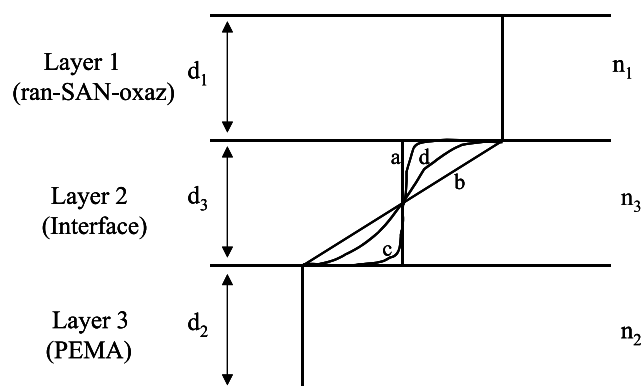


Figure 3.4: 3-layer model for ellipsometer analysis (a) intermix interface layer (b) linear interface layer (c) sharp sigmoidal interface layer (d) shallow sigmoidal interface layer.

The refractive indices of the neat polymers, i.e. n_1 and n_2 , were measured by ellipsometry as a function of temperature and were used for the data analysis of the bilayer system. For the refractive index of the interface layer, only intermix interface layer model has been used so far in the literature. But here four different interface layer models (see Figure 3.4) were considered for the calculation of the interface thickness. In case a, the interface was assumed to be uniform and equal to $n_3 = (n_1+n_2)/2$, as also used by Yukioka and Inoue (1991). Next, the refractive indices of the interface was assumed to vary linearly (case b) between the refractive indexes of the neat polymers followed by the sharp (case c) and shallow (case d) sigmoidal variation of the interface refractive index. A roughness parameter of 15 % of the interface thickness was used in all the analyses.

3.2.6 Elongational flow

To investigate the effect of interface regeneration on the interfacial reaction, bilayer samples were prepared as explained above, but the PEMA-15 layer was replaced by PEMA-9 layer, because of the low MFI. The highly viscous PEMA-9 was used, because the film does not buckle under its own weight. The elongational flow was imposed on the bilayer sample using a Meissner extensional rheometer as schematically shown in Figure 3.5.

The experiment was performed in three steps. First, the bilayer sample was heated at 190 °C for 70 minutes inside the oven until the interfacial reaction reaches a plateau. Secondly, the same sample was held by four rotors and stretched at 130 °C with a rate of 0.001 s^{-1} to an elongation of 100 %. Finally, the sample was heated at 190 °C for another 60 min. The samples were measured before and after each step on a BioRad Excalibur 3000 spectrometer at room temperature. The peak at 1494 cm^{-1} was used as the internal reference.

3.3 Results

The results section is arranged as follows. First, the chemistry of the reaction between oxazoline and acid group is presented for a model system followed by the interfacial reaction

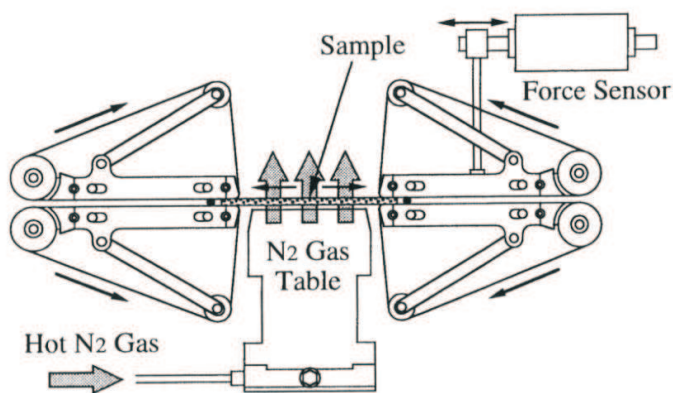


Figure 3.5: Schematics of the Meissner extensional rheometer.

between acid- and oxazoline-containing polymers in a bilayer system. Then, the effect of initial oxazoline concentration, temperature and thickness of the oxazoline layer on the interfacial reaction is presented. Next, the development of interface thickness is presented. Finally, the effect of interfacial regeneration on the interfacial reaction is presented.

3.3.1 Model reaction between acid and oxazoline

To obtain a better insight into the reaction between carboxylic acid and oxazoline groups, a model system of phenylpropionic acid and ethyloxazoline were used as the low molecular weight analogues for PEMA-15 and ran-SAN-oxaz respectively. The two reagents were reacted in 1:1 molar ratio. The reactants and the obtained products were analyzed by transmission FTIR spectroscopy and the results are shown in Figure 3.6.

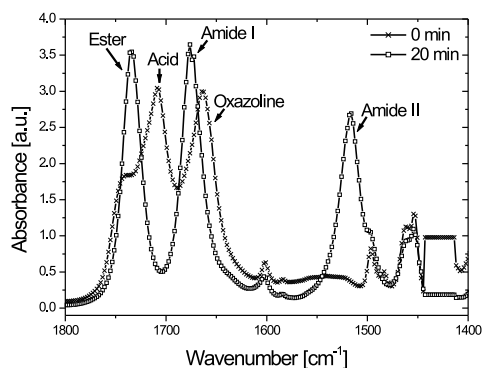


Figure 3.6: FTIR spectra of the mixture of phenylpropionic acid and ethyloxazoline before and after reaction.

Before the start of the reaction, the absorption band at 1700 cm^{-1} corresponding to the car-

bonyl stretching vibration of the acid group and the absorption band at 1660 cm^{-1} assigned to the C=N stretching vibration of the oxazoline-group are clearly visible. Both bands disappear after 20 min of reaction time at $150\text{ }^{\circ}\text{C}$, indicating complete conversion. Meanwhile, strong absorption bands at 1740 cm^{-1} (C=O stretching vibration of ester group), at 1680 cm^{-1} (C=O stretching vibration of amide group) and at 1510 cm^{-1} (C-N-H in-plane bending vibration and C-N stretching vibration (Vien *et al.*, 1991) of the amide group) appear, indicating the formation of an ester-amide linkage (Figure 3.7). The model system was studied at different temperature and the activation energy was found to be 72 kJ/mol . Similar values were reported by Sano (1989) for a system of 2-phenyl-2-oxazoline and n-octanoic acid.

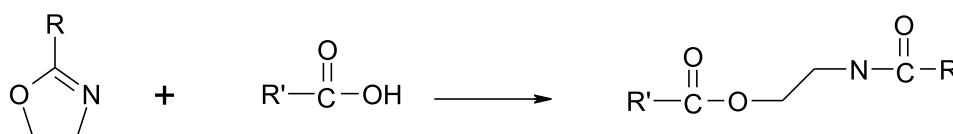


Figure 3.7: Overall reaction between carboxylic acid and oxazoline yielding ester amide.

3.3.2 Interfacial reaction between acid- and oxazoline-containing polymers

To investigate the interfacial reaction between the acid groups in PEMA and the oxazoline groups in ran-SAN-oxaz, the bilayer sample was positioned on the heated ATR crystal. The sample was first heated to $120\text{ }^{\circ}\text{C}$ and kept for 30 min to melt the PE-co-MA according to procedure I. During this time no reaction was observed. The sample was then reacted isothermally at higher temperatures (140 to $190\text{ }^{\circ}\text{C}$) to observe the reaction between acid and oxazoline functionalities and the spectral changes were followed in-situ. Figure 3.8a shows the spectra of a bilayer film, which was reacted at $190\text{ }^{\circ}\text{C}$. The reaction can be followed by the change of three different absorption bands: a) the decrease of the oxazoline band (C=N) at 1660 cm^{-1} , b) the appearance of the amide-I band (C=O) at 1680 cm^{-1} , and c) the appearance of the ester band at 1730 cm^{-1} . The presence of a weak shoulder at 1510 cm^{-1} may be assigned to the amide-II band (C-N-H in-plane bending vibration and C-N stretching vibration (Vien *et al.*, 1991)). The characteristic N-H stretching vibration of amide groups at approximately 3300 cm^{-1} was not observed, which can be explained by a shielding effect of unreacted carboxylic acids (Baker and Saleem, 1987a; Schafer *et al.*, 1996). The weak band at 983 cm^{-1} is assigned to the ring vibration of the oxazoline, also decreased.

Because the bands are not completely separated, it was necessary to apply difference spectroscopy to quantify the extent of reaction. Therefore, all spectra were subtracted from the spectrum obtained after the melting step for 30 min at $120\text{ }^{\circ}\text{C}$. Figure 3.8b shows the difference spectra obtained at $190\text{ }^{\circ}\text{C}$ for different time intervals. The oxazoline band at 1660 cm^{-1} clearly decreases with time. The ester and amide bands at 1730 and 1680 cm^{-1} respectively increase with time. The absorption bands from the ester, amide and oxazoline groups were integrated and then normalized to the ester intensity. The normalized curves were found to be overlapping with each other within an experimental error of 3 %. This shows that the interfacial reaction between oxazoline and acid proceeds similarly as the model reaction, yielding an

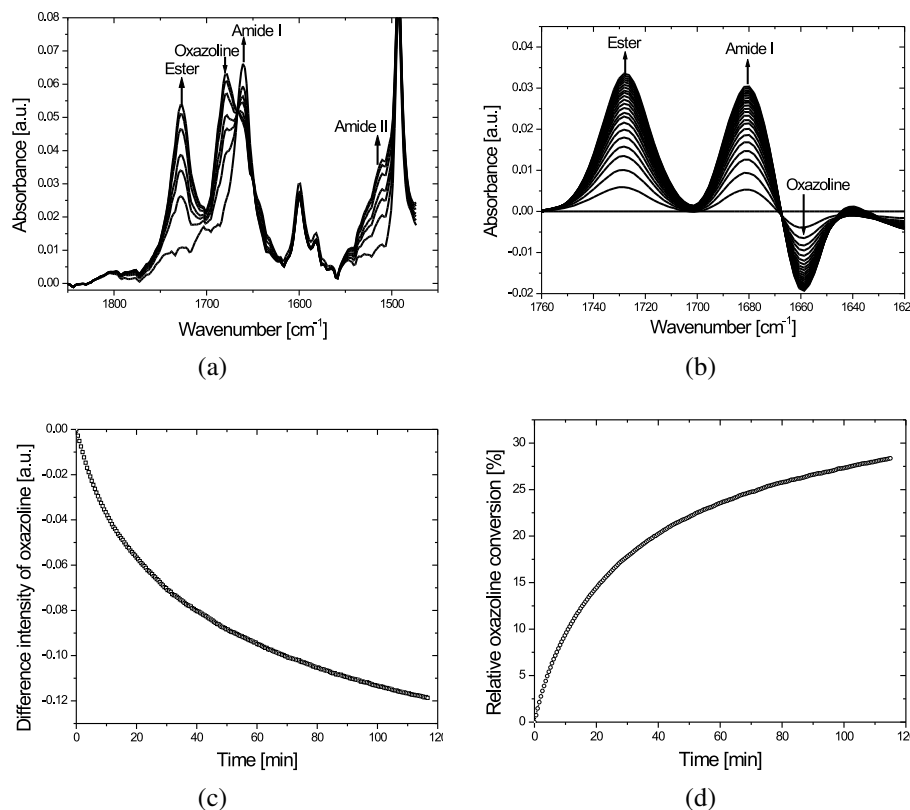


Figure 3.8: Results and analysis of interfacial reaction in bilayer system of PEMA-15 and ran-SAN-oxaz-5.4 at 190 °C: (a) original spectra, (b) difference spectra, (c) difference oxazoline intensity and (d) relative oxazoline conversion versus time.

ester amide (see Figure 3.7) without any major side products. In the subsequent analysis, all the FTIR results are presented in two ways: 1) Difference intensity in arbitrary units (shown in Figure 3.8c), which is defined as $I(t) - I(0)$, where $I(t)$ is the intensity of oxazoline at a given time t and $I(0)$ is the intensity of oxazoline at the start of the annealing temperature. 2) Relative oxazoline conversion (shown in Figure 3.8d), calculated as the difference intensity relative to the original oxazoline intensity. Some experiments were performed five times and the results were reproducible with an experimental error of 4-5 %. Next, the effects of the different parameters on the interfacial reaction were studied and the results are discussed below.

3.3.3 Effect of oxazoline concentration on the interfacial reaction

To determine whether the final conversion and the conversion rate of oxazoline depend on the initial concentration of oxazoline, three different weight percentages of oxazoline (1.9, 3.5 and 5.4 wt %) of ran-SAN-oxaz were chosen and reacted with PEMA-15. The difference intensities of oxazoline are plotted as a function of time in Figure 3.9a. The rate of conversion and the final difference intensity of oxazoline increase proportional to the initial oxazoline

content. The data are also plotted as relative oxazoline conversion as a function of time in Figure 3.9b, and it can be observed that all the curves are similar within 3 %, which is within the experimental error limit. The relative oxazoline conversion is fitted with an exponential growth relation with respect to time ($R^2 = 0.96$) and is concluded that the relative oxazoline conversion follows first-order kinetics with respect to the oxazoline concentration.

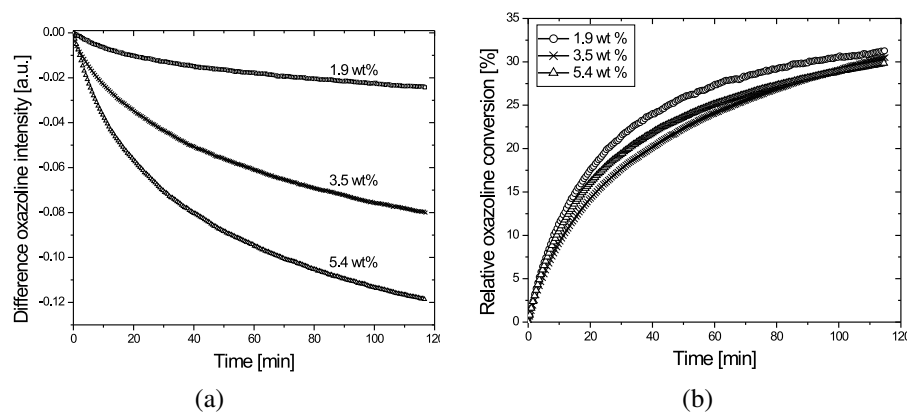


Figure 3.9: (a) Difference oxazoline intensity and (b) relative oxazoline conversion for different starting oxazoline levels in the ran-SAN-oxaz layer in ran-SAN-oxaz/PEMA at 190 °C.

To determine whether the interfacial reaction depends on the distribution of the oxazoline groups over the polymer chain, homogeneous mixtures of ran-SAN-oxaz-5.4 and pure SAN was prepared in CB. This solution was used to prepare a ran-SAN-oxaz-1.9-mix layer for a comparison with the original ran-SAN-oxaz-1.9 layer. The relative conversion as well as the conversion rate for both the original ran-SAN-oxaz-1.9 and ran-SAN-oxaz-1.9-mix layer were found to be similar within 1 % error, indicating that the conversion rate is controlled by the average concentration of reactive oxazoline group and is independent of the oxazoline distribution over the chains including the relative position with respect to other oxazoline groups.

3.3.4 Effect of temperature on the kinetics of interfacial reaction

After studying the effect of the initial oxazoline concentration on the interfacial reaction, the effect of the temperature on the kinetics of the interfacial reaction is investigated in the temperature range of 150 to 190 °C. The relative oxazoline conversion is calculated for all the temperatures (Figure 3.10). At higher temperature the conversion of oxazoline increases fast in the initial stage and then slows down. On the other hand, at lower temperatures the oxazoline conversion increases much slower over the whole time range (2 hr). Unfortunately, kinetics fitting is not possible due to the heterogeneous nature of the reaction. FTIR yields spectra averaged over the whole layer thickness, whereas the reaction occurs only at the interface. Therefore, the initial slopes are plotted against the reciprocal temperature. The data fall on a straight line ($R^2 = 0.97$), indicating that the reaction in the initial stage is chemistry controlled. The activation energy (E_A) for this heterogeneous bilayer reaction between the oxazoline and the carboxylic acid is found to be 73 kJ/mol. Baumert *et al.* (1999) have reported an activation energy of 65 kJ/mol for the homogeneous reaction between oxazoline

and carboxylic acid attached to PS. The activation energy in the heterogeneous system is higher, because the reaction occurs only at the interface. Similar results were reported by Scott and Macosko (1994) for the reaction between anhydride-containing PS and polyamide-11.

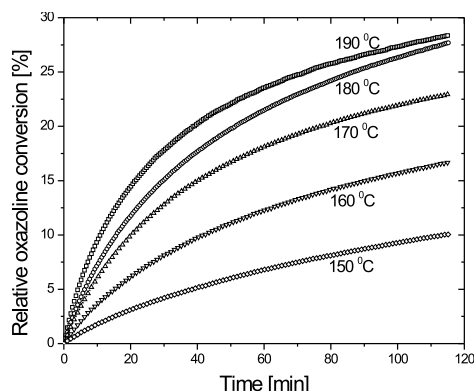


Figure 3.10: Relative oxazoline conversion at different temperatures in ran-SAN-oxaz/PEMA bilayers.

3.3.5 Effect of thickness of oxazoline layer on the interfacial reaction

The effect of thickness of oxazoline layer on both the rate of oxazoline conversion and the final conversion level was studied for two different layer thicknesses, i.e. 100 and 600 nm. The difference intensity of oxazoline for both layers at 190 °C is shown in Figure 3.11. At the initial stage of the reaction, the oxazoline conversion rate is the same for both thicknesses, whereas the conversion rate of oxazoline as well as the final conversion of oxazoline is lower for the thinner layer. For the bilayer samples, the reactive chains first need to diffuse to the interface to react. Hence, the amount of reactive oxazoline groups in the bulk determines the rate of the reaction. For the thinner layer, the amount of oxazoline in the bulk decreases faster as the reaction proceeds compared to the thicker layer. Hence, the conversion rate as well as the final conversion of oxazoline is much lower for the thin layer sample.

3.3.6 Effect of diffusion of reactive chains through nonreactive SAN

To determine whether the copolymer formation is limited by the reaction rate or by the diffusion of reactive chains through the bulk, a trilayer system was used (shown in Figure 3.1b). The time (hereafter called delay time) needed for the reaction to start was measured. The relative conversion of oxazoline for different thicknesses of the SAN-layer was measured at different temperatures and the results for 170 °C are shown in Figure 3.12. For the sample with 0 nm SAN layer, i.e. for the bilayer sample, the oxazoline conversion started to increase at zero time, because the reactive ran-SAN-oxaz is already present at the interface at $t = 0$. Going from the 100 nm to the 400 nm SAN inter layer, the delay time increases because the reactive chains have a longer diffusion path for the thicker samples. The corresponding delay time for two different temperatures is shown in Table 3.2. For a similar thickness, the delay

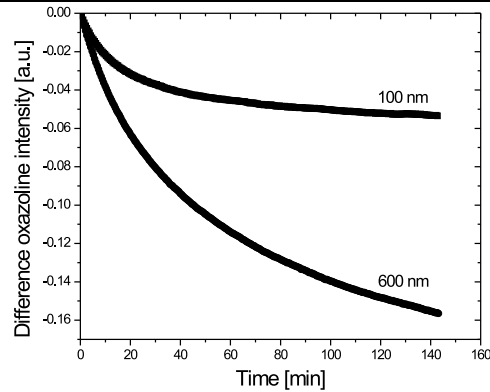


Figure 3.11: Difference oxazoline intensity for 100 and 600 nm thick ran-SAN-oxaz layer in ran-SAN-oxaz /PEMA bilayers at 190 °C.

time decreases with increasing temperature, which is due to the fact that chains diffuse faster at higher temperatures. The diffusion coefficient D at each temperature can be obtained using Fick's law of diffusion (Bird *et al.*, 1994):

$$D = \frac{L^2}{4t_d} \quad (3.1)$$

where L is the thickness of the SAN inter layer and t_d is the delay time. The diffusion coefficient D increases as a function of temperature. The values of the diffusion coefficients are in the order of $10^{-16} - 10^{-17} \text{ m}^2/\text{s}$ (Table 3.2). Similar values were reported in literature for SAN (Kim *et al.*, 1995a,b). The activation energy for diffusion can be calculated by assuming an Arrhenius behavior only at higher temperatures (160-190 °C) (Kim *et al.*, 1995a), which are well above the T_g of ran-SAN-oxaz, i.e. 110 °C. The activation energy was found to be 92 kJ/mol. A value of 100 kJ/mol was reported by (Kim *et al.*, 1995a) for the activation energy, when deuterated SAN diffuse through a SAN layer.

Table 3.2: Delay time and diffusion coefficient for different thicknesses of SAN interlayer in ran-SAN-oxaz /SAN/PEMA trilayer

Thickness of SAN layer [nm]	Temperature [°C]	Dealy time [min]	Diffusion coefficient [m^2/s]
100	170	0.51	8.1×10^{-17}
200	170	1.88	8.8×10^{-17}
400	170	8.05	8.2×10^{-17}
100	190	0.17	2.4×10^{-16}
200	190	0.68	2.4×10^{-16}
400	190	2.74	2.4×10^{-16}

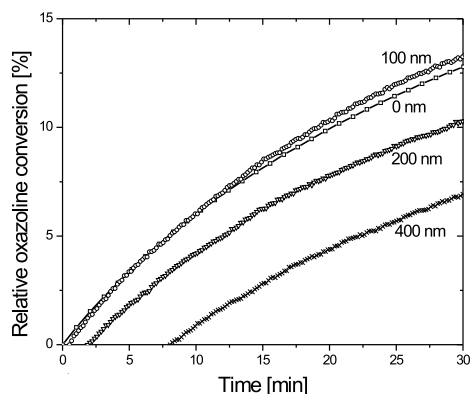


Figure 3.12: Relative oxazoline conversion for different thicknesses of the SAN inter layer in ran-SAN-oxaz /SAN/PEMA trilayer at 170 °C.

3.3.7 Development of interface thickness

After studying the effect of the initial oxazoline concentration, temperature and thickness of the oxazoline layer on the kinetics of the interfacial reaction in the bilayer systems, the actual development of interfacial thickness during the reaction was investigated using ellipsometry. In order to be able to measure the interfacial thickness between two layers of immiscible polymers with ellipsometry, the difference in refractive index between the two polymers should be large enough at the measured temperatures. Therefore, the temperature dependence of the refractive indices of PEMA and ran-SAN-oxaz was measured (Figure 3.13). As expected, the slope of the refractive index of the amorphous ran-SAN-oxaz-5.4 changes at T_g (115 °C). For the crystalline PEMA-15, a discontinuity in the refractive index is observed around the melting point (76 °C). Moreover, the difference in refractive index, i.e. > 0.02 , is sufficient for ellipsometric measurements between ran-SAN-oxaz-5.4 and PEMA-15 at the reaction temperatures of 140 to 180 °C.

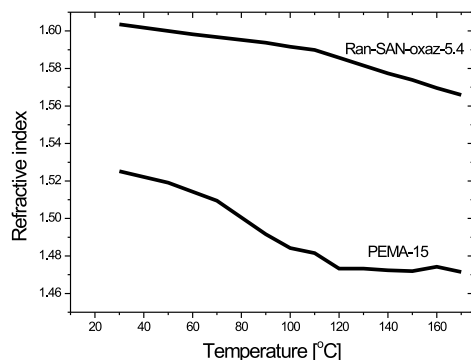


Figure 3.13: Temperature dependence of the refractive indices of ran-SAN-oxaz-5.4 and PEMA-15.

The retardation Δ and the reflection ratio $\tan\Psi$ for the bilayer samples were measured and fitted according the 3-layer model (Yukioka and Inoue, 1991) with three different interface layer models to obtain the value of the interface thickness. The experimental and fitted value of Ψ for three different interface models is shown in Figure 3.14. All the interface models give similar fitting with nearly equal mean square error values.

The interface thickness of the ran-SAN-oxaz-5.4/PEMA-15 system as a function of time at different temperatures is shown in Figure 3.15. The interface thickness increases with time up to 20 minutes and finally reaches a plateau value of 17 nm (± 1.34 nm) for both 150 and 160 °C. This value of the interface thickness is very close to the theoretical prediction by Helfand and Tagami (1972). Similar values for the interface thickness were observed by Yukioka and Inoue (1994) for the system of aPA/SMA8, while much higher value of 30 nm was observed for aPA/SMA23 system. Similarly, Dedecker *et al.* (1998) observed a value of 20 nm for the interface thickness for PA-12/SMA2 system and a higher value of 40 nm for PA-12/SMA14 system. The values obtained in the literature is somewhat higher than the value observed in our system which might be related to the mobility of the systems. In our system (random-random) the mobility is less than the mobility of the system (random-end) used in the literature and hence we expect smaller interfacial thickness in our random-random system as compared to the random-end system. The rate of formation of the interface is faster at higher temperatures because of the higher rate of interfacial chemical reaction, whereas the final interface thickness is the same for both temperatures, which may be due to the saturation of interface at longer times. Interface thickness measurements at temperatures above 160 °C were not possible because the sample started to flow.

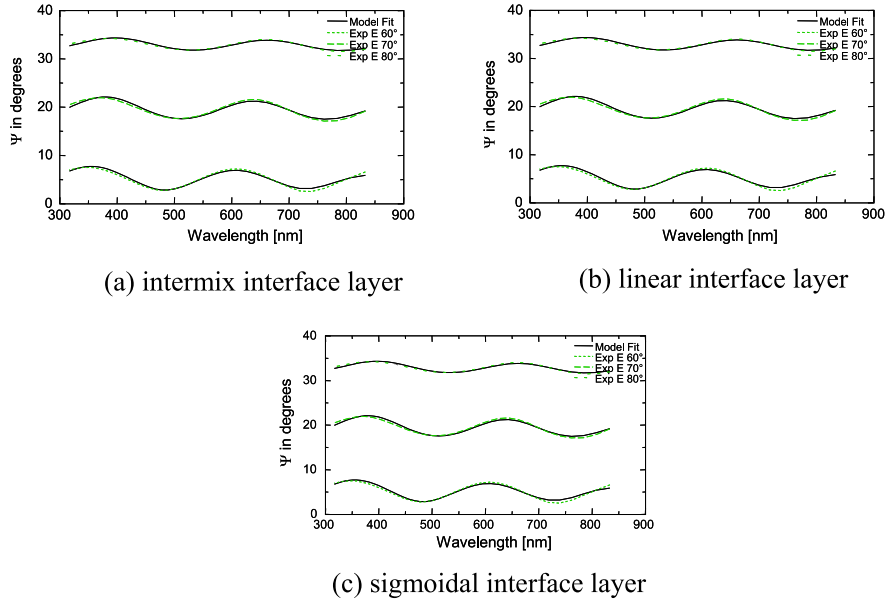


Figure 3.14: Experimental and simulated Ψ for 3 different interface layer (a) intermix interface layer (b) linear interface layer (c) sigmoidal interface layer.

Next, the interfacial growth is compared with the oxazoline conversion at 160 °C as shown in

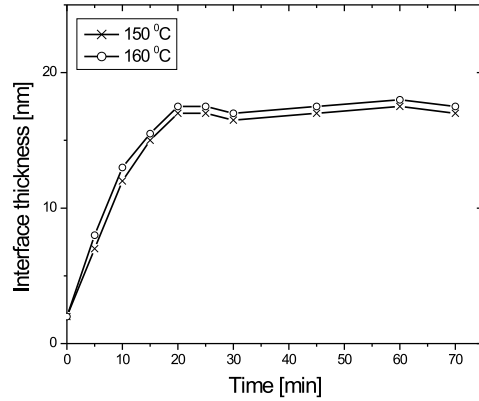


Figure 3.15: Development of interface thickness for ran-SAN-oxaz-5.4/PEMA-15 bilayers at different temperatures.

Figure 3.16. At times below 20 min, both the interface thickness and the oxazoline conversion increase with time and above 20 min, the interface thickness remains constant, whereas the oxazoline conversion continues to increase up to 120 min. This can be explained by assuming that in the initial stage of the interfacial reaction the reactive groups migrate from the bulk to the interface and form graft copolymers and, hence, builds up the interfacial region. But after a certain time (approximately 20 min for the reaction at 160 °C), the interface is saturated with graft copolymers, which form a barrier for new reactive chains and chain segments from the bulk to migrate to the interface. Since for the system studied, many functional groups are attached to the polymer backbone, further 'intra'-copolymer reactions can take place in the interfacial region, resulting in a continuing increase of the oxazoline conversion, but with no further increase in the interface thickness.

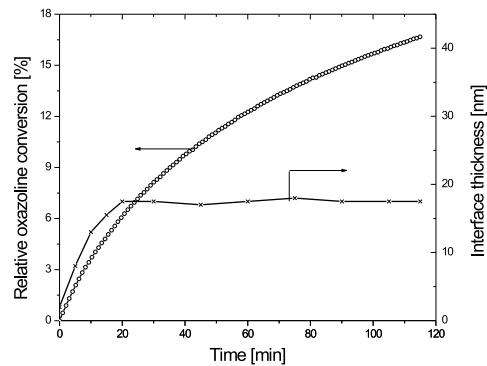


Figure 3.16: Comparison of interface thickness and interfacial oxazoline conversion at 160 °C in ran-SAN-oxaz/PEMA bilayer.

3.3.8 Effect of interface renewal on the late stage of the interfacial reaction

The ellipsometry results show that the interface thickness reaches a plateau value after a reaction time of 20 min at 160 °C, whereas the conversion of oxazoline (see Figure 3.10) does not reach a plateau value even after 120 min of the reaction at 160 °C. To determine whether interface renewal helps in driving the reaction further at high temperatures, the interface of the bilayer samples were refreshed using a Meissner extensional rheometer setup (Figure 3.5). For this experiment, a bilayer system consisting of ran-SAN-oxaz-5.4 and PEMA-9 instead of PEMA-15 was used. Since the FTIR-spectra for this experiment were measured off-line, the reference spectra for the reaction of PEMA-9 with ran-SAN-oxaz-5.4 were measured first on the ATR Golden Gate at 190 °C. Figure 3.17 shows that the oxazoline conversion increases fast in the initial stage but starts to level off after 70 min. The stretching process can be subdivided into three steps as explained in the experimental section. In the first step, the sample was heated in the oven at 190 °C for 70 min. Samples were taken at 10 min intervals and measured with FTIR spectroscopy and the results are shown as full circles in Figure 3.17. The differences between the on-line and offline-measured spectra are small and within an experimental error of 2 %. After 70 min (step II), the sample was stretched at 130 °C to twice its initial length. The thickness of the interface was halved after stretching, whereas the oxazoline conversion remained constant, because during stretching no further reaction occurred. In the third step (III), the sample was annealed for another 60 min at 190 °C. The oxazoline conversion was increased further by 8 %. On the other hand, the reference spectra showed that the oxazoline conversion would have increase by 2 % when there is no interface refreshment. This indicates that the stretching process increases the extent of reaction because of interface renewal.

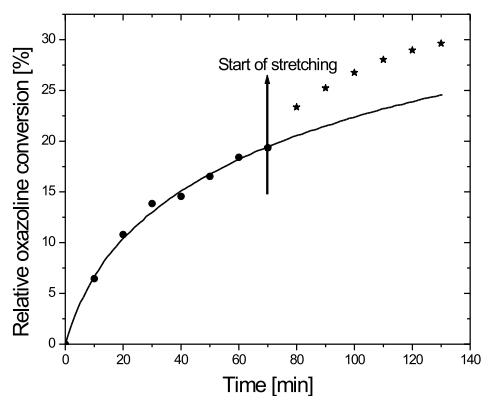


Figure 3.17: Relative oxazoline conversion versus time for on-line measurement (○), off-line measurement before stretching (●) off-line measurement after stretching (★) in ran-SAN-oxaz/PEMA bilayer.

3.4 Discussion

In this section, an attempt will be made to capture the presented results on the interfacial reaction between high-molecular-weight polymers containing randomly distributed acid and oxazoline functionalities in a model, of which the schematics are presented in Figure 3.18. Before describing the model in detail, it has to be mentioned that schematic models often suffer from simplicity and do not capture all features. In addition, some of the phenomena discussed as occurring sequentially, may partially occur simultaneously. Throughout the discussion, the term 'interface' is used instead of 'interphase', as being used by some other authors, to represent the interfacial region in which the reactions occur.

The model is divided in three different, sequential stages: viz. the initial, intermediate and late stage of the interfacial reaction. At $t = 0$, the two layers are brought into contact with each other and the reactive oxazoline groups of ran-SAN-oxaz, denoted by x, and the reactive carboxylic groups of PEMA, denoted by \square , are located on both sides of the sharp, infinitely thin interface, represented by a double line (Figure 3.18a).

The initial stage is first characterized by the inter-diffusion of reactive chains to form an interface, which is in the order of 2-3 nm as calculated from the interaction parameter (Helfand and Tagami, 1972) without undergoing reaction (Figure 3.18b). Next, the initial stage is also characterized by the migration of reactive chain segments from the bulk to the interface, which occurs very fast and by the reaction between oxaz and acid (\bullet) resulting in the formation of graft copolymers at the interface (Figure 3.18c). This is evident from the results of the effect of different thickness of the oxazoline layer (Figure 3.11) and the effect of diffusion through the nonreactive SAN layer on the interfacial reaction (Figure 3.12). The oxazoline conversion rate does not depend on the thickness of the oxazoline layer at the initial stage, as is shown in Figure 3.11. Furthermore, it is evident from Figure 3.12 that the diffusion is much faster than the reaction, which is confirmed by the observation that the delay time for different thicknesses of the SAN layer varies from 1-8 min, whereas the oxazoline conversion is only about 2 % within 10 min. From the ellipsometry results in Figure 3.15, it is also evident that the interface thickness increases considerably in the same time interval.

The intermediate stage (Figure 3.18d) is characterized by immobilization of the interface, because of the formation of highly branched graft copolymers in the interfacial region. Correspondingly, the migration of reactive chains through the interface is slower than in the initial stage. Further reactions at the interface can occur between reactive groups of new chains and chain segments coming from the bulk as well as 'intra'-copolymer reactions can occur between reactive groups of the graft copolymers already present at the interface. This is evident from the results presented in Figure 3.10 on the interfacial reaction at different temperatures and the corresponding ellipsometry results (Figure 3.16). Figure 3.10 shows that the conversion rate is lower in the intermediate stage than in the initial stage, while Figure 3.16 illustrates that the interface thickness develops slower in the intermediate stage than in the initial stage.

The late stage (Figure 3.18e) is characterized by saturation of the interface with highly branched grafted copolymers and, concomitantly, no migration of reactive chains from the bulk to the interface can occur. The interface thickness remains constant, whereas the reaction between the acid and oxazoline groups still proceeds, but with a slower rate than for the initial and intermediate stages. Since no new reactive chains migrate to the interface, only 'intra'-copolymer reactions are responsible for the observed progress of the reaction. This is confirmed by both the IR and ellipsometry results (Figure 3.16), which show that the interfa-

cial reaction still proceeds, while the interface thickness remains constant. At the end of the late stage (e.g. after 2 hr at 190 °C), interfacial reactions are not observed and the interface thickness does not change.

Next, the schematic model for the static situation described above is extended for the dynamic situation. Hence, the interface was refreshed by applying elongational flow from both sides of the bilayer films at 130 °C with an elongational rate of 0.001 s^{-1} (Figure 3.19a) followed by reaction at 190 °C. The time scale of elongation is approximately 15 min at 130 °C, whereas the diffusion time at that temperature is more than 15 min (extrapolated value from the delay time shown in Table 3.2). Hence, the interface thickness is halved with no diffusion of new chains to the interface (Figure 3.19b) with most likely the development of some Rayleigh disturbances on the interface, as observed by other authors with TEM (Kim *et al.*, 2003, 2005; Jiao *et al.*, 1999). Finally, at 190 °C, the diffusion of reactive chains is much faster giving rise to a further increase in oxazoline conversion and the formation of graft copolymers (see the results of Figure 3.17). The increase in oxazoline conversion may be due to both 'inter'- and 'intra'-copolymer reaction resulting in a further increase of interface thickness (Figure 3.19c).

These results show that for the random-functionalized acid (PEMA) and random-functionalized oxazoline (ran-SAN-oxaz) systems, interface refreshing enhances the interfacial reaction.

3.5 Conclusions

Ran-SAN-oxaz with different concentrations of oxazoline were prepared by modification of the nitrile group in SAN and used as reactive polymer in reactive blending. Poly(ethylene-*co*-methacrylic acid) (PEMA-15 and PEMA-9) was used as the other reactive polymer. The interfacial reaction was monitored by FTIR spectroscopy and ellipsometry. From the FTIR results, it was found that the interfacial reaction is a first order reaction with respect to the oxazoline concentration with an activation energy of 73 kJ/mol, whereas 65 kJ/mol was reported for the homogeneous reaction between oxazoline and carboxylic acid groups attached to PS. The effect of diffusion was studied with a trilayer approach, with a third, nonreactive SAN layer positioned in between the reactive layers and an Arrhenius-type dependency was found with an activation energy of 92 kJ/mol for diffusion. The ellipsometry results showed that the interface thickness reached a plateau value of 17 nm after a reaction time of 20 min at 160 °C, whereas the conversion of oxazoline did not reach a plateau value even after 120 min of the reaction at 160 °C. At 190 °C, the oxazoline conversion also reached a plateau value after 70 min.

Thus, the interface was refreshed at lower temperature, i.e. at 130 °C, which facilitated the migration of new reactive chains from the bulk to the interface at higher temperature, thereby increased the further oxazoline conversion.

Based on the FTIR and ellipsometry results, a model was proposed to describe the bilayer interfacial reaction in which three stages can be distinguished. In the initial stage, both the conversion of the interfacial reaction and the interface thickness increase because of the migration of reactive chain segments from the bulk to the interface and the formation of graft copolymers at the interface. In the intermediate stage, the migration of reactive chain segments slows down because of the formation of densely grafted copolymers. In the late stage, no migration of reactive chains from the bulk to the interface takes place, because the inter-

face is saturated with the densely grafted copolymers and only intra-chain copolymerization reactions can occur. Interface refreshing by imposing an elongational flow on the bilayer system promotes migration of new reactive chains from the bulk to the interface, thereby reinitiating the interface reaction.

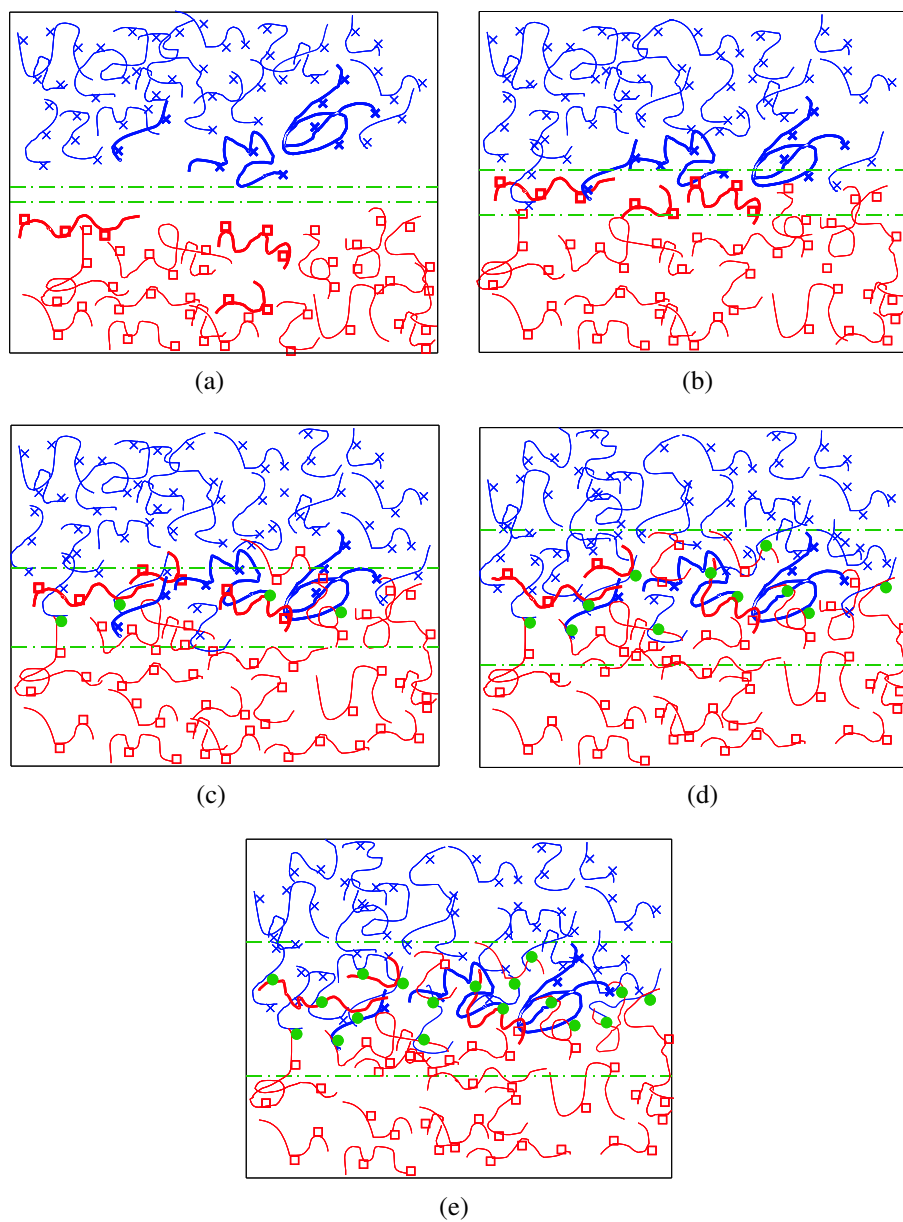


Figure 3.18: Schematic model describing the different stages of the interfacial reaction in the ran-SAN-oxaz/PEMA bilayer (a) $t = 0$, (b) migration and (c) reaction during initial stage, (d) intermediate stage, and (e) late stage of reaction.

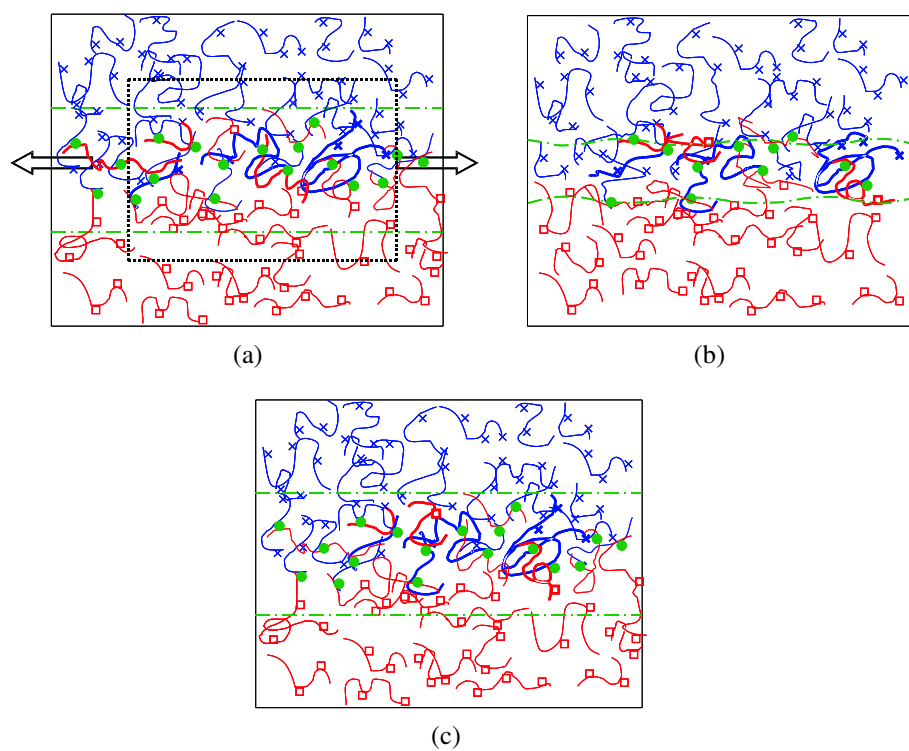


Figure 3.19: Schematic model describing the interfacial reaction and development of the interface during refreshment of the interface: (a) the end of the late stage (b) effect of interface refreshing and (c) final situation after stretching.

Chapter 4

Interfacial reaction between random acid functionalized and end oxazoline functionalized polymers

4.1 Introduction

Blending of polymers offers an attractive opportunity for the development of novel materials with useful combinations of properties (Paul and Newman, 1997). However, most polymer pairs are thermodynamically immiscible and usually display poor properties upon blending, due to a high interfacial tension and concomitantly an unstable morphology. This can be overcome by the addition of compatibilizers, i.e. block or graft copolymers, to modify the interfacial properties during processing. The different blocks of the copolymers have affinity for either of the two blend phases. The efficiency of block and graft copolymers in reducing the interfacial tension and stabilizing the morphology against coalescence has been extensively discussed in literature (Fayt *et al.*, 1981, 1986; Scott and Macosko, 1991) and can be premade or preferably generated in-situ using a reactive blending process, i.e. reactive compatibilization. The later has the advantage of forming the copolymers at the interface, where they are required.

The kinetics of the interfacial reaction plays a major role in polymer blends prepared by reactive compatibilization. The interfacial reaction kinetics determines the amount of in-situ formed compatibilizers and, ultimately, the properties of the polymer blends (Utracki, 1989; Pagnoulle, 2000). The molecular structure of the in-situ formed copolymer has an influence on the residence time at the polymer interface. Inoue et al. compared the residence time for in-situ formed linear block copolymers and graft copolymers of the same molecular weight (Charoensirisomboon *et al.*, 1999, 2000) and found that block copolymers leave the interface easily, whereas graft copolymers with the graft situated in the dispersed phase resides within the interfacial region. Pagnoulle (2000) investigated the influence of the architecture of the graft copolymer formed by interfacial reaction of mutually reactive PP and SAN chains on

the mechanical properties of blends and found that highly grafted copolymers formed at the SAN/PP interface lead to a relatively lower toughness than single graft copolymers.

In Chapter 3, the interfacial reaction between random acid-functionalized PE (PEMA) and random oxazoline-functionalized SAN (ran-SAN-oxaz) was studied and a model for the bilayer systems was proposed. The graft copolymer formed in the initial stage of the reaction stays at the interface and hinders further migration of reactive chains towards the interface. The rate of the interfacial reaction thus becomes very slow in the late stages. Interface refreshing promotes the continuation of the interfacial reaction by allowing further migration of reactive chains from the bulk to the interface. Note that, in most reactive blends, the graft copolymers are formed by reactions between copolymers with functional groups randomly distributed along the chain and polymers with the functional groups positioned at the end of the chain, such as polyamides and polyesters.

The objective of this chapter is to study the interfacial reaction in bilayer systems comprising random acid-functionalized and oxazoline end-functionalized polymers. Therefore, low-molecular-weight end oxazoline-functionalized SAN (end-SAN-oxaz) were prepared from end acid-functionalized SAN (end-SAN-acid), prepared by Reversible Addition Fragmentation chain Transfer (RAFT) mediated polymerization. Poly(ethylene-co-methacrylic acid) (PEMA) was used as the high molecular weight random acid-functionalized polymer. The interfacial reaction was monitored by Attenuated Total Reflection FTIR (ATR-FTIR). Further, the results are confronted with the model proposed in Chapter 3 and modifications are implemented.

4.2 Experimental

4.2.1 Materials

The styrene and acrylonitrile monomers of the highest available purity were purchased from Aldrich. Styrene was purified by filtration through a aluminum oxide filled column (Al_2O_3 , activated basic Brockmann I, standard grade, ca. 150 mesh) and acrylonitrile was purified by filtration through a column filled with inhibitor remover to remove hydroquinone and monomethyl ether hydroquinone stabilizers. The 1,1'-azobis(1-cyclohexanecarbonitrile) (V-40, purity > 98 %) initiator was obtained from WAKO and used as received. Toluene (Hi-DryTM, anhydrous solvent), obtained from Romil Ltd., and tetrahydrofuran (THF), obtained from Aldrich, were used as received. The RAFT agent S-dodecyl-S'-(isobutyric acid) trithiocarbonate (DIBTTC) was prepared according to the procedure used by Lai *et al.* (2002). 1,3-phenylene-bisoxazoline (PBO) was obtained from Degussa and used without purification. Poly(ethylene-co-methacrylic acid) with 15 wt% methacrylic acid (PEMA-15) was obtained from Sigma Aldrich; $M_n = 11$ kg/mol and $M_w = 51$ kg/mol with a Melt Flow Index (MFI) (ASTM D 1238, 190 °C/2.16 kg) of 21 g/10 min and a melting temperature of 76 °C. Anthracene, obtained from Aldrich, and trichloroacetyl isocyanate (TAI), obtained from Acros, were used as received. 1,2-dichlorobenzene (DCB), methanol, chloroform and chlorobenzene were purchased from Sigma Aldrich and used without further purification.

4.2.2 Synthesis of end acid-functionalized SAN (end-SAN-acid)

The copolymerization was carried out in a three-necked, round-bottom flask equipped with a magnetic stirrer. First, 0.5 g of DIBTTC was added to a mixture of styrene (3.95 g) and

acrylonitrile (1.2 g). Then, 5 g of toluene was added followed by the addition of the AZO initiator V-40 (0.03 g). The mixture was then purged with argon for approximately 45 min at room temperature. Next, the reaction mixture was placed in an oil bath thermostated at 85 °C. The reaction was stopped after 24 hrs and the SAN-copolymer was precipitated from toluene with a 10-fold excess of methanol. The copolymer was then dried overnight in a vacuum oven at 50 °C. The details of the reaction scheme to produce end-SAN-acid (1) from styrene and acrylonitrile monomer are shown in Figure 4.1.

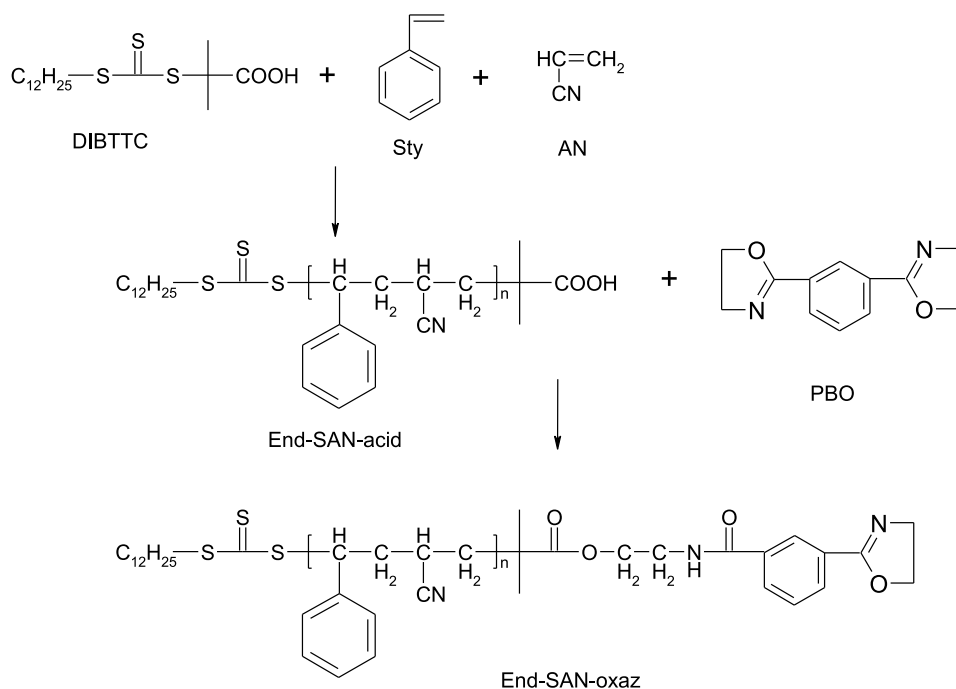


Figure 4.1: Schematic representation of preparation of end-SAN-acid (1) and end-SAN-oxaz (2).

4.2.3 Synthesis of end oxazoline-functionalized SAN (end-SAN-oxaz)

A mixture of end acid-functionalized SAN and 1,3-PBO in 1:10 molar ratio was dissolved in DCB at 150 °C in a Schlenk flask. The reaction was performed for 24 hrs to obtain end oxazoline-functionalized SAN (2) as shown in Figure 4.1. To remove the unreacted excess of PBO, a 2-fold amount of chloroform relative to the total reaction mixture was added to obtain a homogeneous solution. The polymer was then precipitated with a 5-fold excess of methanol. This procedure was repeated 4 times for complete removal of the low-molecular-weight PBO. The purified sample was dried at 45 °C under vacuum for 2 days.

4.2.4 Preparation of bilayer samples

End-SAN-oxaz was dissolved in chlorobenzene and thin films were prepared by spin coating using a KarlSus, RC8-apparatus. Spin coating of thin films of PEMA-15 at room temperature was impossible, since no solvent was available. Thus, 0.5 mm-thick films of PEMA-15 were prepared by compression molding at 180 °C for 30 min in a Collin compression press. For the ATR-FTIR-measurements on the bilayer systems, thinner films (approximately 600 nm) of end-SAN-oxaz were spin-coated on top of PEMA-15 films. Samples were dried in an oven set at 50 °C for 2 hrs to remove residual solvent.

4.2.5 MALDI-TOF-MS

Measurements were performed on a Voyager-DE STR (Applied Biosystems, Framingham, MA) instrument, equipped with a 337 nm nitrogen laser. Trans-2-[3-4-(tert-butylphenyl)-2-methyl-2-propenylidene]malononitrile was used as the matrix. The matrix was dissolved in THF at a concentration of 40 mg/ml. Potassium trifluoroacetate was added as cationic ionization agent and was dissolved in THF at a concentration of 1 mg/ml. The polymer concentration in THF was approximately 1 mg/ml. In a typical MALDI experiment, the matrix, salt and polymer solutions were mixed in a ratio of 5 μ l sample, 5 μ l matrix and 0.5 μ l salt. Approximately 0.5 μ l of this mixture was spotted on the target plate by hand. Positive-ion spectra were recorded in reflector mode. For each spectrum 1000 laser shots were accumulated. The data obtained were analyzed using in-house developed software (Willemse *et al.*, 2004; Willemse, 2005; Staal, 2005).

4.2.6 Nuclear Magnetic Resonance Spectroscopy (NMR)

All solution ^1H -NMR spectra were recorded on a Varian 400 MHz spectrometer at 25 °C and at a resonance frequency of 400.164 MHz. All chemical shifts are reported in ppm downfield from anthracene, used as an internal standard. The spectra were acquired using 128 scans. First, a 1 mg/ml stock solution of anthracene in CDCl_3 was prepared. 15-20 mg of the polymer was dissolved in 1 ml of the stock solution. The polymer solution was transferred to a NMR tube. Subsequently, an excess of TAI was added (approximately 5 μ l) and mixed by shaking.

4.2.7 LC-MS

LC-MS measurements were performed on an Agilent 1100 series HPLC-setup, equipped with a degasser (G1322A), a quaternary pump (G1311A), an autosampler (G1313A) and an UV diode-array detector (G1315B). For the MS detection an Agilent MSD type SL (G1946D) mass spectrometer with an atmospheric pressure electrospray interface was used (drying gas temperature: 350 °C, drying gas flow: 13 l/min, nebuliser pressure: 30 psi, capillary voltage: 4 kV). A 50/50 % (V/V) water/methanol mixture was used as the eluent. A flow rate of 0.25 ml/min was used with an injection volume of 1 μ l. All the measurements were carried out at room temperature. Spectra were recorded in the mass range of 50-500 atomic mass units (a.m.u).

4.2.8 Triple-SEC

Size exclusion chromatography was performed on a system consisting of a gradient pump (Waters Alliance 2695, flow rate 1.0 ml/min under isocratic conditions), a guard column (PL gel 5 μm , Polymer Laboratories), a three-column set (three PL gel Mixed-C 5 μm columns from Polymer Laboratories) with a photodiode-array detector (Waters 2996) and a differential refractive-index detector (Waters 2414) as concentration detectors, a light-scattering detector (Viscotek), and a viscosity detector (Viscotek, dual detector 250). THF (Biosolve) was used as the solvent and was filtered twice (0.2 μm filter, Alltech) and stabilized with BHT (0.01 vol%, Merck, > 99 % pure). Data were acquired with the Empower Pro software.

4.2.9 ATR-FTIR spectroscopy

The bilayer samples were put upside down on the temperature-controlled Golden Gate ATR top-plate. The thinner end-SAN-oxaz layer was brought in contact with the ATR-crystal, while the thicker PEMA-layer was positioned at the top. The bilayer sample was covered with a steel plate flushed with a continuous nitrogen gas flow. The temperature of the ATR topplate was adjusted from ambient temperature to 200 °C by a Eurotherm 3000 series temperature controller. The angle of incidence of the ATR was set at 45° with diamond as the ATR crystal material. The penetration depth was 1.0-1.5 μm for the spectral range of interest (1000-2000 cm^{-1}). The spectra were recorded using a BioRad Excalibur 3000 FTIR apparatus coupled to a MCT-detector cooled with liquid nitrogen. A spectral resolution of 4 cm^{-1} was used for all measurements in order to minimize the spectra accumulation time. The time resolution was 30 sec and the number of scans was 100. Peak integrations were carried out with the BioRad Win-IR Pro software.

4.3 Results

First, the results of the synthesis and characterization of end acid-functionalized SAN are presented followed by the oxazoline modification of the end acid-functionalized SAN. Subsequently, the results from the interfacial reaction of the bilayer sample as obtained by FTIR spectroscopy are presented.

4.3.1 Preparation of end acid-functionalized SAN (end-SAN-acid) via RAFT

Low-molecular-weight SAN copolymers end-functionalized with carboxylic acid was prepared via RAFT mediated polymerization. The product was characterized with FTIR spectroscopy, $^1\text{H-NMR}$ and MALDI-TOF-MS.

Figure 4.2 shows the FTIR spectra of the end acid-functionalized SAN and the spectrum of pure SAN. Two additional absorption bands are observed for the end-SAN-acid, one at 1740 cm^{-1} , which can be attributed to the carbonyl stretching vibration of the carboxylic acid, and one at 1700 cm^{-1} , which can be attributed to the carbonyl stretching vibration of dimers of the carboxylic acid (Vien *et al.*, 1991).

For determination of the terminal carboxylic acid in the functionalized SAN copolymer, a drop of TAI was added to the mixture of end-SAN-acid/ CDCl_3 before recording the $^1\text{H NMR}$ spectrum. The reaction between TAI and carboxylic acid (Donovan and Moad, 2005; Postma

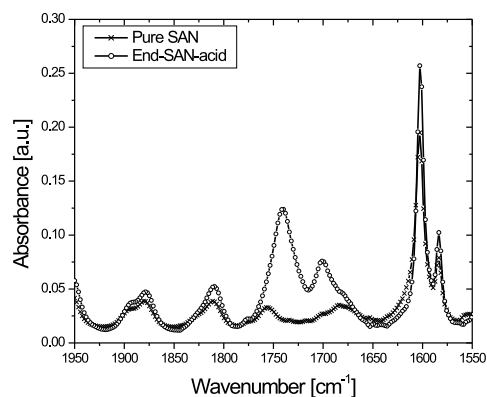


Figure 4.2: FTIR-spectra of pure SAN and end-SAN-acid.

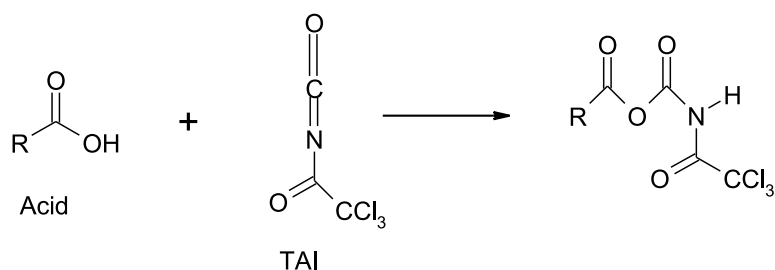


Figure 4.3: Reaction between carboxylic acid end group and TAI.

et al., 2006) at room temperature proceeds instantaneously to completion (see Figure 4.3) and the resulting spectra of the reaction products are shown in Figure 4.4. A single imidic hydrogen resonance from the product is found at approximately 10.3 ppm (Donovan and Moad, 2005). The concentration of the carboxyl end groups was calculated by integration of the peak of the end group normalized with the peak integral of anthracene (Choi *et al.*, 2004). From this a number-average molecular weight of 2800 g/mol was calculated, which agrees with the value determined with SEC (2900 g/mol).

Table 4.1: Peak assignment of the MALDI-TOF-MS spectra shown in Figure 4.5

Peak	E ₁	E ₂	K ⁺	Na ⁺
1	C ₁₂ H ₂₅ -CS ₃	C ₃ H ₆ COOH	+	-
1	C ₁₂ H ₂₅ -CS ₃	C ₃ H ₆ COOH	-	+

The MALDI-TOF-MS spectrum of the low-molecular-weight SAN end-capped with DIBTTC

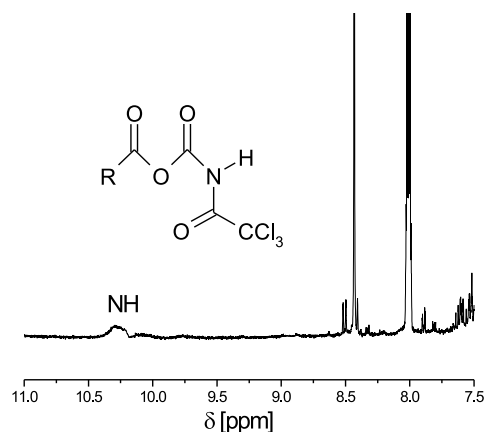


Figure 4.4: Region of interest of the $^1\text{H-NMR}$ spectrum of TAI derivatized with acid end-functionalized SAN.

(RAFT agent) is shown in Figure 4.5. For comparison, simulated spectra of SAN with the expected end-groups, cationized either with K^+ or Na^+ , are also shown in Figure 4.5, while the assignments of peaks 1 and 2 are presented in Table 4.1. The enlargement of the experimental spectrum is shown in Figure 4.5b from 2400 - 2650 a.m.u. The most abundant polymer chains with the expected end groups from the RAFT agent, i.e. dodecyl-trithiocarbonate ($\text{C}_{12}\text{H}_{25}\text{CS}_3$) and isobutyric acid ($\text{C}_3\text{H}_6\text{COOH}$), cationized with potassium and sodium, marked as peak 1 and peak 2 are pictured in Figure 4.5c and 4.5d respectively. The main reaction product is isobutyric acid end-functionalized SAN. The remaining peak in the spectrum (Figure 4.5) can be assigned to sodium or potassium salt of carboxylic acid (simulated spectrum is not shown here).

To determine the copolymer composition distribution, the MALDI-TOF-MS results are plotted with two-dimensional graphical representations of three dimensions (number of repeat units of A, number of repeat units of B and the intensity), called contour plots (Staal, 2005; Willemse, 2005). The contour plot for end-SAN-acid is shown in Figure 4.6a with the number of styrene units and acrylonitrile units on the two axes. The highest intensity in the contour plot corresponds to 17 styrene units and 8 acrylonitrile units, i.e. 32 mol% of acrylonitrile repeat unit. This is fairly close to the azeotropic condition used for the recipe. It is evident that the styrene and acrylonitrile monomers were incorporated in the polymer chain with the expected carboxylic acid end groups originated from the RAFT agent.

4.3.2 End oxazoline-functionalized SAN (end-SAN-oxaz)

The end oxazoline-functionalized SAN was prepared by reacting end acid-functionalized SAN with an excess of PBO. The presence of unreacted PBO after washing the product was checked with LC-MS and triple-SEC. The purified end-SAN-oxaz was characterized using FTIR spectroscopy, $^1\text{H-NMR}$ and MALDI-TOF-MS.

To determine whether the unreacted PBO is still present in end-SAN-oxaz after washing the sample with excess of methanol, the samples were analyzed with LC-MS and triple-

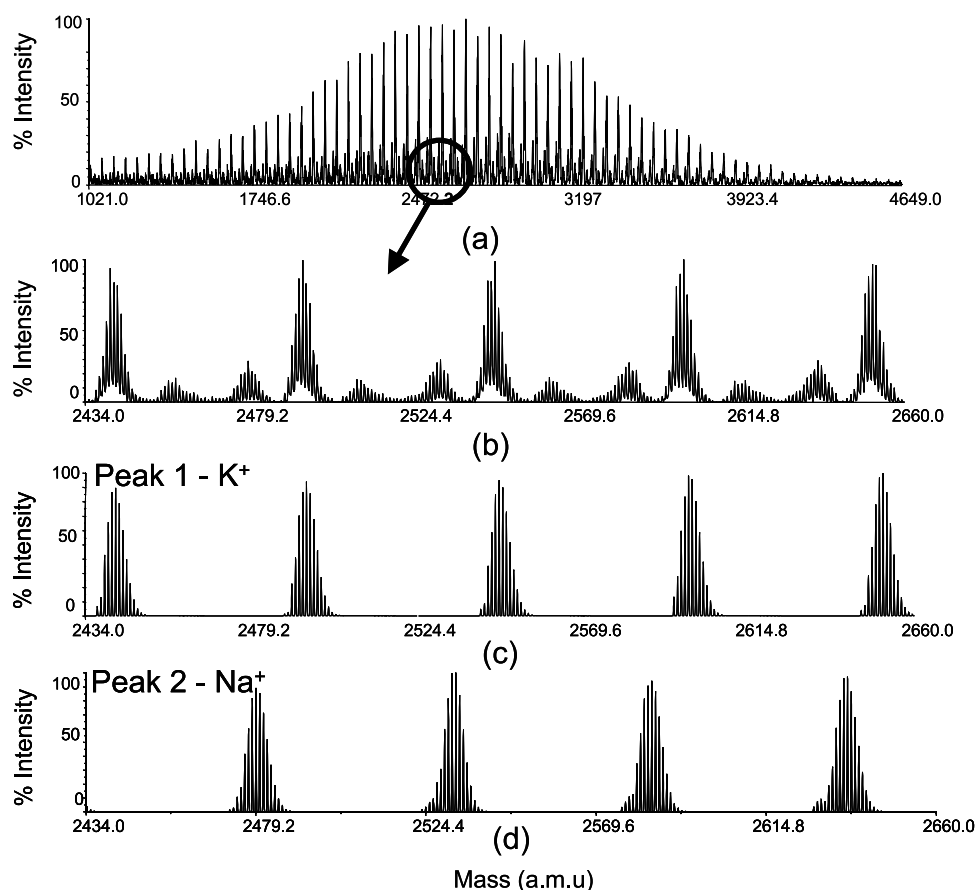


Figure 4.5: Comparison between experimental and simulated spectra for end acid-functionalized SAN: (a) entire spectrum, (b) enlarged spectrum between 2450 and 2650 a.m.u., (c) simulated spectra for peak1 from potassium salt and (d) peak2 from sodium salt.

SEC before and after washing (Figure 4.7a and 4.7b respectively). Large PBO peaks can be observed both with LC-MS (retention time of 5 min) and triple-SEC (retention time of 30 min) for the non-purified sample, indicating levels of more than 10 mg/ml of PBO before the first washing. The peaks are almost absent (less than 0.1 mg/ml) after washing the reaction product for four times in an excess of methanol. It is concluded that the product of reaction after washing does not contain unreacted PBO (<10 ppm in end-SAN-oxaz).

The reaction of end acid-functionalized SAN with PBO was studied with FTIR (Figure 4.8). Before the start of the reaction, the peak at 1740 cm^{-1} corresponding to the carbonyl stretching vibration of the acid group is clearly visible. This peak completely disappears upon reaction with PBO, indicating complete conversion of acid. Meanwhile, strong absorption bands at 1660 cm^{-1} due to the C=N stretching vibration of the oxazoline-group, at 1740 cm^{-1} , originating from the C=O stretching vibration of the ester group, at 1680 cm^{-1} , from the C=O stretching vibration of the amide group, and at 1510 cm^{-1} , from the C-N-H in-plane

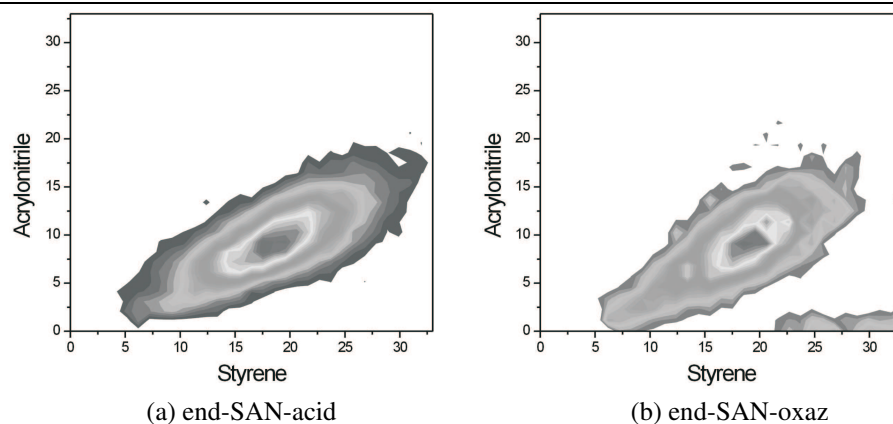


Figure 4.6: Contour plots of styrene and acrylonitrile in (a) end-SAN-acid and (b) end-SAN-oxaz.

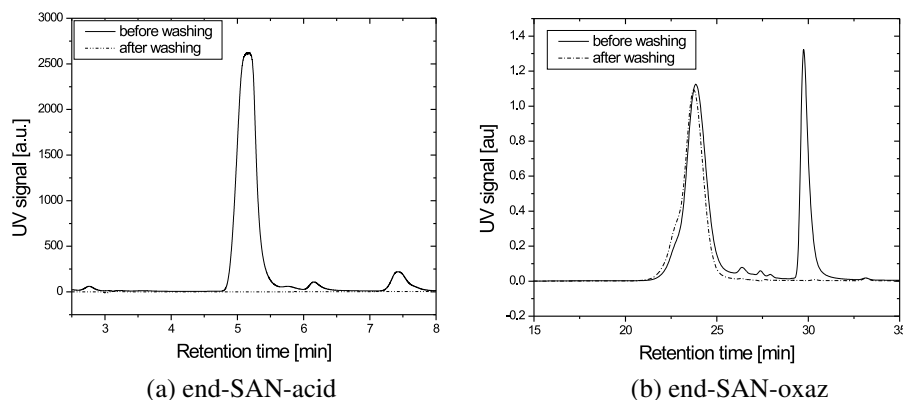


Figure 4.7: (a) LC-MS spectra and (b) triple-SEC spectra of reaction products before and after washing with excess of methanol.

bending vibration and C-N stretching vibration (Vien *et al.*, 1991) of the amide group, appear, indicating the formation of an ester-amide linkage with end-functionalized oxazoline.

For the NMR-analysis, end-SAN-oxaz was reacted with TAI similar to the procedure of end-SAN-acid and the resulting spectra are shown in Figure 4.9. The spectrum of end-SAN-oxaz does not show the imide NH-peak at 10.3 ppm, which was present in that of end-SAN-acid, thereby confirming the complete conversion of the acid with PBO.

The MALDI-TOF-MS spectrum of the end-SAN-oxaz is shown in Figure 4.10a. The enlargement of the experimental spectrum is shown in Figure 4.10b from 2400-2650 a.m.u. The most abundant polymer chains with the expected end group from dodecyl-trithiocarbonate ($C_{12}H_{25}-CS_3$), originating from the RAFT-agent, and oxazoline ($C_{16}H_{19}O_4N_2$), originating from PBO cationized with potassium and sodium is shown in Figure 4.10c and 4.10d respectively. No further attempt is made to assign the other peaks with lower intensities. The peak assignments are similar to that for the end-SAN-acid, where isobutyric acid is replaced by the oxazoline group.

The contour plot of the copolymer after the reaction with PBO was also obtained from the

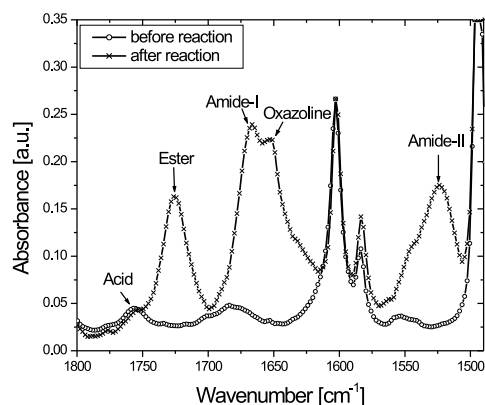


Figure 4.8: FTIR spectra of end acid-functionalized SAN before and after reaction with PBO.

MALDI-TOF-MS analysis (Figure 4.6b). The highest intensity shows that the average composition of SAN copolymer is 32 mol% of acrylonitrile repeat unit, which is in close agreement with the average composition of the SAN copolymer before reaction. The results from Figure 4.6a and 4.6b show that the contour plots before and after reaction with PBO are almost identical, which indicates that the end group modification does not change the chemical composition of the polymer backbone as expected.

4.3.3 Interfacial reaction between a bilayer sample of PEMA and end-SAN-oxaz

To study the interfacial reaction kinetics between end oxazoline-functionalized SAN (end-SAN-oxaz) and random acid-functionalized PE (PEMA), the bilayer film was first heated to 120 °C on the ATR crystal and kept for 30 min for pre-melting and then annealed isothermally at higher temperatures (140-190 °C). Figure 4.11a shows the spectra of the bilayer films, which were reacted at 190 °C. The reaction can be followed by the change of three different absorption bands as described in Chapter 3: 1) the decrease of the oxazoline band (C=N) at 1660 cm^{-1} , 2) the appearance of the amide-I band (C=O) at 1680 cm^{-1} , and 3) the appearance of the ester band (C=O) at 1730 cm^{-1} . Since the intensity changes of all absorption bands are very small and all bands are also not completely separated, difference spectroscopy was applied on the spectra from Figure 4.11a. All spectra were subtracted from the spectrum obtained after pre-melting at 120 °C for 30 min. The relative oxazoline conversion (as defined in Chapter 3) was calculated and the results are shown in Figure 4.11b for all investigated temperatures. The oxazoline conversion rate increases steeply in the initial stage of the reaction and slows down at the later stage for higher temperatures, but does not reach a plateau. On the other hand, at lower temperatures, the oxazoline conversion rate increases much slower for the entire time range (2 hr) of the reaction. Unfortunately, the experimental data cannot be fitted with a kinetic equation, because of the heterogeneous nature of the interfacial reaction. Therefore, the initial slopes were calculated and plotted against the reciprocal temperature. The Arrhenius plot showed a straight line, indicating that the oxazoline conversion in the initial stage is chemically controlled. The activation energy (E_A) for this

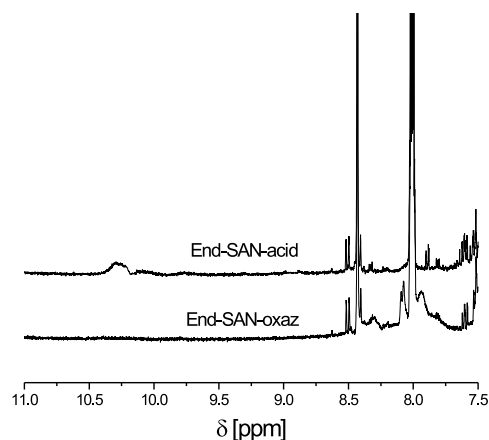


Figure 4.9: Comparison of ^1H -NMR spectra between end-SAN-acid and end-SAN-oxaz with TAI.

heterogeneous bilayer reaction between end-SAN-oxaz and PEMA is 110 kJ/mol. The initial oxazoline conversion rate is 2 to 3 times slower than the rate observed for the reaction between PEMA and ran-SAN-oxaz as discussed in Chapter 3. This is related to the oxazoline concentration in the end-functionalized system, which is approx. 2 wt% versus 5.4 wt% for the random-functionalized system.

4.4 Discussion

The interfacial reaction for the bilayer of end oxazoline-functionalized and random acid-functionalized polymers was studied with FTIR spectroscopy. Unfortunately, the development of the interfacial thickness by ellipsometry and the effect of interface refreshment by extensional rheometry on the interfacial kinetics could not be studied, since not enough end-SAN-oxaz was available.

The results are only discussed with the help of the FTIR-results and the observations from literature on similar systems and in analogy with Chapter 3, the results on the interfacial reaction are confronted with the model presented in Chapter 3 to see in which stage(s) deviations occur and how the model should be refined.

As discussed in Chapter 3, the model (Figure 4.12) can be divided in three different, sequential stages: viz. the initial, intermediate and late stage of the interfacial reaction, though the distinction is not so strict. At $t = 0$, the layers are brought into contact with each other and the reactive oxazoline groups of end-SAN-oxaz, denoted by x , and the reactive carboxylic acid groups of PEMA, denoted by \square , are located on both sides of the sharp, infinitely thin interface, represented by a double line (Figure 4.12a).

The initial stage is similar to the initial stage for random-random system, which is characterized first by the inter diffusion of reactive chains forming an interface without undergoing reaction (Figure 4.12b). Second, it is also characterized by the fast diffusion of reactive chains from the bulk to the interface and the reaction between oxaz and acid (\bullet) resulting in the formation of graft copolymers at the interface (Figure 4.12c). However, the shape of

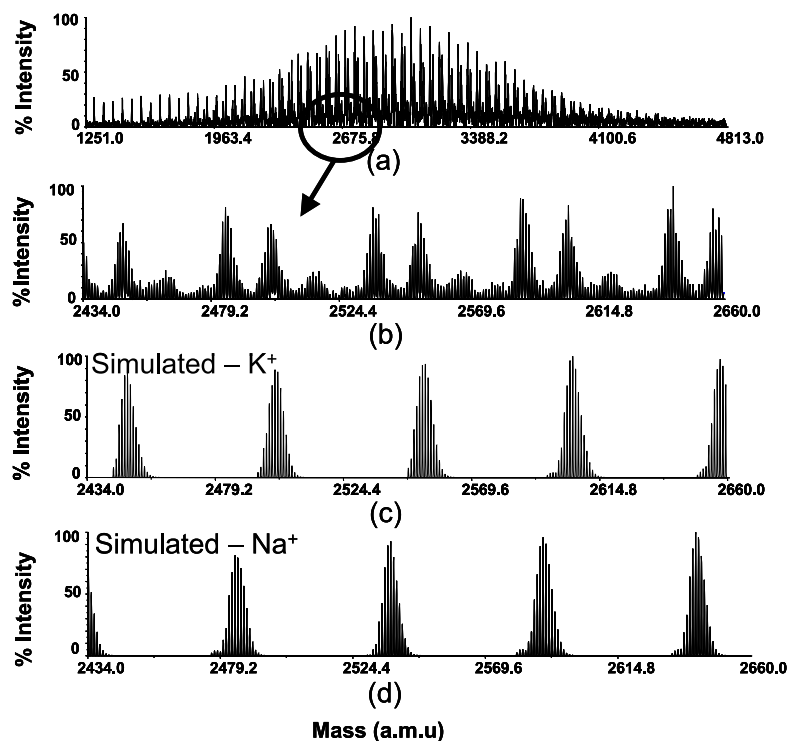


Figure 4.10: Comparison between experimental and simulated spectra for end oxazoline-functionalized SAN: (a) entire spectrum, (b) enlarged spectrum between 2450 and 2650 a.m.u., (c) simulated spectra for peak1 from potassium salt and (d) peak2 from sodium salt.

the graft copolymer formed in this case is Y-shaped, whereas for the random-random system, used in Chapter 3, H-shaped graft copolymers is formed. Although diffusion experiments were not performed for this system, it can be argued that the diffusion of end-SAN-oxaz is faster, because SAN copolymers with a lower molecular weight are used in comparison to the ran-SAN-oxaz used in Chapter 3.

The intermediate stage (Figure 4.12d) is characterized by slow migration of reactive chain segments to the interface compared to the initial stage, because of the presence of graft copolymers. The oxazoline conversion rate is lower than observed in the initial stage (Figure 4.11). Jiao *et al.* (1999) reported that the interfacial tension decreases with the formation of graft copolymer at the interface, when an end-functional chain reacts with a random-functional chain at the interface. This decrease in interfacial tension leads to the spontaneous formation of a corrugated interface, because of Rayleigh disturbances. In our system, undulations on the interface start to grow as shown in Figure 4.12d, which is less likely for the random-random system studied in Chapter 3.

The late stage is characterized by large undulations of the interface due to the formation of more graft copolymers at the interface. Hence, the polymer/polymer interfacial tension

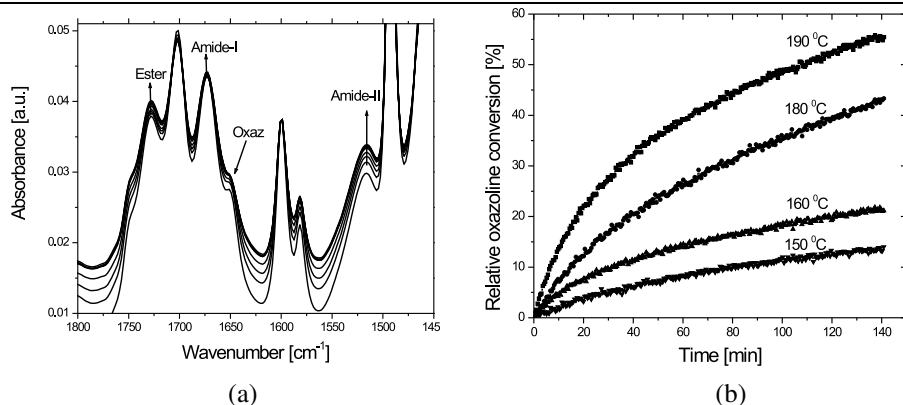


Figure 4.11: (a) Original spectra and (b) relative oxazoline conversion versus time at different temperatures.

decreases substantially, eventually leading to micelle formation in the phase with random functionalized polymer with low molecular weight polymers forming the core of the micelles via pinching mechanism (Jiao *et al.*, 1999; Kim *et al.*, 2005). In our system, low molecular weight SAN copolymer forms the core of the micelles (dotted circle in Figure 4.12e) and could be pinched off to the poly(ethylene) phase (Charoensirisomboon *et al.*, 1999, 2000; Pagnouille, 2000). The migration of these graft copolymers facilitate the further migration of the reactive chain segments from the bulk to the interface. This is in sharp contrast compared to the late stage in random-random system (Chapter 3), where the migration of reactive chains is almost absent. This is evident from the FTIR results (Figure 4.11), where the rate of conversion did not decrease even after 2 hrs of reaction. On the other hand, the rate of conversion reached a plateau value after 2 hrs of reaction (Figure 3.10, Chapter 3) for the random oxazoline and random acid system.

From the above discussions, it is found that the graft copolymers pinches off from the interface to the bulk in the system of end oxazoline-functionalized SAN and random acid-functionalized PE, which facilitates the further migration of reactive chains from the bulk to the interface. Hence, the interface refreshing might not be needed in the bilayer system of end-SAN-oxaz and PEMA.

4.5 Conclusions

End-SAN-acid was prepared via RAFT mediated polymerization, which was further converted into end-SAN-oxaz by reacting with PBO. The end-functionalization with acid and oxazoline was demonstrated with FTIR, ¹H NMR and MALDI-TOF-MS. The interfacial reaction in end-SAN-acid and PEMA bilayer was monitored with FTIR spectroscopy. A model with three different stages was proposed and compared with that of the random-random system studied in Chapter 3. In the initial stage of the reaction, diffusion of reactive chain segments is faster, but slows down with time. The migration of graft copolymers occurs in the intermediate and late stage resulting micelles in the PEMA phase. This facilitated further migration of reactive chains from the bulk to the interface and hence the interfacial reaction did not reach a plateau even after 2 hrs of reaction. Therefore, the interfacial refreshment is not necessary for the system of end-SAN-oxaz and PEMA.

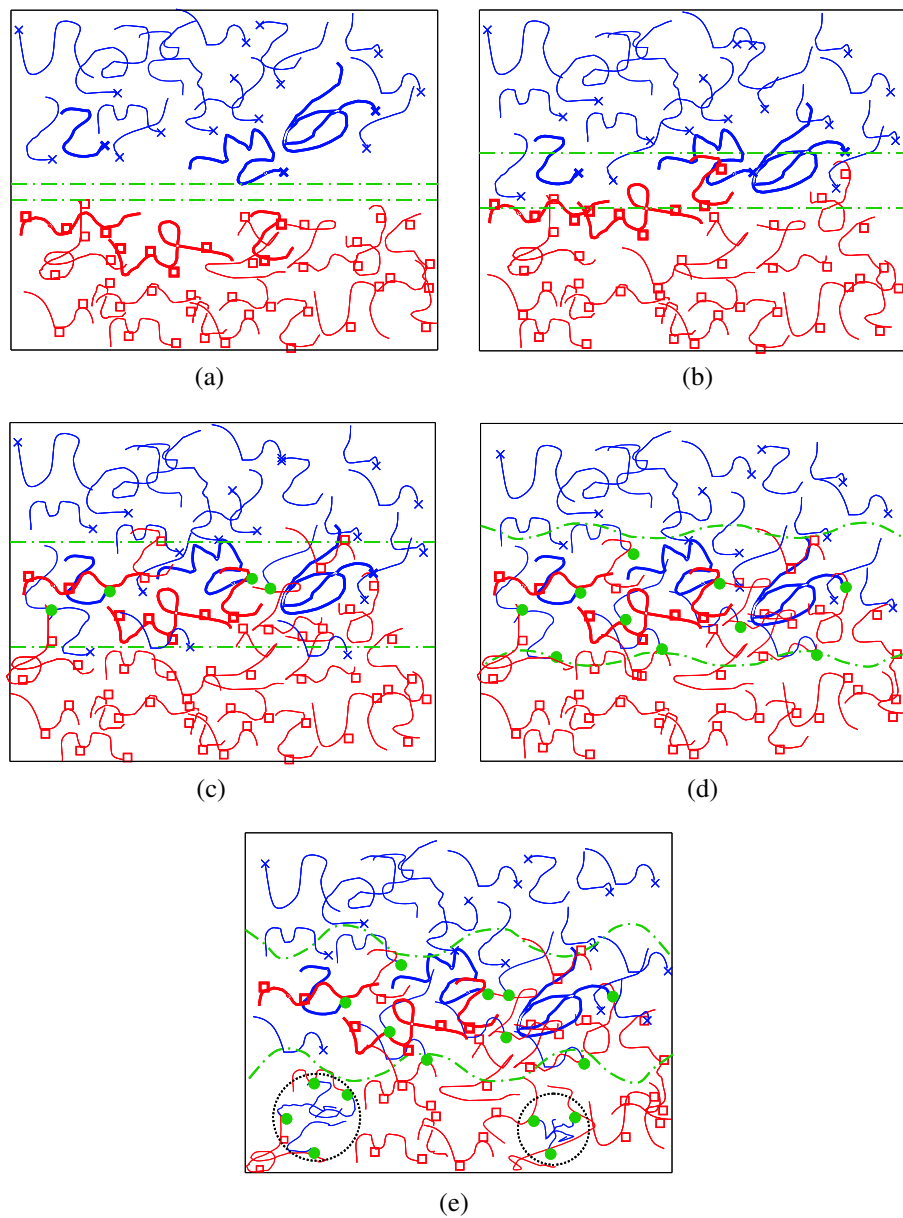


Figure 4.12: Schematic model for the different stages of the interfacial reaction in the end-SAN-oxaz/PEMA bilayer (a) $t = 0$, (b) migration and (c) reaction during initial stage, (d) intermediate stage, and (e) late stage of the reaction.

Chapter 5

Phase behavior of PMMA/SAN systems with reactive groups

5.1 Introduction

Blending of polymers has been extensively studied and used in industry to improve the properties of polymers (Paul, 1978; Utracki, 1989; Culberston, 1989). Generally, polymer blends are classified into three categories depending upon the miscibility, e.g. immiscible, partially miscible and fully miscible (Utracki, 1989). Immiscible polymer blends are an important family of materials, especially in comparison to fully miscible and partially miscible blends, since they usually combine a number of desirable characteristics of the individual components. A key issue in the blending of immiscible polymers is the control of the morphology, as well as of the size and shape of the dispersed phase and the interfacial properties. The ability to control these parameters is effectively achieved through the addition of a polymeric compatibilizer, which tends to concentrate in the interfacial region and acts as an emulsifier. Typically, block or graft copolymers are used in this respect. It was shown (Culberston, 1989; Noolandi and Hong, 1984; Leibler, 1991) that these copolymers provide an efficient method in controlling the blend morphology by reducing the size of the dispersed phase domains and also by enhancing the phase adhesion. Alternatively, functionalized polymers capable of reacting and forming copolymers in-situ during blending at the interface, a process known as reactive blending, are also quite effective.

For partially miscible blends, of which the polymers are miscible in a limited range of temperatures and/or compositions, phase separation can occur either upon lowering the temperature or upon increasing the temperature, called upper critical solution temperature (UCST) and lower critical solution temperature (LCST) respectively (Utracki, 1989). Phase separation in partially miscible blends is also suppressed by the addition of block copolymers. Park and Roe (1991) studied the late-stage coarsening behavior of PS/PB blends in the presence of PS-b-PB block copolymers. The block copolymer retarded the coarsening rate and the extent of retardation increased with increasing amounts of block copolymer and upon increasing the molecular weight of the copolymer. These results were consistent with the light scattering results obtained by Roe and Kuo (1990) on similar blend systems. Hashimoto and Izumitani (1993, 1994) found that the coarsening rate decreased significantly with increasing amounts

of block copolymer up to 6 % in a ternary system containing PB, SBR and SBR-b-PB block copolymers. Although there are a number of studies in the literature focussing on the effect of addition of pre-made block copolymers on the phase behaviour of binary blends, studies concerning the effect of in-situ reaction on the phase behaviour of binary blends are scarce. The only in-situ reaction reported in literature is that between PC and PMMA (Rabeony *et al.*, 1992). (Rabeony *et al.*, 1992) found that the low temperature phase separated system of PC/PMMA homogenizes at higher temperatures due to formation of graft copolymers as a result of the transesterification reaction between PC and PMMA. A similar behaviour was reported by Ko *et al.* (1995) for the PC/PMMA blend, although they ascribed their experimental observations to thermodegradative rather than transesterification reactions. Debier *et al.* (1995) explained the mixing of PC/PMMA systems with a reaction mechanism having both thermodegradative and transesterification reactions.

The phase behaviour of binary blends is not only affected by the graft copolymer, but also by the nature of the end group (Schacht and Koberstein, 2002; Van Durme *et al.*, 2006; Lee *et al.*, 2001). Schacht and Koberstein (2002) demonstrated that the incorporation of a fluorosilane group at the end of polystyrene chains enhances the miscibility with poly(vinyl methyl ether) (PVME). An increase of the LCST of approx. 10 °C was observed. Van Durme *et al.* (2006) also showed that different hydrophilic/hydrophobic end groups have a large influence on the LCST behaviour of PVME in water. Hydroxy-terminated PVME shifts the miscibility gap to higher temperatures, whereas a hydrophobic Br-containing end group causes PVME to be insoluble at room temperature. Lee *et al.* (2001) also showed that by varying the end group from methyl to amide attached to poly(dimethylsiloxane) (PDMS), the UCST of poly(isoprene)/PDMS decreases by 165 °C.

The aims of this chapter are to study: 1) the effect of introducing functional groups, i.e. acid and oxazoline on PMMA and SAN respectively, on the LCST behaviour of PMMA/SAN system and 2) the effect of the reaction between the acid and oxazoline groups on the phase diagram of end acid-functionalized PMMA (end-PMMA-acid)/random oxazoline-functionalized SAN (ran-SAN-oxaz). The phase diagram was investigated with cloud point measurement and the phase separation kinetics with small-angle light scattering experiments.

5.2 Experimental

5.2.1 Materials

Poly(styrene-co-acrylonitrile) (SAN), containing 28 wt% acrylonitrile (AN), was obtained from the DOW Chemical Company (M_n of 41 kg/mol and M_w of 91 kg/mol). SAN with 25 wt% and 34 wt% AN was obtained from GE Plastics. Poly(methyl methacrylate) (PMMA), was obtained from Atofina (M_n of 51 kg/mol and M_w of 103 kg/mol). PMMA end-functionalized with carboxylic acid (end-PMMA-acid) was obtained from Polymer Source, Canada (M_n of 68 kg/mol and M_w of 90 kg/mol). Oxazoline modified SAN (ran-SAN-oxaz) was prepared by reaction of SAN with 2-aminoethanol as explained in Chapter 2. Tetrahydrofuran (THF) was obtained from Merck and used as received.

5.2.2 Sample preparation

First, mixtures of two polymers (SAN/PMMA, SAN/end-PMMA-acid, ran-SAN-oxaz/PMMA, ran-SAN-oxaz/end-PMMA-acid) were dissolved in THF. The polymer concentration of the

solution was approximately 30 wt%. The solution was cast onto a thin glass slide and a doctor blade was used to control the thickness of the film. The solvent-cast samples were put into an oven for 3 days at 60 °C followed by a final drying step for 3 more days at 120 °C to ensure complete removal of the solvent. The final thickness of the samples was between 40-50 μm .

5.2.3 Cloud point measurements

Cloud point measurements were used to establish the phase boundaries for PMMA/SAN and end-PMMA-acid/SAN systems. The set-up consisted of a HeNe laser ($\lambda = 632.8 \text{ nm}$) of which the light is directed through the sample positioned on the silver block of a Linkam THMS600 hot-stage, and a light-sensitive diode that is placed under a fixed angle with respect to the incident light. The cloud point was taken as the temperature at which the scattered light intensity deviates from the baseline as the temperature was increased. Cloud point data were obtained at three heating rates i.e. 2, 5 and 10 °C/min, and for convenience, the phase transition temperature was calculated by a linear extrapolation of the three experimental cloud points to a temperature corresponding to zero heating rate.

5.2.4 Fourier-Transform Infrared Spectroscopy (FTIR)

FTIR was used to study the interaction between different groups attached to the two polymers. The sample was put on top of a glass plate and the spectra were recorded with a slide-on ATR crystal (silicon) using a BioRad UMA 500 infrared microscope coupled to a BioRad FTS6000 spectrometer. 100 scans were taken for each measurement with a spectral resolution of 4 cm^{-1} .

5.2.5 Size Exclusion Chromatography

Size exclusion chromatography (SEC) measurements were performed on a Shimadzu system with a SCL-10A system controller, a LC-10AD pump, a RID-10A refractive index detector, a SPD-10A UV detector and three PLgel 10 M Mixed-B columns in series. N,N-dimethylacetamide with 5 mmol LiCl was used as eluent at 1 mL/min and the column oven was set to 40 °C. Data acquisition and processing were performed using Shimadzu Class VP 7.3 software.

5.3 Results and Discussion

The results and discussion section is arranged as follows. First, the phase diagram of the SAN/PMMA system is presented and discussed. Next, the effect of end-functionalized carboxylic acid on the phase diagram is presented for the system of SAN/end-PMMA-acid. Subsequently, the effect of SAN randomly functionalized with oxazoline on the phase diagram of ran-SAN-oxaz/PMMA is presented. Finally, the effect of the reaction between the acid and oxazoline groups attached to PMMA and SAN respectively on the phase separation of ran-SAN-oxaz/end-PMMA-acid system is discussed.

5.3.2 Effect of acid groups on the phase behaviour of PMMA/SAN blends

Before studying the effect of the reaction between acid and oxazoline groups attached to PMMA and SAN respectively on the phase behaviour of the PMMA/SAN systems, the effect of the individual reactive groups is studied separately. First, the effect of acid end groups on the phase behaviour is studied by measuring the cloud point curve of SAN with end-PMMA-acid (Figure 5.3). The lower critical solution temperature changes from 203 °C to 250 °C, when the end group of the PMMA is modified with carboxylic acid. The increase of the LCST in case of the end-PMMA-acid/SAN blend may be due to two reasons. The first reason is the enhanced interaction between the nitrile group in SAN and the carboxylic acid group in PMMA, which was confirmed by the FTIR results, shown in Figure 5.4. The nitrile absorption band for SAN/end-PMMA-acid shifts from 2239 cm^{-1} to 2236 cm^{-1} when heated to 160 °C, whereas the peak remains constant at 2239 cm^{-1} for SAN/PMMA system even on heating. Therefore, this shift can be attributed to hydrogen bonding between the carboxylic acid group in end-PMMA-acid and the nitrile group of SAN (see Figure 5.5). Similarly to the shift of the nitrile absorption band, the band at 1725 cm^{-1} due to the carbonyl vibration also shifts to lower wavenumbers upon heating, but this shift is not as prominent. This is because the shift of the carbonyl band to lower wavenumbers due to the interaction between the carboxylic acid group in end-PMMA-acid and the nitrile group in SAN (see Figure 5.5), is counterbalanced by the shift of the carbonyl band to higher wavenumbers due to the formation of isolated carboxylic acid by dissociation of intermolecular carboxylic acid dimers at elevated temperature (Earnest and MacKnight, 1980; Lee *et al.*, 1988). The second explanation for the increase of the LCST is the lower weight-average molar mass of the end-PMMA-acid in comparison to the unmodified PMMA. From the Flory-Huggins theory, it can be estimated that the increase of the weight-average molar mass results in an increase of LCST by approx. 20 °C (for detailed calculation see Chapter 6). This implies that the additionally observed increase of approx. 30 °C can be ascribed to the enhanced interaction of the acid group in end-PMMA-acid with the nitrile group in SAN as discussed above.

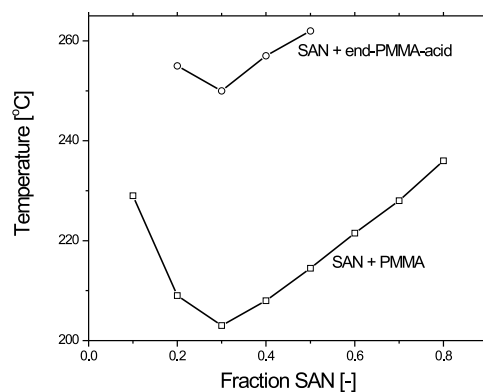


Figure 5.3: Cloud point temperatures as a function of composition of SAN in the mixture of SAN/PMMA and SAN/end-PMMA-acid.

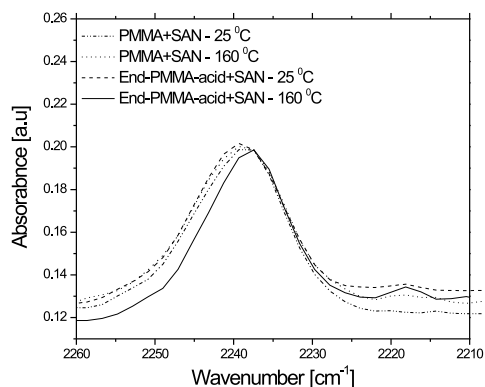


Figure 5.4: FTIR spectra of SAN/PMMA and SAN/end-PMMA-acid at room temperature and at 160 °C.

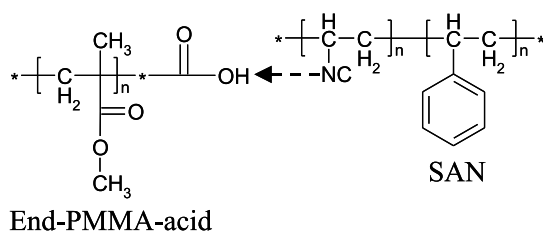


Figure 5.5: Hydrogen bonding between the nitrile and acid groups in the SAN/end-PMMA-acid blend.

5.3.3 Effect of oxazoline groups on the phase behaviour of PMMA/SAN blends

Next, the effect of the oxazoline group in ran-SAN-oxaz on the phase behaviour of PMMA/SAN was studied. In the measured temperature and composition range complete miscibility was observed and hence we may conclude that the LCST is increased above 300 °C when 3 wt% oxazoline in ran-SAN-oxaz is used in combination with PMMA. This may be due to the higher repulsion between the styrene, acrylonitrile and oxazoline units in ran-SAN-oxaz than the repulsion between styrene and acrylonitrile units in SAN copolymer.

5.3.4 Effect of reaction between acid and oxazoline group in the phase behaviour of PMMA/SAN

Next, the effect of reaction between oxazoline and acid group on the phase behaviour of PMMA/SAN was studied by using ran-SAN-oxaz with end-PMMA-acid. This miscibility increase is due to three reasons. Along with the two reasons described for the ran-SAN-oxaz/PMMA system, an additional third reason is due to the formation of graft copolymer during the reaction (Figure 5.6), which enhances the miscibility further. An additional shoulder was found at lower retention time with increase in reaction time.

Finally, the effect of the reaction between ran-SAN-oxaz and end-PMMA-acid on the phase behaviour of PMMA/SAN was studied. The reactive mixture of ran-SAN-oxaz/end-PMMA-acid was observed to be miscible up to 300 °C, which was the maximum temperature the experiment was carried out. This increase in miscibility is due to three reasons. The first two reasons are due to the higher molar volume effect and repulsion effect as explained in the previous section for the ran-SAN-oxaz/PMMA system. An additional third reason may be due to the formation of graft copolymer during the reaction, which enhances the compatibility further. The formation of graft copolymer was confirmed from SEC analysis (Figure 5.6). Compared to the original mixture of ran-SAN-oxaz/end-PMMA-acid before reaction, an additional shoulder at a retention time of 18 min was observed with increase in reaction time indicating the formation of copolymer. Unfortunately, the absorption of the ester groups from the copolymer could not be detected with FTIR because of the overlap of the ester band from PMMA.

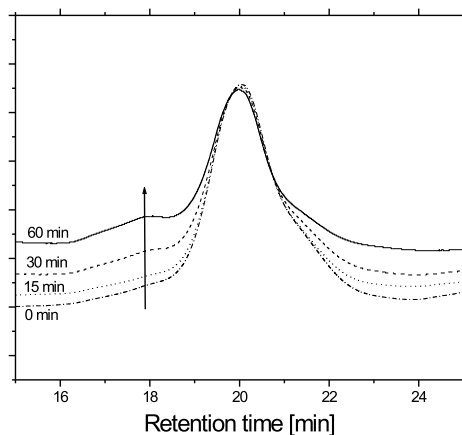


Figure 5.6: RI signal from SEC traces of ran-SAN-oxaz/end-PMMA-acid system heated for different reaction time.

5.4 Conclusions

The phase separation in PMMA/SAN system is studied with the cloud point measurement with light scattering. First the effect of acid groups was studied and enhanced miscibility was found because of the additional interaction between acid groups and nitrile groups. The miscibility is enhanced further when end-functionalized acid group is replaced by random-functionalized oxazoline group which may be due to the enhanced repulsion effect between styrene, acrylonitrile and oxazoline segments in ran-SAN-oxaz copolymer. For ran-SAN-oxaz/end-PMMA-acid, the system becomes homogeneous up to 300 °C, which is due to the formation of graft copolymers from the reaction between acid and oxazoline groups.

Chapter 6

Experimental and computational study on structure development of PMMA/SAN blends

6.1 Introduction

Polymer blending is a convenient route to develop new materials with specific properties that are superior to those of the constituent polymers (Koning *et al.*, 1998). However, most polymer pairs are immiscible and have a coarse morphology due to a high interfacial tension. The interface thickness is also small resulting in poor mechanical properties (Datta and Lohse, 1996). To reduce the interfacial tension and concomitantly to obtain finer morphologies, compatibilizers are added to polymer blends. The compatibilizers lower the interfacial tension, which influences the fibre break-up process (Koning *et al.*, 1998). Secondly, the presence of the compatibilizers at the interface reduces the tendency of the domains to coalesce. Both factors lead to stable morphologies and smaller domain sizes and hence better mechanical properties. Many compatibilized blends are used in the polymer industry (Utracki, 1998).

Apart from these fully immiscible blends, blends can be classified into two other types depending on the miscibility. The first type is called a fully miscible blend, where the polymers are miscible over a wide range of temperatures and at all compositions due to specific interactions. A well-known example is poly(styrene)/poly(phenylene oxide) (PS/PPO). The second type is called a partially miscible blend, where miscibility is only observed in a specific temperature and/or concentration window. For this type of blends, the morphology is generally controlled by the phase separation kinetics (Utracki, 1998). It is well known that the phase separation in partial miscible blends may occur via two different mechanisms: binodal decomposition, for which the system is thermodynamically metastable, and spinodal decomposition, for which the system is thermodynamically unstable.

In literature, a large number of comprehensive experimental and theoretical studies on spinodal decomposition have been reported. Many researchers (Olabisi *et al.*, 1979; Paul, 1978; Gunton *et al.*, 1983) studied experimentally the spinodal decomposition behavior of polymer blends having either a lower critical solution temperature (LCST), for which phase separation occurs by increasing the temperature, or an upper critical solution temperature (UCST),

for which phase separation occurs by decreasing the temperature. UCST-systems containing poly(butadiene) (PB)/poly(isoprene) (PI) and poly(isoprene) (PI) and poly(ethylene-co-propylene) (PEP) were studied by Hashimoto *et al.* (1991) and Cumming *et al.* (1992), respectively. Hashimoto *et al.* (1991) distinguished three stages of spinodal decomposition, i.e. early, intermediate and late stage, for PB/PI blends (Figure 6.1). The phase separation process generally starts with concentration fluctuations around the initial concentration ϕ_i after a temperature jump into the spinodal region of the binary phase diagram. In the early stage (top picture of Figure 6.1), concentration fluctuations start to develop with different correlation lengths, but only the concentration fluctuations with a certain dominant correlation length, Λ_m , continue to increase, while the concentration fluctuations with other correlation lengths damp out. In the intermediate stage, the concentration fluctuations with the dominant correlation length continue to grow, while also the correlation length increases: the structure coarsens. In the late stage, the correlation length still changes, but the concentration fluctuations have reached the equilibrium concentrations ϕ' and ϕ'' .

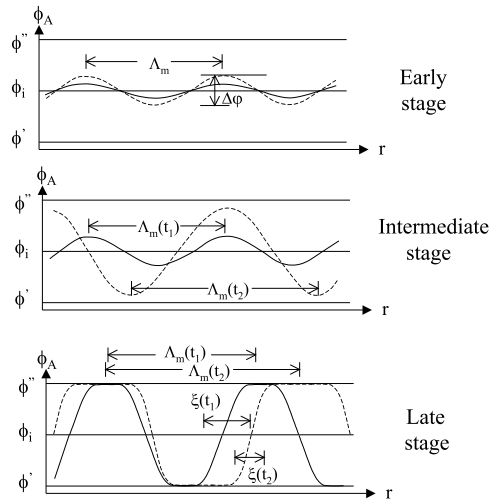


Figure 6.1: The different stages of the spinodal decomposition process, characterized by the concentration difference $\Delta\phi = \phi'' - \phi'$, dominant correlation length Λ_m and interface thickness ξ .

Similar studies were reported on the spinodal decomposition of poly(carbonate) (PC)/poly(styrene-co-acrylonitrile)(SAN), poly(vinyl methyl ether) (PVME)/PS and poly(methyl methacrylate) (PMMA)/SAN, having a LCST behavior. From all these blends, the combination of PMMA and SAN is most suitable for experimentation. The refractive index difference between PMMA and SAN is large enough to yield enough contrast for small-angle light scattering measurements, the primary technique to study phase separation kinetics and both polymers have similar glass transition temperatures, meaning that differences in mobility factors cancel out. Furthermore, by varying the acrylonitrile(AN) content of the SAN-copolymer, the miscibility of SAN with PMMA can be systematically adjusted (Suess *et al.*, 1987; Cowie and Lath, 1988).

Apart from the experimental investigations cited above, several computational methods have

also been applied to study the spinodal decomposition process. Microscopic numerical approaches, such as Monte Carlo simulations (Petschek and Metiu, 1983; Meakin and Deutch, 1983) and molecular dynamics (Mruzik *et al.*, 1978), have been used to study the spinodal decomposition in polymer blends, but also mesoscopic approaches, such as the density particle dynamic approach (Vliet *et al.*, 2000), have been adopted. Similar results have also been reported with macroscopic models using the Cahn-Hilliard model (Tran *et al.*, 2005). In our study, we use macroscopic diffuse-interface modeling based on the Cahn-Hilliard theory, in which the thermodynamics and hydrodynamics are coupled through the momentum equation. The advantage of this approach is that the thermodynamic and hydrodynamic parameters for the model can be derived from experiments.

The objective of this work is to study different stages of phase separation as well as the effect of hydrodynamics on the phase separation kinetics for the PMMA/SAN system by combining both experiments and computations. The input parameters for the description of the thermodynamics are obtained from experimental cloud point data, while the input parameters for the hydrodynamics description are obtained from the analysis with the linearized Cahn-Hilliard-Cook model (Cook, 1970) of the initial stage of the experimental phase separation results. The computational results are then compared with experimental observed phase separation kinetics.

6.2 Model equations

The classical expression for the specific Helmholtz free energy used in diffuse-interface modeling is based on the work of Cahn and Hilliard (1958):

$$f(c, \nabla c) = f_0(c) + \frac{1}{2}\kappa |\nabla c|^2 = -\frac{1}{2}\alpha c^2 + \frac{1}{4}\beta c^4 + \frac{1}{2}\kappa |\nabla c|^2, \quad (6.1)$$

where α and β are positive constants and κ is the gradient energy parameter that is proportional to the interaction parameter χ and c is the mass fraction of one of the two components. The chemical potential can be obtained from the variational derivative with respect to the concentration of the specific Helmholtz free energy given by Eq. (6.1) and reads as:

$$\mu = \frac{\delta f}{\delta c} = -\alpha c + \beta c^3 - \kappa \nabla^2 c. \quad (6.2)$$

This generalized chemical potential allows for the description of the interface between the two fluids by a continuously varying concentration profile. For example, for a planar interface, with x being the direction normal to the interface, the analytical solution of equation (6.2) can be written as :

$$c(x) = \sqrt{\frac{\alpha}{\beta}} \tanh \frac{x}{\sqrt{2\xi}}, \quad (6.3)$$

with $\pm\sqrt{\alpha/\beta}$ being the equilibrium bulk solutions (in the approach outlined here ± 1) and ξ ($= \sqrt{\kappa/\alpha}$) defines interfacial thickness. To comply with mass conservation for both components, the following balance equation should be fulfilled:

$$\rho \left(\frac{\partial c}{\partial t} + \mathbf{v} \cdot \nabla c \right) = \nabla \cdot M \nabla \mu, \quad (6.4)$$

where M is the mobility, which is known to be dependent on the volume fraction of component (Pincus, 1981; De Gennes, 1980), but here for simplicity considered as a constant. The diffusion flux is assumed to be proportional to the gradient of the chemical potential, which is more general than the commonly used Fickian diffusion, based on the concentration gradients, that does not hold for multi-phase systems, even at equilibrium. The more general expression used in Eq. (6.4) reflects Gibbs' findings that the chemical potential becomes uniform in non-ideal mixtures at equilibrium, and is known as the Cahn-Hilliard equation (Cahn and Hilliard, 1959). This equation was first used by Cahn (1964) to describe the initial stages of spinodal decomposition.

To obtain conservation of momentum, a generalized Navier-Stokes equation can be derived for the velocity field (Lowengrub and Truskinovsky, 1998; Verschueren, 1999):

$$\rho \left[\frac{\partial \mathbf{v}}{\partial t} + (\mathbf{v} \cdot \nabla) \mathbf{v} \right] = -\rho \nabla g + \nabla \cdot \eta \left(\nabla \mathbf{v} + \nabla \mathbf{v}^T \right) + \rho \mu \nabla c, \quad (6.5)$$

where g is the modified pressure $g = f + p/\rho$, with p the local pressure, ρ the density and \mathbf{v} the velocity. The viscosity η and density ρ generally depend on c . Here, we consider the iso-viscous and density-matched case (where for simplicity η and ρ will be set equal to one hereafter) which gives for the equation of continuity:

$$\nabla \cdot \mathbf{v} = 0. \quad (6.6)$$

6.2.1 Non-dimensionalization of the equations

To study the effect of hydrodynamics on the phase separation kinetics, we have used the dimensionless equations for component balance, momentum balance and chemical potential. The dimensionless variables used for non-dimensionalization read:

$$c^* = \frac{c}{c_B}; \quad \nabla^* = L \nabla; \quad \mu^* = \frac{\mu \xi^2}{\epsilon c_B};$$

$$\mathbf{v}^* = \frac{\mathbf{v}}{V}; \quad t^* = \frac{tV}{L}; \quad g^* = \frac{gL}{\rho \eta V}.$$

The characteristic velocity V is the diffusion velocity (in the absence of external flow) and the characteristic length scale is the average domain size. The system of equations (Eq. (6.2), (6.4- 6.6)) reads, (after dropping the asterix notation and in absence of inertia):

$$\frac{\partial c}{\partial t} + \mathbf{v} \cdot \nabla c = \frac{1}{\text{Pe}} \nabla^2 \mu, \quad (6.7)$$

$$\mu = c^3 - c - \text{C}^2 \nabla^2 c, \quad (6.8)$$

$$\mathbf{0} = -\nabla g + \nabla \cdot [(\nabla \mathbf{v}) + (\nabla \mathbf{v})^T] + \frac{1}{\text{CaC}} (\mu \nabla c), \quad (6.9)$$

$$\nabla \cdot \mathbf{v} = 0. \quad (6.10)$$

The dimensionless groups that appear are: the Péclet number Pe , the capillary number Ca and the Cahn number C which are defined as:

$$Pe = \frac{\xi^2 LV}{M\kappa}; \quad Ca = \frac{\xi\eta V}{\rho\kappa c_B^2}; \quad C = \frac{\xi}{L}.$$

Pe is the ratio of convection to the diffusion, Ca is the ratio of the viscous forces to the interfacial tension ($\eta V/\Gamma$) (Davis and Scriven, 1982) and C is the ratio of interface thickness to the domain size. This system of partial differential equations is solved with bi-periodic boundary conditions for c , μ and \mathbf{v} .

6.3 Numerical methods

For the concentration problem, the two second-order differential Eq. (6.7) and (6.8) are solved in a coupled way. For the temporal discretization of Eq. (6.7) a first-order Euler implicit scheme was employed. The non-linear term in Eq. (6.8) was linearized by a standard Picard method. A second-order finite element method is used for spatial discretization of the set of equations.

The fully discretized set of linearized equations for c and μ , written in matrix form, reads:

$$\begin{bmatrix} \mathbf{M} + \Delta t \mathbf{N}^{n-1} & \frac{\Delta t}{Pe} \mathbf{S} \\ [1 - (c_{i-1}^n)^2] \mathbf{M} - C^2 \mathbf{S} & \mathbf{M} \end{bmatrix} \begin{bmatrix} c_i^n \\ \mu_i^n \end{bmatrix} = \begin{bmatrix} \mathbf{M} c_0^{n-1} \\ \mathbf{0} \end{bmatrix}, \quad (6.11)$$

where c_i^n is the discretized concentration at the i^{th} Picard-iteration at time step n , μ_i^n is the discretized chemical potential at the i^{th} Picard-iteration at time step n , c_0^{n-1} is the discretized concentration at time step $n - 1$, \mathbf{M} is the mass matrix, \mathbf{N} is the convection matrix, and \mathbf{S} is the diffusion matrix. This set is solved using an iterative solver. Details about the iteration scheme can be found in Keestra *et al.* (2003) and Khatavkar *et al.* (2006).

The flow problem is solved using the velocity-pressure formulation and discretized by a standard Galerkin finite element method. The effect of the interface, i.e. $\mu \nabla c$, is included as a known volume source term. Taylor-Hood quadrilateral elements with continuous pressure that employ a biquadratic approximation for the velocity and a bilinear approximation for the pressure are used. The resulting discretized set of linear algebraic equations is solved using a direct method based on a sparse multifrontal variant of Gaussian elimination (HSL/MA41) (Amestoy and Duff, 1989a,b; Amestoy and Puglisi, 2002).

6.4 Experimental

6.4.1 Materials

Poly(methyl methacrylate) (PMMA), obtained from Atofina, and poly(styrene-*co*-acrylonitrile) (SAN), obtained from the DOW Chemical Company, were used as received. SAN is a random copolymer containing 28 wt% acrylonitrile and an weight-average molar mass (M_w)

of $113 \text{ kg} \cdot \text{mol}^{-1}$ ($M_w/M_n = 2.6$), measured with size exclusion chromatography (SEC) based on polystyrene standards. PMMA has a M_w of $103 \text{ kg} \cdot \text{mol}^{-1}$ ($M_w/M_n = 2.0$). Tetrahydrofuran (THF) was obtained from Merck and used as received.

6.4.2 Sample preparation

First, SAN and PMMA were dissolved in THF. The polymer concentration in the solution was approximately 30 wt%. The solution was cast onto a thin glass slide and a doctor blade was used to control the thickness of the film. The solvent-cast samples were put into an oven at $60 \text{ }^\circ\text{C}$ for 3 days followed by a drying step at $120 \text{ }^\circ\text{C}$ for 3 more days to ensure complete solvent removal. The final thickness of the samples was between $40\text{-}50 \text{ }\mu\text{m}$.

6.4.3 Cloud point measurements

Light scattering was used to determine the cloud point curve of the PMMA/SAN system. The set-up consisted of a HeNe laser ($\lambda = 632.8 \text{ nm}$) of which the light is directed through the sample positioned on the silver block of a Linkam THMS600 hot-stage, and a light-sensitive diode that is placed under a fixed angle with respect to the incident light. The output signal of the diode, which is coupled to an xt -recorder, registered the scattered light.

6.4.4 Small-Angle Light Scattering (SALS)

Small-Angle Light Scattering (SALS) was used to follow the kinetics of phase separation. A 1 mW HeNe laser was used as incident light source and the light was guided through a pinhole collimator and the sample, of which the temperature was controlled by a Linkam THMS600 hotstage. The scattered light was projected on a semi-transparent polypropylene screen. The scattering patterns were captured with a 16 bit 2D-CCD camera (Versarray:512B Princeton CCD with a ST-133 controller), equipped with a Rodenstock Rodagon 50 mm f 1:2.8 lens with a variable focal distance. The CCD-camera was linked to a personal computer for data acquisition and analysis. The scattering patterns were radially averaged using the Fit2D-program developed by dr. Andy Hammersley from the European Synchrotron Radiation Facility (ERSF), Grenoble, France.

6.5 Results and discussion

The results and discussion section is arranged as follows. First, all experimental results are shown starting with the phase diagram of PMMA/SAN. The different stages of spinodal decomposition are then evaluated from the SALS-measurements. The effect of hydrodynamics on the phase separation is then illustrated with the numerical calculations. Finally, a quantitative comparison between the experimental and the numerical results is presented.

6.5.1 Phase diagram

The experimental phase diagram was measured to obtain the thermodynamics parameters for the diffuse-interface model. The PMMA/SAN28 composition ratios varied between 80/20 and 10/90. The cloud points were measured in duplo by using three heating rates (10, 5 and $2 \text{ }^\circ\text{C}/\text{min}$) and a linear extrapolation to a heating rate of zero. The extrapolated values are

plotted in Figure 6.2 (open circles) as a function of composition. The phase diagram shows a LCST behavior with a critical condition at 203 °C and 70 wt% PMMA.

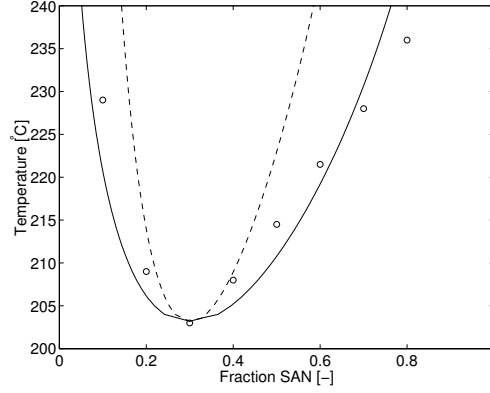


Figure 6.2: Cloud point temperature as a function of compositions: Extrapolated cloud point (o)temperature, calculated spinodal (- - -) and binodal (—) curves as a function of SAN fraction in PMMA/SAN mixture.

The temperature and concentration dependence of the χ -parameter can be obtained by fitting the experimental cloud point data with the binodal equation obtained from the Flory-Huggins free energy equation neglecting the polydispersity of the polymer. The fitted equation for χ -parameter (taking $N_1 = 990$ for PMMA and $N_2 = 1068$ for SAN) can be written as:

$$\begin{aligned} \chi(T, c) &= \chi_0 + \frac{\chi_1}{T} + \chi_2 T + \chi_3 c \\ &= -0.009758 - 0.000025T - 0.0013904c . \end{aligned} \quad (6.12)$$

The resulting binodal (solid line) and spinodal (dotted line) curves of the phase diagram using the calculated χ -parameter are shown in Figure 6.2.

6.5.2 Different stages of phase separation

Knowing the phase behavior and the critical temperature and composition for the PMMA/SAN28 system, the different stages of the spinodal decomposition were studied by several temperature jump experiments at the critical composition (70 wt% PMMA). The scattering patterns obtained at 235 °C collected after different time intervals are shown in Figure 6.3. The first two images show only the scattered light of the incident beam. The third image of the first row shows a diffuse scattering ring at higher scattering angle, indicating that the phase separation process has started and that periodic structures develop, characteristic for the spinodal decomposition process. The intensity of the ring progressively increases, implying that the refractive index differences increase, i.e. the concentration fluctuations strengthen. After the fifth pattern, also the scattering angle of the ring decreases as a function of time, indicating that the structure size is growing.

The 2D-scattering images were radially integrated to obtain a better signal-to-noise ratio and subsequently presented as 3-D plots of the scattered intensity as a function of the scattering

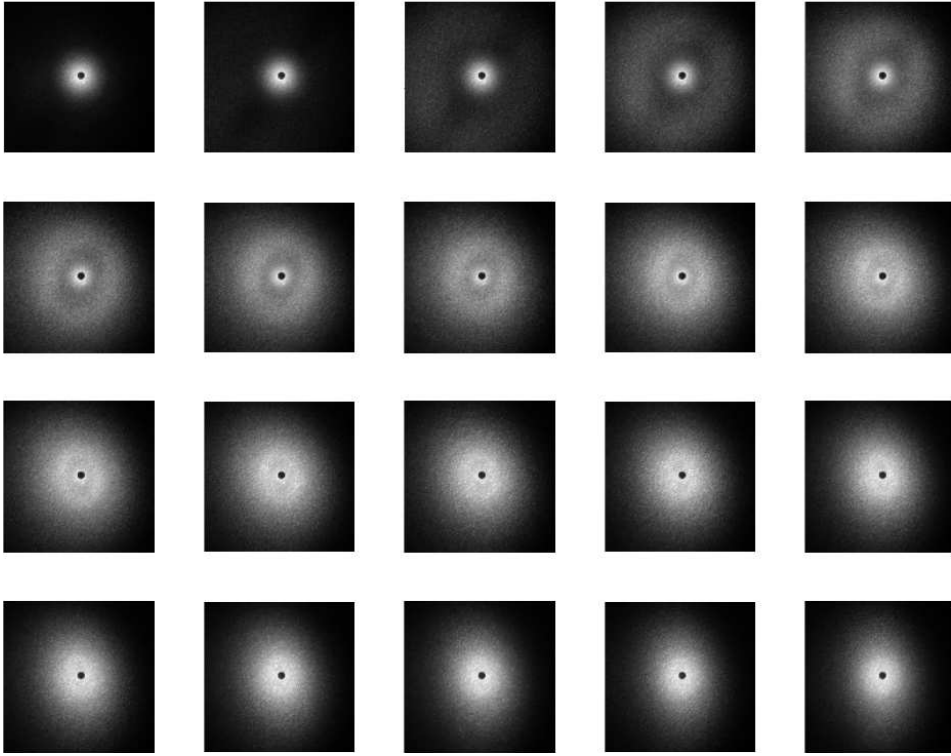


Figure 6.3: Time evolution of the 2D-scattering patterns of a 70/30 mixture PMMA/SAN collected at 235 °C.

vector q (defined as: $q = \frac{4\pi}{\lambda} \sin\theta$, where 2θ is the scattering angle and λ is the wavelength of the incident beam = 632.8 nm) and time in Figure 6.4. It is evident that the growth of structure as a result of the phase separation is strongly nonlinear. It is also found that the initial peak develops at $q = 3.5 \mu\text{m}^{-1}$ corresponding to an average structure size of $\bar{d} (= \frac{2\pi}{q}) = 1.8 \mu\text{m}$. Then, the structure coarsens to a size of $12 \mu\text{m}$ in approximately 30 min.

When the scattered intensity I is plotted against q for both the initial time interval and the late time (shown in Figure 6.5), a clear difference can be observed. In the early stage (Figure 6.5a), it is found that the peak at q_{max} is only growing in intensity but the peak position remains constant. However, in the subsequent intermediate and late stage (Figure 6.5b), not only the intensity increases but also the peak position of the maximum starts to shift to lower q -values, indicating that the structure grows. The analysis of the initial stage of the phase separation is done separately from the intermediate and late stage phase separation to obtain different parameters, which will be used later for the numerical simulation and also to compare the experimental results with the numerical results.

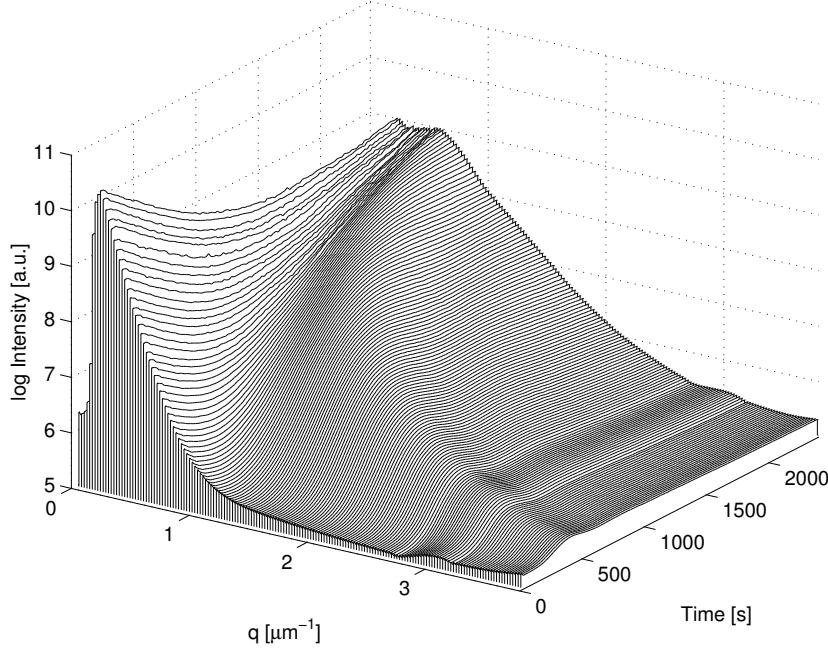


Figure 6.4: 3-D plot of the scattered intensity of a 70/30 PMMA/SAN mixture at 235 °C as a function of scattering vector q and time.

6.5.3 Analysis of early stage of phase separation

The results of the early stage of the phase separation are analyzed with the linearized Cahn-Hilliard-Cook (CHC)-model to obtain respectively the interface thickness ξ , diffusion coefficient D_{app} and the gradient energy parameter κ . The CHC-model equation (Cook, 1970) reads as:

$$I(q, t) = I(q, 0) \exp(2R(q)t), \quad (6.13)$$

where $I(q, 0)$ is the scattered intensity as a function of q at time $t = 0$ and $R(q)$ is the relaxation rate. The values of apparent diffusivity and gradient energy parameter can be obtained from the relaxation rate with the following relation:

$$R(q) = -q^2 \left(D_{\text{app}} + 2M\kappa q^2 \right). \quad (6.14)$$

The relaxation rate is plotted versus q^2 in Figure 6.6. From the intercept and slope of the curve, the apparent diffusivity D_{app} and $2M\kappa$ values are obtained for 235 °C. Similarly, the values for different temperatures could be obtained and these are summarized in Table 6.1. The apparent diffusivity values are in the order of $10^{-4} - 10^{-5} \mu\text{m}^2/\text{s}$. Similar values were also reported by Kim *et al.* (1994) for the PMMA/SAN23 system using forward recoil spectrometry.

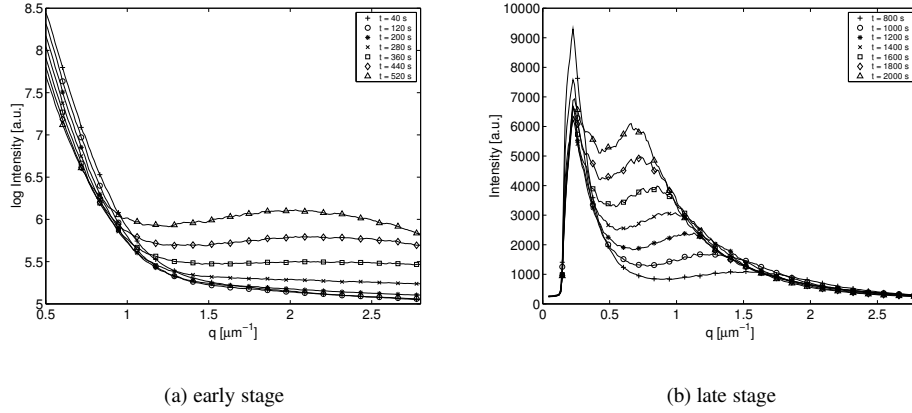


Figure 6.5: 1-D scattering curves as a function of q in the (a) early and (b) late stage of the phase separation for the 70/30 mixture of PMMA/SAN at 235 °C.

Table 6.1: Results of the Cahn-Hilliard-Cook fit (slope and intercept) at different temperatures.

Temperature [°C]	D_{app} [$\mu\text{m}^2/\text{s}$]	$2M\kappa$ [$\mu\text{m}^4/\text{s}$]
215	1.09×10^{-5}	2.38×10^{-7}
220	4.30×10^{-5}	1.11×10^{-6}
225	6.42×10^{-5}	1.53×10^{-6}
230	1.28×10^{-4}	4.30×10^{-6}
235	1.92×10^{-4}	4.08×10^{-6}
240	3.80×10^{-4}	9.54×10^{-6}

The experiments were performed at different temperatures to investigate the temperature dependence of the diffusivity. The experimental data at different temperatures were fitted with the Williams-Landell-Ferry (WLF)-equation (Zheng *et al.*, 2001) and the results are shown in Figure 6.7. From the slope and intercept of the linear curve of the insert in Figure 6.7, the constants of the WLF-equation can be obtained. Using these constants, the final temperature dependence of the diffusivity can be written as:

$$\log [D_{app}(403)/D_{app}(T)] = \frac{-2.52(T - 503)}{53.85 + (T - 503)}, \quad (6.15)$$

where 230 °C is used as the reference temperature.

The interface thickness at the early stage of the phase separation for different temperatures can be obtained from the D_{app} and $2M\kappa$ values (shown in Table 6.1) according to the follow-

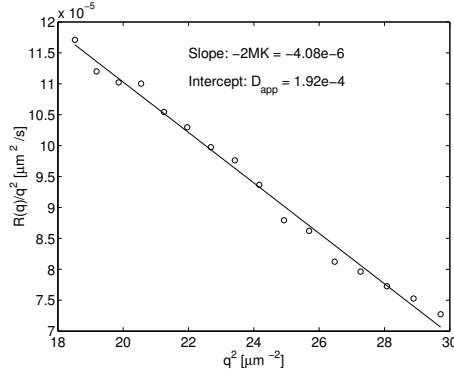


Figure 6.6: The results from the Cahn-Hilliard-Cook-analysis ($R(q)/q^2$) for the initial stage of the phase separation at 235 °C.

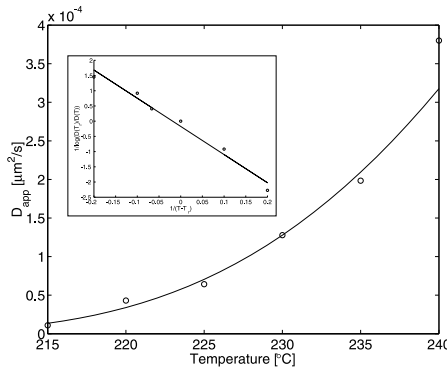


Figure 6.7: The apparent diffusivity as a function of temperature. The insert shows the WLF-plot. The dots represent the measured values, while the solid line is the results of the WLF-fit.

ing equation (Keestra, 2004):

$$\xi = \sqrt{\frac{2M\kappa}{D_{app}}} \tag{6.16}$$

The calculated interface thickness for different temperatures is shown in Figure 6.8 and is found to be approximately 0.15 μm for the temperature range investigated (215 °C - 240 °C).

6.5.4 Analysis of intermediate and late stage of phase separation

The intermediate and late stage results from Figure 6.5b were analyzed with a power-law scaling equation to obtain the scaling coefficients at different temperatures to investigate whether

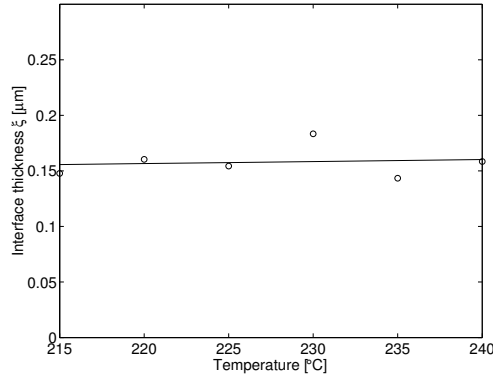


Figure 6.8: Interface thickness versus temperature calculated with the Cahn-Hilliard-Cook analysis.

hydrodynamics play a role in the phase separation kinetics. The results of the late stage are also analyzed with the Porod's law to obtain the interface thickness.

For the intermediate and late stage of the phase separation, the position of the scattering ring, $q_{\max}(t)$, and the corresponding intensity at that q -value, $I_{\max}(t)$, as a function of time can be captured with a power-law:

$$q_{\max}(t) \propto t^{-\alpha}, \quad (6.17)$$

where α is a scaling coefficient varying from $\alpha = 0.33$ (diffusion controlled) to $\alpha = 1.0$ (hydrodynamics controlled), and

$$I_{\max}(t) \propto t^{\beta}. \quad (6.18)$$

where β is again a power-law scaling coefficient. Siggia (1979) showed that in the intermediate and late stage for most phase separating polymer-polymer binary blends a hyper-scaling relation $\alpha = 3\beta$ exists. For our system, the results for the intermediate and late stage phase separation at 235 °C are analyzed from Figure 6.5b and the corresponding $I_{\max}(t)$ and $q_{\max}(t)$ as a function of time are shown in Figure 6.9. The scaling coefficient α varies from 0.55 to 0.86 going from the intermediate stage to the late stage. This shows that at the intermediate stage the system is more dominated by diffusion, whereas at the late stage the system is more dominated by hydrodynamics. The other coefficient β varies from 1.69 to 2.62 going from the intermediate to the late stage. From the above analysis, the hyper-scaling relation $\beta = 3\alpha$ is found in our system, which is consistent with the results obtained by Siggia (1979).

To study the effect of hydrodynamics as a function of temperature, the blends were phase separated at other temperatures and the results for q_{\max} are shown in Figure 6.10. First, at different temperatures, some variation in the slope of the curves is found, but no relation exists in the sense that with increasing temperature the extent of hydrodynamic interactions increases. Second, within a certain degree of accuracy, the curves appear to be evenly shifted with respect to time as a function of temperature. We can conclude that the temperature dependence of the structure development is very important. After approximately two hours at 215 °C, a morphology has developed with a maximum at $q = 2 \mu\text{m}^{-1}$, corresponding to an average periodicity of $d = 3.1 \mu\text{m}$. A similar average structure size is obtained after

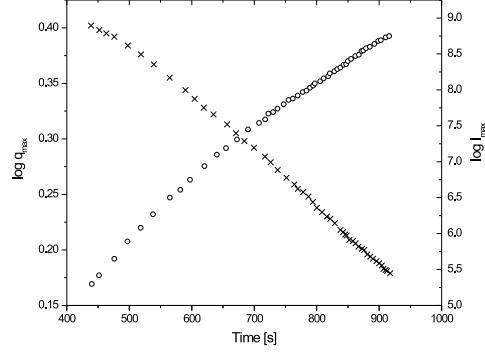


Figure 6.9: $q_{\max}(x)$ and $I_{\max}(o)$ at 235 °C as a function of time.

approximately ten minutes at 240 °C. A similar time-temperature behavior was observed by Zheng *et al.* (2001) for PMMA/SAN32. From Figure 6.10, it can be concluded that the temperature is the most important parameter in this phase separation process.

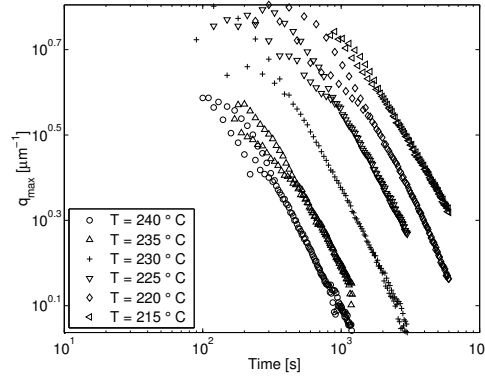


Figure 6.10: The maximum q -values as a function of time for a range of temperatures.

To check the validity of the diffuse-interface model used in the numerical calculations, the interface thickness for the late stage is calculated using Porod's law. For sharp interfaces, the scattering relation in the limit of high scattering vectors takes the form (Porod, 1951):

$$\lim_{q \rightarrow \infty} I(q) = K_p/q^4, \quad (6.19)$$

where K_p is the Porod constant. However, for real polymer systems the product $I(q)q^4$ does not reach a constant value. In the limit $q \rightarrow \infty$, the modified Porod's model for diffuse interfaces as proposed by Koberstein and Stein (1983) for a pinhole collimator can be used:

$$\lim_{q \rightarrow \infty} I(q) = e^{-4\pi^2\xi^2q^2} K_p/q^4, \quad (6.20)$$

where ξ is the diffuse-interface thickness. The interface thickness calculated with Eq. (6.20) is shown in Figure 6.11 as a function of time. It is found that the interface thickness is constant at the late stage of phase separation and is approximately $0.03 \mu\text{m}$.

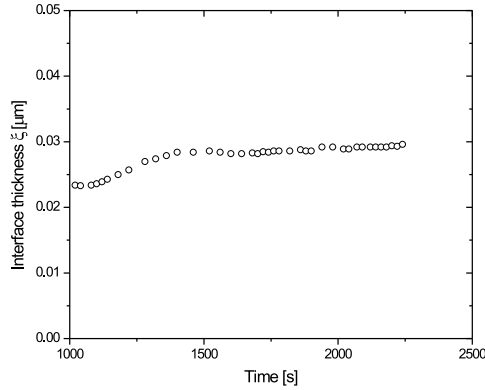


Figure 6.11: Interface thickness as a function of time with the modified Porod's analysis.

6.6 Numerical results

In this section, the effect of hydrodynamics on the phase separation kinetics is studied with varying capillary number. In the next section, a quantitative comparison of numerical phase separation kinetics with experimental phase separation kinetics is presented.

6.6.1 System definition

The numerical analysis of the phase separation was studied on a rectangular domain with dimensions of $(-1, -1)$ in the left bottom corner to $(1, 1)$ in the top right corner. In each simulation a 60×60 mesh was used with second-order elements. The time step used for simulation was $\Delta t = 0.01$. The thermal fluctuations were imposed ($c_i = \mathcal{O}(10^{-5})$) by introducing a random noise on the concentration level, which was five orders lower than the equilibrium concentration ($c_{eq} = \mathcal{O}(1)$). A bi-periodic boundary condition was applied for c , μ and v .

6.6.2 Effect of hydrodynamics

To study the effect of hydrodynamics on the phase separation kinetics, two different capillary numbers were chosen. First, phase separation for a system with high viscous forces and low interfacial forces, i.e. high capillary number ($\text{Ca} = 10$), was studied and the results of the simulation are shown in Figure 6.12. The concentration fluctuation is first observed at the dimensionless time $t = 0.75$ and it increases up to $t = 1.65$. On the other hand, the average structure size remain constant from $t = 0.75$ to $t = 1.05$ and increases afterwards up to $t = 3.00$. From the above observations, it is found that the phase separation has started at $t = 0.75$ and the initial stage of phase separation is observed up to $t = 1.05$. Then the

intermediate and late stage of phase separation is observed with a slow increase in the average structure size.

The results of a simulation for a system with lower viscous force and higher interfacial force, i.e. low capillary number ($Ca = 0.5$), is shown in Figure 6.13. In this case, the concentration fluctuation starts at the same dimensionless time $t = 0.75$, whereas the average size increases faster compared to the case for the higher capillary number.

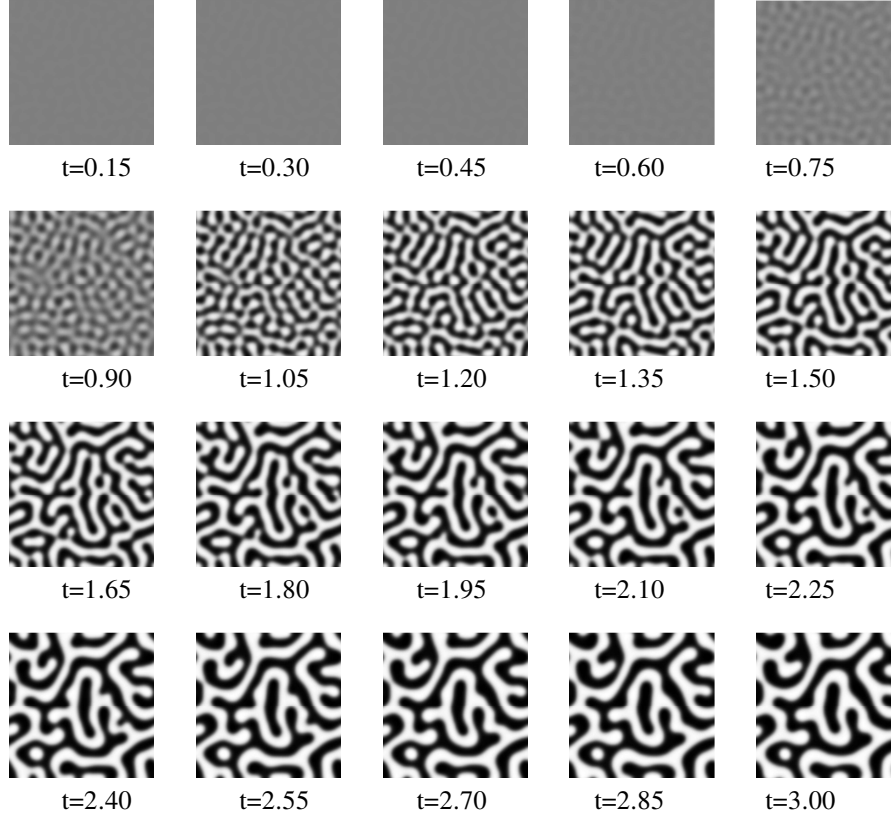


Figure 6.12: Simulation of the phase separation process with $Ca = 10$, $Pe = 50$ and $C = 0.02$.

The kinetics of the phase separation can be described with a power-law relation, similar to the SALS-results:

$$\bar{d} \sim t^n, \quad (6.21)$$

where t is the dimensionless time, n is the power-law coefficient and \bar{d} is the average domain size. The average domain size can be calculated using a correlation function defined as:

$$G(\mathbf{r}, t) = \frac{1}{N^d} \sum (c(\mathbf{x} + \mathbf{r}, t) - c_{av}) \cdot (c(\mathbf{x}, t) - c_{av}), \quad (6.22)$$

where \mathbf{r} and \mathbf{x} are the lattice vectors, N is the number of grid points, c_{av} the average concentration and d the dimensionality, $d = 2$. Radial averaging is carried out using a Brillouin

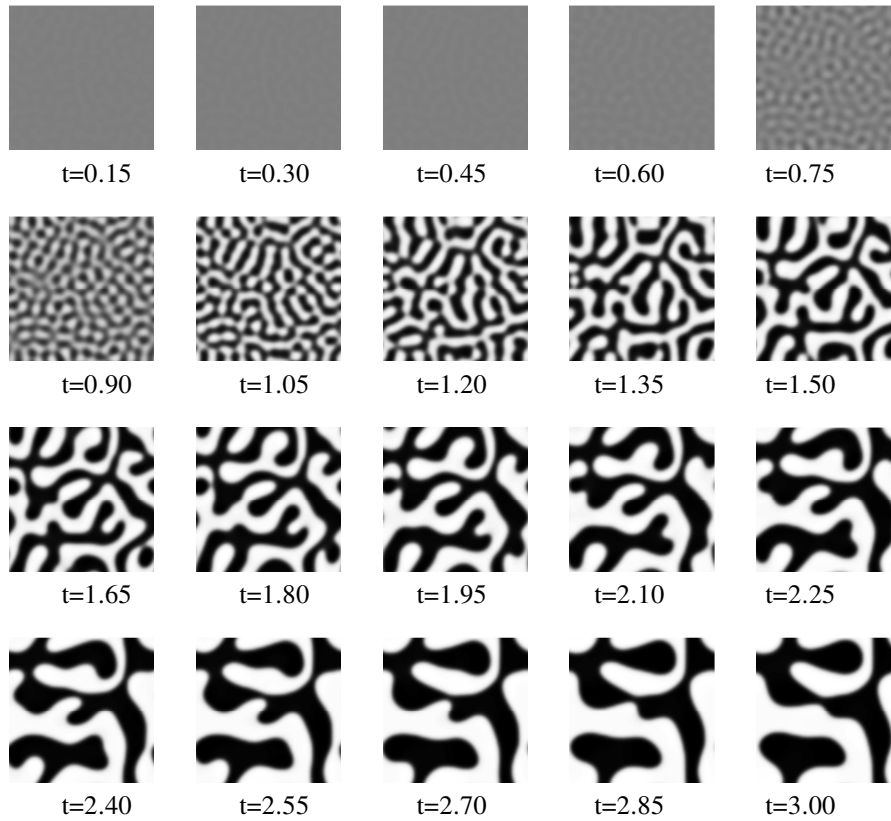


Figure 6.13: Simulation of the phase separation process with $Ca = 0.5$, $Pe = 50$ and $C = 0.02$.

zone function to eliminate any directional effects (Keestra, 2004):

$$g(r, t) = \frac{1}{N_r} \sum_{r-\Delta(r/2) \leq |x| < r+\Delta(r/2)} g(r, t). \quad (6.23)$$

The results are shown in Figure 6.14a. It can be seen that with increasing time the first local maximum, which is representative for the average structure size, shifts to higher values (ranging from 0.25 to 0.45), indicating that the periodicity is increasing. In the remainder of the discussion however, the first intersection of the correlation function with the x -axis is used as a measure for the growth of the structure. The resulting data are plotted in Figure 6.14b as a function of time. It is found that for the higher capillary number, the power-law coefficient n is equal to 0.38, in line with literature observations, for which a theoretical coefficient of $\frac{1}{3}$ is found. For the small capillary number, the coefficient is 0.69, close to the theoretical value $\frac{2}{3}$ for a two-dimensional system. A linear relation ($n = 1$) is expected for 3D-simulations with low capillary numbers (Vasishtha and Nauman, 1994).

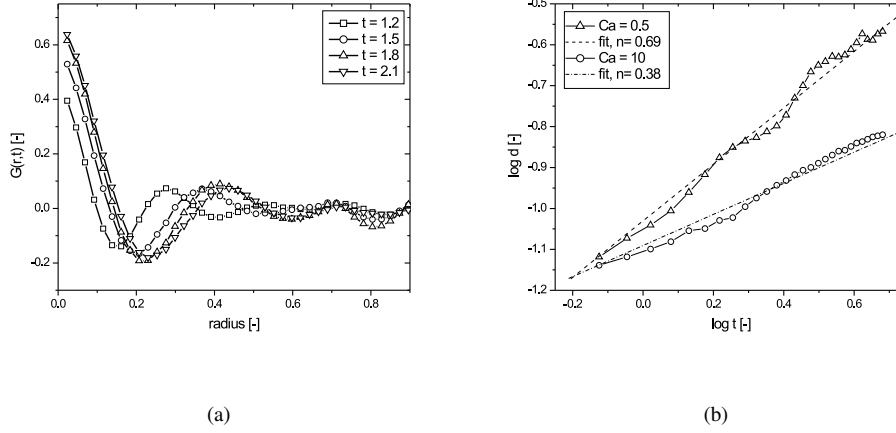


Figure 6.14: Results of the simulations with different capillary numbers: (a): correlation function at different time steps, (b): structure size as a function of time for $Ca = 0.5$ (o) and $Ca = 10$ (*) and the power-law fit.

6.7 Quantitative comparison between numerical and experimental results

The quantitative comparison between the experimental SALS-results and the results from the numerical analysis is done for a temperature of 230 °C. All parameters used for the simulations are calculated for 230 °C. The average density of PMMA/SAN (70/30) blend is taken as $\rho_{av} = 1.13 \text{ g/cm}^3$, based on the density of the individual components $\rho_{\text{PMMA}} = 1.18 \text{ g/cm}^3$ and $\rho_{\text{SAN}} = 1.08 \text{ g/cm}^3$ (Braun and Saechtling, 1982). The interaction parameter χ at the specific temperature and concentration is calculated with equation (6.12) giving a value of 0.0024. Correspondingly, the value of α is 9.172×10^{-4} . The values of ξ and D_{app} are taken from the calculated data from the linearized Cahn-Hilliard-Cook analysis. All the experimental parameters used to calculate the simulation parameters are summarized in Table 6.2.

Table 6.2: Parameters used in the simulation of the phase separation of a PMMA/SAN 70/30 mixture at $T = 230 \text{ °C}$.

parameter	value	dimension
ξ	0.158	μm
η	2.12×10^3	$\text{Pa}\cdot\text{s}$
D_{app}	1.27×10^{-16}	m^2/s
ρ	1.13×10^3	kg/m^3
κ	1.05×10^{-15}	Jm^2/kg

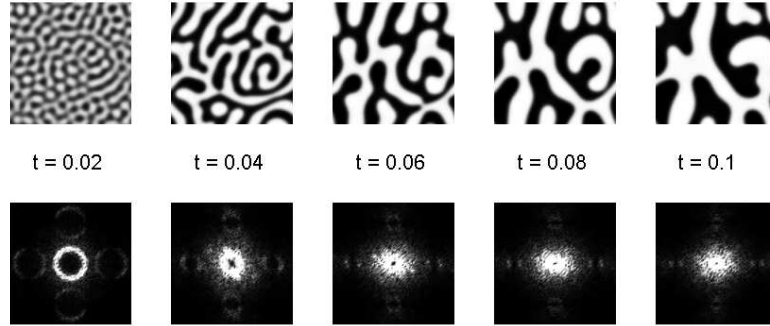


Figure 6.15: Simulated morphologies and the corresponding 2D-FFTs. The secondary reflections are the result of the limited periodic domain.

Since the simulations are compared with experiments under quiescent conditions, i.e. in the absence of external flow, the dimensionalization of the equations in section 6.2.1 is slightly changed. The convective term of the composition equation can be scaled with the apparent diffusivity $V = D_{\text{app}}/L$. Consequently, the Péclet number is now scaled to unity. The other non-dimensionalized parameters used in the simulation can then be defined as:

$$\text{Ca} = \frac{\xi \eta D_{\text{app}}}{\rho c_B^2 \kappa L} \quad t^* = \frac{t D_{\text{app}}}{L^2} .$$

Using the hydrodynamic and thermodynamic data from Table 6.2, the capillary number is calculated to be 0.029. The results of simulations with $\text{Ca} = 0.029$, $\text{Pe} = 1.0$ and $C = 0.02$ are shown as a function of time in the top row of Figure 6.15. The corresponding Fourier transforms are shown in the bottom row. It is observed that the structure is growing on a dimensionless time scale up to $t^* = 0.1$, corresponding to a time of $t = t^* L^2 / D_{\text{app}} = 0.1 * 6 \times 10^{-11} / 1.27 \times 10^{-16} = 4.7 \times 10^4$ seconds.

The q -values of the scattering rings can be calculated from the two-dimensional-FFT images and are plotted as a function of time in Figure 6.16 along with the experimental SALS-data obtained at 230 °C. The predicted q_{max} -values are substantially different from the experimentally measured values. First of all, it is found that the scaling coefficient (slope) obtained from the numerical simulations is larger than the coefficient obtained from the experiments. This might be due to the fact that the capillary number used in the simulation is lower than the experimental (true) capillary number, which depends on both interfacial thickness and diffusion coefficient. Further, the onset of phase separation as predicted with the numerical calculations is slower than the onset observed with the experiments by a factor of thirty. A possible explanation for the mismatch can be found in the initially imposed concentration fluctuations. The initial homogeneous concentration used for the simulation described in Figure 6.16 is perturbed with a random noise scaled with 10^{-5} (Kestra *et al.*, 2003). However, we found that the onset of phase separation can be decreased by a factor of four, when we changed the random noise level from 10^{-5} to 10^{-4} .

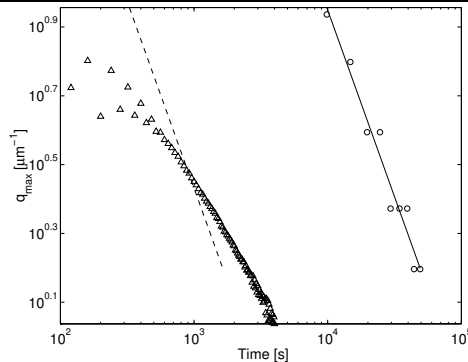


Figure 6.16: Maximum scattering vector as a function of time for the PMMA/SAN mixture at 230 °C (Δ) and predicted values (\circ). The solid line (—) represents the linear fit through the predicted values and the broken line (- -) the same fit shifted by a factor of 30 with respect to time.

6.8 Conclusions

The kinetics of spinodal decomposition for PMMA/SAN blends, containing 28 wt% AN, was studied experimentally with small-angle light scattering and numerically with a diffuse-interface model based on the Cahn-Hilliard theory. The thermodynamic input parameters for the numerical simulations were obtained from experimental cloud point measurements. The data were fitted with the binodal equation yielding the temperature- and concentration-dependent interaction parameter: $\chi(T, c) = -0.009758 - 0.000025T - 0.0013904c$. The critical point of the PMMA/SAN28 blend is 203 °C at 70 wt% PMMA. The SALS-study revealed all three stages of the spinodal decomposition process. The initial stage was analyzed with the linearized CHC-model yielding the apparent diffusivity, which is in the order of 10^{-16} m²/sec, and an interface thickness of approximately 0.15 μ m. The interface thickness development during the intermediate and late stage was analyzed with the modified Porod's model and an end value of 0.03 μ m was obtained. The power-law scaling coefficient (α) may vary from 0.33 (diffusion controlled) to 1.0 (hydrodynamics controlled). In the investigated system, this coefficient varied from 0.55 in the intermediate stage to 0.86 in the late stage, indicating that the system becomes more dominated by hydrodynamics in the late stage of phase separation. The computational analysis showed that the power-law coefficient changed from 0.38 to 0.69 when the capillary number (Ca) was reduced from 10 to 0.5.

The quantitative comparison between the experimental results and the simulations was done using the experimentally determined input parameters D_{app} , ξ and η at $T = 230$ °C. The experimental time scale for the onset of the phase separation was slower than the numerically predicted value. This might be due to the lower random noise level used for the simulation. The experimental coarsening rate was slower than the numerically-predicted coarsening rate which might be due to lower capillary number used for the numerical calculation.

Chapter 7

Computational study on the initial stage of phase separation in ternary blends of homopolymers and block copolymers

7.1 Introduction

Blending of polymers provides an efficient route to develop materials with specific properties that are superior to the constituent polymers (Paul, 1978). However, most polymer pairs are immiscible and have a high interfacial tension. Consequently, immiscible polymer blends have a coarse morphology resulting in poor mechanical properties. Compatibilizers such as block or graft copolymers are commonly added to polymer blends to stabilize the morphology. These additives lower the interfacial tension as well as hinder the coalescence and drive the incompatible polymers to form small, well-dispersed, domains and hence better mechanical properties (Lyatskaya *et al.*, 1996; Koning *et al.*, 1998). The effectiveness of these interfacial agents may, however, be limited by the formation of copolymer micelles in one of the polymeric domains (Fayt *et al.*, 1981, 1986). To circumvent this problem, polymers have been used with functional groups attached to it, which react to form block copolymers at the interface during blending (Tan *et al.*, 1996; Wu, 1985; Scott and Macosko, 1994). Although this strategy has been successful, complete understanding of the morphology evolution with time in case of reactive blending is still lacking.

For a partially miscible system of homopolymers, the evolution of morphology was reported in Chapter 6. The coarsening dynamics for homopolymer blends showed only macrophase separation with three different stages of phase separation, viz. initial, intermediate and late stage. For polymers with end functional groups block copolymers are formed upon reaction. The block copolymers can undergo an order-disorder transition, frequently referred to as microphase separation, and at least three ordered morphologies, such as lamellar, cylindrical, spherical structures (Leibler, 1980; Ohta and Kawasaki, 1986; Khandpur *et al.*, 1995) can be identified. Thus upon reaction the system changes from a binary, homopolymer mixture to

a ternary system consisting of the two homopolymers and the formed block copolymer of which the composition depends on the extent of the reaction.

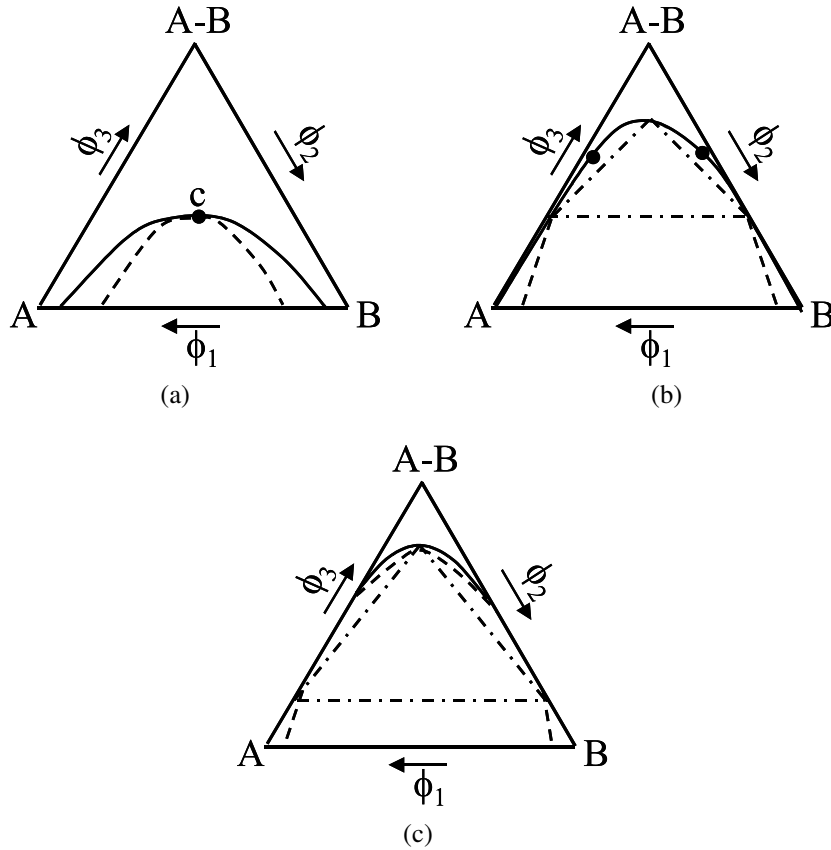


Figure 7.1: Phase diagram for homopolymer/random copolymer mixture for (a) $\chi N = 3$, (b) $\chi N = 7$ and (c) $\chi N = 9$ respectively. Φ_A , Φ_B and Φ_{AB} is the volume fraction of A, B and AB random copolymer, (—) coexistence curve (---) spinodal curve (- · - · -) triphase region (based on the original phase diagram of Leibler (1981)).

Next, for the ternary homopolymer/copolymer mixture, first the phase diagram was studied by Leibler (1981) in the weak segregation limit. The possibility of microphase separation was not considered by Leibler (1981) who only focused on the effect of the degree of incompatibility characterized by the product $\chi N \Delta$ in the phase diagram of the ternary mixture with Δ being the difference in chemical composition of the copolymer chains. He observed different situations (Figure 7.1) depending upon the degree of incompatibility. In the case of nearly miscible species ($2 < \chi N < 6$), the addition of copolymers cause a two-phase homopolymer blend to become one phase (Figure 7.1a). As the incompatibility increases, i.e. $6 < \chi N < 8$ (Figure 7.1b) and $\chi N > 8$ (Figure 7.1c), a relatively small content of copolymers in the system separates the system into two phases containing very little amount of homopolymer A and homopolymer B, respectively. Both phases contain the same fraction of copolymer, so there is no complete demixing into pure A and pure B phases. For a higher copolymer content

the segregation into three phase occurs as shown in Figure 7.1b and 7.1c. Similar results were obtained by Broesta and Fredrickson (1990) for a random copolymer/homopolymer mixture. There have been very few theoretical works on the ordered phases of ternary mixture consisting of a block copolymer and two homopolymers. One of the first studies was by Banaszak and Whitemore (1992), who used the weak segregation theory of Leibler (1980) and limited their consideration to the lamellar structure only. To complete this rather limited work, Janert and Schick (1997) calculated the full phase diagram for the ternary mixture consisting of A and B homopolymers in presence of diblock copolymers having nearly a symmetric composition. Out of all the parameter space for the ternary system of A/B/A-b-B, i.e. chain-length ratios, volume fractions of homo- and block copolymer, fraction of A in block copolymer (f) and χN , Janert and Schick (1997) focused only on the chain length dependency on the phase diagram. They found that homopolymers longer than the diblock are expelled from the ordered phase. This was due to the loss of configurational entropy that they would suffer were they confined to the microstructure. Large regions of coexistence, between an ordered phase and a disordered one which contains most of the homopolymers were formed. Homopolymers that are slightly shorter or comparable to length of block copolymer can swell the microphase indefinitely. Later on Huh and Jo (2002) extended the work of Janert and Schick (1997) to include asymmetric contributions of the diblock copolymer.

For convenience, we have chosen system containing A/B/A-b-B block copolymer with equal fraction of A and B in block copolymer and chain length of homopolymer half that of the block copolymer and $\chi N = 9$. The phase diagram for the above system can be illustrated in Figure 7.2, which is taken from Huh and Jo (2002) for the same system but with $\chi N = 10$. Both biphasic and triphasic coexistence could be observed depending upon the volume fraction of homo- and block copolymer in the ternary mixture. Note that a value of $\chi N = 10$ used for the phase map in Figure 7.2 is slightly smaller than the value for the order-disorder transition of a symmetric block copolymer melt ($\chi N = 10.5$), so that the phase near the apex of $(\phi_{AB}, \phi_A, \phi_B) = (1,0,0)$ is still disordered. As the point at $(1,0,0)$ in the map is vertically moved in the direction perpendicular to the $\phi_A - \phi_B$ lattice in the triangular map, the phase structure undergoes $D \rightarrow L \rightarrow LDD \rightarrow DD$, where D and L stands for disordered and lamellar phase. The order-disorder transition of $D \rightarrow L$ is attributed to the swelling effect caused by addition of homopolymers of comparable size of A and B block. When the content of the block copolymers further decreases along the vertical line from the L region, microphase separated domains cannot accommodate all the homopolymers, and thus some A and B homopolymers are expelled from the swollen lamellar phases and form their own phases, leading to a triphasic coexistence LDD of the swollen lamellar, the disordered A-rich phase, and the disordered B-rich phase. An even further decrease of the block copolymer content results in the biphasic demixing into two disordered A- and B-homopolymer-rich phases (DD).

During reactive blending, all the phases described in the above phase diagram could be encountered by the formation of diblock copolymer dynamically from the reaction of homopolymers containing functional groups. Thus, apart from the phase diagram of the ternary system, a large number of experimental and theoretical studies on the time evolution of morphology in ternary systems containing homopolymers and block copolymers have been reported. Roe and Kuo (1990) and Park and Roe (1991) studied the late-stage phase separation kinetics of poly(styrene) (PS)/poly(butadiene) (PB)/PS-PB block copolymer (PS-b-PB) blends with light scattering and optical microscopy. The homopolymers were considerably shorter than the corresponding blocks of the diblock copolymer. They reported that the block copolymer accumulates at the interface and retards domain growth. Similar observations were

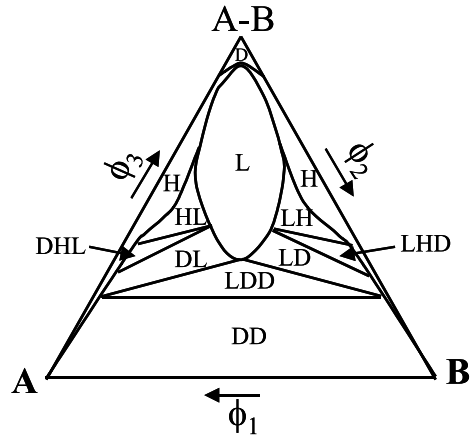


Figure 7.2: Phase diagram of homopolymer/block copolymer mixture (L-lamellar, H-hexagonal, B-bcc, D-disorder) for $\chi N = 10$ (based on the original phase diagram of Huh and Jo (2002))

reported by Sung and Han (1995) on a PS/PB/PS-*b*-PB system and by Hashimoto and Izumitani (1993, 1994) on poly(styrene-*ran*-polyisoprene)(SBR)/PB/SBR-*b*-PB. Lin *et al.* (1995) studied ternary blends with shorter diblock copolymers than of the homopolymers for a system of poly(methylene butylene) (PMB), poly(ethyl butylene) (PEB) and PMB-*b*-PEB. The shorter block copolymers were found to be homogeneously distributed in the homopolymer melt.

Apart from the experimental investigations on ternary systems, theoretical studies were performed using the time-dependent Landau-Ginzburg equation (Cahn and Hilliard, 1959; Cahn, 1964; Cook, 1970). Kawakatsu (1994) and Kawakatsu *et al.* (1993, 1994) studied ternary homopolymer/block copolymer mixtures for the monomer system in two dimensions without hydrodynamic interaction, for which the polymerization index was taken as one. The domain growth was observed to slow down by the presence of surfactants/block copolymers. Kawakatsu (1994) observed that the phase separation of the ternary system was dominated by macroscopic phase separation of the homopolymers with shorter block copolymers. The phase separation kinetics was governed by microphase separation when longer block copolymers were used in the system. Kielhorn and Muthukumar (1999) studied the ternary symmetric homopolymer/diblock copolymer system with the time-dependent Ginzburg-Landau equation for the time evolution of the order parameter. They observed for the polymer system that the diblock copolymer accumulates at the interface of the domains through expulsion from the interior of the domains.

For the reactive system of partially miscible polymers, first the morphology evolution for the non-reactive homopolymers was studied in Chapter 6, where macrophase separation was observed with three different stages of phase separation, i.e. initial, intermediate and late stage. Then, the morphology development for the pure symmetric diblock copolymers was studied (not shown in this chapter), where only lamellar morphology was observed. For the reactive system, block copolymers are produced from the reaction between the homopolymers and hence different equilibrium structures can be obtained depending upon the volume percent-

age of block copolymers in the ternary mixture as shown in Figure 7.2. Since for the reaction system, the set of equations contains logarithmic terms, it is difficult to start the system with zero percent of block copolymer. First, a system containing 20 vol% of block copolymer in homopolymer/block copolymer mixture was chosen. In this work, the study is focussed only on the dynamics of phase separation in the ternary blend of homopolymer/block copolymer mixture containing 20 vol% block copolymer without neglecting hydrodynamic interactions. The diffuse-interface approach was followed with the model proposed by Kawakatsu (1994). For the ternary system, the computation was done first for the monomer system and then for the polymer system where the polymerization index was chosen as hundred.

7.2 Free energy of the system

7.2.1 System definition

The system is considered to be a mixture of two homopolymer species A and B and a diblock copolymer consisting of an A and a B block. It is assumed that each homopolymer species consists of N segments and that the diblock copolymer is made up of $2N$ segments and that the segment volume v is the same for all segments. Assuming that the system is composed of n_{AH} , n_{BH} and n_{AB} molecules of homopolymer A , homopolymer B and diblock copolymer AB , respectively the total volume is

$$V = Nv\{n_{AH} + n_{BH} + 2n_{AB}\}. \quad (7.1)$$

The segments are considered to be located in a lattice with Z the coordination number and a the lattice parameter. So, $1/v$ is the site density and $N\{n_{AH} + n_{BH} + n_{AB}\}$ the total number of sites. The functions ϕ_{AH} and ϕ_{AD} denote the fractions of sites occupied by A -type segments of the homopolymers and di-block copolymers, respectively. The functions ϕ_{BH} and ϕ_{BD} have a similar meaning for the B -type segments. Vacancies are assumed to be absent meaning that

$$\phi_{AH} + \phi_{BH} + \phi_{AD} + \phi_{BD} = 1,$$

and that the volume V is constant.

The total density fractions of A and B -type segments are denoted by ρ_A and ρ_B , respectively. So

$$\rho_A = \phi_{AH} + \phi_{AD}; \quad \rho_B = \phi_{BH} + \phi_{BD},$$

each segment of type A is surrounded by a total of Z other segments of which, on average, a number $Z\rho_A$ are segments of type A and $Z\rho_B$ of type B (mean field approach).

The total Helmholtz free energy of the system is the sum of the homogeneous free energy contribution, the long range contribution due to block copolymers and the gradient contribution (Kawakatsu, 1994). The details of each term are described below.

7.2.2 Homogeneous part

Let ϵ_{AA} , ϵ_{BB} and ϵ_{AB} be the energy associated with segment interaction between type A segments, type B segments and between type A and type B segments. The energy associated

with each segment of type A is then

$$u_A = \frac{Z}{2} (\rho_A \epsilon_{AA} + \rho_B \epsilon_{AB}) ,$$

and the energy associated with each segment of type B is

$$u_B = \frac{Z}{2} (\rho_B \epsilon_{BB} + \rho_B \epsilon_{AB}) .$$

For each volume element dV , we have $\rho_A dV/v$ segments of type A and $\rho_B dV/v$ of type B. The total internal energy U of the system is then

$$U = \int_V \frac{Z}{2v} (\epsilon_{AA} \rho_A^2 + \epsilon_{BB} \rho_B^2 + 2\epsilon_{AB} \rho_A \rho_B) dV . \quad (7.2)$$

The energy of the unmixed system is

$$U_{nm} = \int_V \frac{Z}{2v} (\epsilon_{AA} \rho_A + \epsilon_{BB} \rho_B) dV , \quad (7.3)$$

because in the volume V_A we have $\rho_A = 1$ and $\rho_B = 0$, whereas in V_B $\rho_B = 1$ and $\rho_A = 0$ applies. So, the energy of mixing U_m is

$$\begin{aligned} U_m &= U - U_{nm} \\ &= \int_V \frac{Z}{2v} \left[(\epsilon_{AA} \rho_A^2 + \epsilon_{BB} \rho_B^2 + 2\epsilon_{AB} \rho_A \rho_B) - (\epsilon_{AA} \rho_A + \epsilon_{BB} \rho_B) \right] dV . \end{aligned} \quad (7.4)$$

Defining the order parameters of the system by

$$X = \phi_{AH} - \phi_{BH} ; \quad Y = \phi_{AD} - \phi_{BD} ;$$

$$\Phi = \phi_{AH} + \phi_{BH} ; \quad \Psi = \phi_{AD} + \phi_{BD} ,$$

one finds

$$\begin{aligned} \rho_A &= \frac{1}{2} (1 + X + Y) , \\ \rho_B &= \frac{1}{2} (1 - X - Y) , \\ \rho_A \rho_B &= \frac{1}{4} [1 - (X + Y)^2] . \end{aligned} \quad (7.5)$$

Substituting the above relations in Eq. (7.2) and Eq. (7.3) leads to

$$\begin{aligned} U &= \int_V \frac{Z}{2v} \left(\left[\frac{\epsilon_{AA}}{4} + \frac{\epsilon_{BB}}{4} + \frac{\epsilon_{AB}}{2} \right] + (X + Y)^2 \left[\frac{\epsilon_{AA}}{4} + \frac{\epsilon_{BB}}{4} - \frac{\epsilon_{AB}}{2} \right] \right. \\ &\quad \left. + 2(X + Y) \left[\frac{\epsilon_{AA}}{4} - \frac{\epsilon_{BB}}{4} \right] \right) dV , \end{aligned} \quad (7.6)$$

and

$$U_{nm} = \int_V \frac{Z}{2v} \left(\epsilon_{AA} \left[\frac{1}{2} (1 + X + Y) \right] + \epsilon_{BB} \left[\frac{1}{2} (1 - X - Y) \right] \right) dV . \quad (7.7)$$

The mixing energy U_m is now

$$\begin{aligned} U_m &= U - U_{nm} \\ &= \int_V \frac{Zw}{4v} (1 - (X + Y)^2) dV, \end{aligned} \quad (7.8)$$

where the energy parameter, $w = \epsilon_{AB} - \frac{1}{2}(\epsilon_{AA} + \epsilon_{BB})$ was introduced. The mixing energy in units of $k_b T$ is then (using $V = vN$)

$$\frac{U_m}{k_b T} = \int_V \left[-(X + Y)^2 \frac{wZ}{4k_b T v} \right] dV + constant, \quad (7.9)$$

where k_b is the Boltzman's constant and T is the temperature. Without loss of generality, the constant in Eq. (7.9) is taken equal to zero. The lattice site volume density of the mixing energy u_m is

$$u_m = -\frac{\chi Z}{4v} (X + Y)^2, \quad (7.10)$$

in which χZ is the Flory-Huggins interaction parameter

$$\chi = \frac{w}{k_b T}.$$

For the entropy of mixing, we follow the approach of Kawakatsu (1994) and treat the system at first as a mixture of three independent species with volume fractions ϕ_{AH} , ϕ_{BH} and ϕ_{AB} ($\phi_{AD} + \phi_{BD}$) respectively. For a volume element ΔV , containing Δn_{AH} , Δn_{BH} and Δn_{AB} molecules, one can find the entropy of mixing :

$$\Delta S_m = -k_b (\Delta n_{AH} \ln \phi_{AH} + \Delta n_{BH} \ln \phi_{BH} + \Delta n_{AB} \ln \phi_{AB}), \quad (7.11)$$

using

$$\Delta n_{AH} = \frac{\Delta V}{v} \frac{\phi_{AH}}{N}, \quad \Delta n_{BH} = \frac{\Delta V}{v} \frac{\phi_{BH}}{N}, \quad \Delta n_{AB} = \frac{\Delta V}{v} \frac{\phi_{AB}}{2N}.$$

We now get

$$S_m = -\frac{k_b}{vN} \int_V \left[\phi_{AH} \ln \phi_{AH} + \phi_{BH} \ln \phi_{BH} + \frac{\phi_{AB}}{2} \ln \phi_{AB} \right] dV. \quad (7.12)$$

In terms of the order parameters the contribution to the mixing entropy in units of k_b is then

$$\frac{S_m}{k_b} = -\frac{1}{2vN} \int_V [(\Phi + X) \ln(\Phi + X) + (\Phi - X) \ln(\Phi - X) + \Psi \ln \Psi] dV. \quad (7.13)$$

So, this entropic part contributes to the volume density of the free energy and the term is

$$s_m = -\frac{1}{2vN} [(\Phi + X) \ln(\Phi + X) + (\Phi - X) \ln(\Phi - X) + \Psi \ln \Psi]. \quad (7.14)$$

After collecting Eq. (7.10) and Eq. (7.14), the homogeneous part of the Helmholtz energy density f_s reads:

$$f_s = \frac{1}{v} \left\{ -\frac{1}{4} Z \chi (X + Y)^2 + \frac{1}{2N} [(\Phi + X) \ln(\Phi + X) + (\Phi - X) \ln(\Phi - X) + \Psi \ln \Psi] \right\}. \quad (7.15)$$

Although f_s depends on X , Y , Φ and Ψ , one of the last two order parameters can be eliminated from the problem because $\Phi + \Psi = 1$.

7.2.3 The long range contribution

In diblock copolymers, A -type blocks are connected to B -type blocks by means of a chemical bond preventing macrophase separation (Kawakatsu, 1994; Ohta and Kawasaki, 1986). The long range contribution imposes a penalty on the long wavelength fluctuations in the field $Y(\mathbf{r})$. Following Ohta and Kawasaki (1986), we can write this penalty as:

$$\frac{F_l}{k_b T} = \frac{\alpha}{2v} \int_V \int_{V'} dV dV' G(\mathbf{r} - \mathbf{r}') [Y(\mathbf{r}) - \bar{Y}] [Y(\mathbf{r}') - \bar{Y}] dV, \quad (7.16)$$

where the Green's function $G(r)$ satisfies $\nabla^2 G(r) = -\delta(r)$ and \bar{Y} is the spatial average of $Y(r)$ and α is a positive constant, which depends on the polymerization index N of the block copolymer chain as $\alpha \sim N^{-2}$ (Ohta and Kawasaki, 1986).

The density f_l is then found to be

$$f_l = \frac{\alpha}{2v} \int_{V'} G(\mathbf{r} - \mathbf{r}') [Y(\mathbf{r}) - \bar{Y}] [Y(\mathbf{r}') - \bar{Y}] dV'. \quad (7.17)$$

7.2.4 The gradient contribution

For the diffuse-interface modeling, we consider the interface to have a non-zero thickness, allowing a continuous change in the properties of the system. For a binary system, one term is added which takes into account the gradient in concentration (De Gennes, 1980):

$$F_g = \int_V [\kappa(\phi)(\nabla\phi)^2] dV. \quad (7.18)$$

The parameter $\kappa(\phi)$ describes the free energy cost of the concentration fluctuations and it has two sources: an enthalpic term related to the effective range of interaction r_0 and a term whose origin is the configurational entropy of the Gaussian coils (Binder, 1983; De Gennes, 1980). The prefactor of the square-gradient term in the binary case reads

$$\kappa(\phi) = \frac{k_b T}{v} \left[\frac{r_0^2}{6} \chi_{\text{eff}} + \frac{a^2}{\lambda\phi(1-\phi)} \right]. \quad (7.19)$$

For polymer systems, usually the first term in $\kappa(\phi)$ is neglected. Nevertheless, in this work we consider both contributions to make our model applicable to either polymer and/or monomer systems. According to Cahn and Hilliard (1958) and Binder (1983), r_0 is in the same order as the lattice spacing a and χ_{eff} is well represented by the interaction parameter $Z\chi$; therefore $\kappa(\phi)$ simplifies to

$$\kappa(\phi) = a^2 k_b T \left[\chi + \frac{1}{\lambda \phi (1 - \phi)} \right], \quad (7.20)$$

where $\lambda = 36$ when a partially miscible system is considered. In these kinds of systems, the wavelength of the concentration fluctuation is large. On the other hand, $\lambda = 24$ holds for segregated systems, where the wavelength of the concentration fluctuations is short.

In our case we identify ϕ with $\phi_{AH} + \phi_{AD}$ and obtain for the contribution of the gradient part by choosing $\lambda = 36$

$$\frac{F_g}{k_b T} = \frac{a^2}{2} \int_V \left[\frac{\chi}{2} + \frac{1}{36(X+Y)(1-X-Y)} \right] |\nabla(X+Y)|^2 dV, \quad (7.21)$$

which leads to the free energy density

$$f_g = \frac{a^2}{2v} \left[\frac{\chi}{2} + \frac{1}{36(X+Y)(1-X-Y)} \right] |\nabla(X+Y)|^2. \quad (7.22)$$

Note that the above expression for f_g , apart from the term $\chi/2$, is the same as suggested by Ohta and Kawasaki (1986) and Kawakatsu (1994).

7.2.5 The total Helmholtz energy density

The total Helmholtz energy density can be obtained by collecting all the terms derived above and can be written as:

$$\begin{aligned} f_T = \frac{1}{2v} \left\{ -\frac{Z\chi}{2} (X+Y)^2 + a^2 \left[\frac{\chi}{2} + \frac{1}{36(X+Y)(1-X-Y)} \right] |\nabla(X+Y)|^2 \right. \\ \left. + \left[\frac{(\Phi+X)}{N} \ln(\Phi+X) + \frac{(\Phi-X)}{N} \ln(\Phi-X) + \frac{\Psi}{N} \ln \Psi \right] \right. \\ \left. + \alpha \int_{V'} dV' G(\mathbf{r}-\mathbf{r}') [Y(\mathbf{r}) - \bar{Y}] [Y(\mathbf{r}') - \bar{Y}] \right\} \end{aligned} \quad (7.23)$$

and the total Helmholtz energy functional is $F_T = \int f_T dV$. The above expression is used to determine the evolution equation for the order parameters.

7.3 The evolution equations

7.3.1 For a ternary system without reaction

If p is any order parameter, then its evolution equation is given by

$$\frac{1}{v} \frac{\partial p}{\partial t} = \nabla \cdot (D^p \nabla \mu_p), \quad (7.24)$$

where μ_p is the chemical potential for p and D^p is the diffusion coefficient. Here, we assume that v and D^p are constants although D^p is a function of concentration (Pincus, 1981), leading to

$$\frac{\partial p}{\partial t} = v D^p \nabla^2 (\mu_p), \quad (7.25)$$

as the generic form of the evolution equation for the order parameter. The chemical potential μ_p is equal to the variational derivative of the Helmholtz energy functional F_T with respect to the order parameter p ,

$$\mu_p = \frac{\delta F_T}{\delta p}.$$

For X , Y and Ψ , this leads to :

$$\begin{aligned} \frac{\partial X(\mathbf{r}, t)}{\partial t} = & \frac{1}{2} D^X \nabla^2 \left\{ -Z\chi(X+Y) - a^2 \chi \nabla^2(X+Y) + \frac{1}{N} \ln \left(\frac{\Phi+X}{\Phi-X} \right) \right. \\ & \left. - \frac{a^2}{36(X+Y)(1-X-Y)} \left[\frac{1-2X-2Y}{(X+Y)(1-X-Y)} |\nabla(X+Y)|^2 \right. \right. \\ & \left. \left. + 2\nabla^2(X+Y) \right] \right\}, \end{aligned} \quad (7.26)$$

$$\begin{aligned} \frac{\partial Y(\mathbf{r}, t)}{\partial t} = & \frac{1}{2} D^Y \nabla^2 \left\{ -Z\chi(X+Y) - a^2 \chi \nabla^2(X+Y) \right. \\ & \left. - \frac{a^2}{36(X+Y)(1-X-Y)} \left[\frac{1-2X-2Y}{(X+Y)(1-X-Y)} |\nabla(X+Y)|^2 \right. \right. \\ & \left. \left. + 2\nabla^2(X+Y) \right] - 2\alpha(Y-\bar{Y}) \right\}, \end{aligned} \quad (7.27)$$

and

$$\frac{\partial \Psi(\mathbf{r}, t)}{\partial t} = \frac{D^\Psi \nabla^2}{2N} (1 + \ln \Psi). \quad (7.28)$$

To dimensionalize the above equations, the following set of dimensionless variables are introduced:

$$t^* = \frac{D^X t}{2a^2 \chi}; \quad \nabla^* = a\sqrt{\chi} \nabla; \quad \mathbf{r}^* = \frac{\mathbf{r}}{a\sqrt{\chi}}; \quad \tilde{D}^Y = \frac{D^Y}{D^X}; \quad \tilde{D}^\Psi = \frac{D^\Psi}{D^X},$$

where D^X , D^Y and D^Ψ are diffusion coefficients for X , Y and Ψ respectively.

Now, the evolution equations (Eq. (7.26) - Eq. (7.28)) in dimensionless form after dropping the asterisk notation read

$$\begin{aligned} \frac{\partial X(\mathbf{r}, t)}{\partial t} = & \nabla^2 \left\{ -Z\chi(X+Y) - \nabla^2(X+Y) + \frac{1}{N} \ln \left(\frac{\Phi+X}{\Phi-X} \right) \right. \\ & \left. - \frac{1}{36\chi(X+Y)(1-X-Y)} \left[\frac{1-2X-2Y}{(X+Y)(1-X-Y)} \right. \right. \\ & \left. \left. |\nabla(X+Y)|^2 + 2\nabla^2(X+Y) \right] \right\}, \end{aligned} \quad (7.29)$$

$$\begin{aligned} \frac{\partial Y(\mathbf{r}, t)}{\partial t} = & \tilde{D}^Y \nabla^2 \left\{ -Z\chi(X+Y) - \nabla^2(X+Y) \right. \\ & \left. - \frac{1}{36\chi(X+Y)(1-X-Y)} \left[\frac{1-2X-2Y}{(X+Y)(1-X-Y)} \right. \right. \\ & \left. \left. |\nabla(X+Y)|^2 + 2\nabla^2(X+Y) \right] - 2\tilde{\alpha}(Y-\bar{Y}) \right\}, \end{aligned} \quad (7.30)$$

and

$$\frac{\partial \Psi(\mathbf{r}, t)}{\partial t} = \frac{\tilde{D}^\Psi \nabla^2}{N} (1 + \ln \Psi) . \quad (7.31)$$

7.3.2 For a ternary system with reaction

When block copolymers are formed by the reaction of two reactive homopolymers, only the evolution equation in Ψ will change, whereas no change in the evolution equations of X and Y will occur. Assuming the reaction to be first order in both A and B and second order overall, the rate expression can be written as: (Maurits *et al.*, 1999)

$$\begin{aligned} \frac{\delta \phi_{AH}}{\delta t} &= -k \phi_{AH} \phi_{BH} , \\ \frac{\delta \phi_{BH}}{\delta t} &= -k \phi_{AH} \phi_{BH} , \\ \frac{\delta \phi_{AD}}{\delta t} &= k \phi_{AH} \phi_{BH} , \\ \frac{\delta \phi_{BD}}{\delta t} &= k \phi_{AH} \phi_{BH} , \end{aligned} \quad (7.32)$$

where k is the chemical reaction rate constant. Rearranging all the terms, the evolution equation of Ψ can be written as:

$$\frac{\partial \Psi}{\partial t} = \frac{\tilde{D}^\Psi \nabla^2}{N} (1 + \ln \Psi) + 2k \phi_{AH} \phi_{BH} . \quad (7.33)$$

Again $\phi_{AH} \phi_{BH}$ can be rewritten in terms of order parameters Φ and X ,

$$\begin{aligned} 2\phi_{AH} \phi_{BH} &= \frac{1}{2} \left[(\phi_{AH} + \phi_{BH})^2 - (\phi_{AH} - \phi_{BH})^2 \right] \\ &= \Phi^2 - X^2 \\ &= (1 - \Psi)^2 - X^2 . \end{aligned} \quad (7.34)$$

The evolution equation for Ψ is read as:

$$\frac{\partial \Psi}{\partial t} = \frac{\tilde{D}^\Psi \nabla^2}{N} (1 + \ln \Psi) + 2k \left[(1 - \Psi)^2 - X^2 \right] . \quad (7.35)$$

7.4 Balance equation of mass and momentum

From the conservation of momentum, a generalized Navier-Stokes equation can be derived for the velocity field (Lowengrub and Truskinovsky, 1998; Verschueren, 1999) in absence of inertia:

$$\mathbf{0} = -\rho \nabla g + \nabla \cdot \eta \left(\nabla \mathbf{v} + \nabla \mathbf{v}^T \right) + \rho (\mu_X \nabla X + \mu_Y \nabla Y + \mu_\Psi \nabla \Psi) , \quad (7.36)$$

where g is the modified pressure $g = f + p/\rho$, with p the local pressure, ρ the density and \mathbf{v} the velocity. Compared to the classical Navier-Stokes equation, in Eq. (7.36) an extra

capillary term $\rho(\mu_X \nabla X + \mu_Y \nabla Y + \mu_\Psi \nabla \Psi)$ appears reflecting the interfacial tension via the chemical potential. This modification accounts for hydrodynamic interactions, i.e. the influence of the concentration fields X , Y and Ψ on the velocity field and, hence, describes the spatial variations of the velocity field due to the presence of interfaces. The viscosity η and density ρ generally depend on X , Y and Ψ . Here, we consider the iso-viscous and density-matched case (where for simplicity η and ρ will be set equal to one hereafter) which gives for the equation of continuity:

$$\nabla \cdot \mathbf{v} = 0. \quad (7.37)$$

7.5 Numerical methods

The concentration problems (Eq. (7.29) - Eq. (7.31)) for X , Y and Ψ and the flow problem (Eq. (7.36) - Eq. (7.37)) are solved by a finite element method. The details about the temporal and spatial discretization can be found in Khatavkar *et al.* (2006). The phase separation was studied on a rectangular domain of $(0, 0)$ to $(128, 128)$ for the monomer system whereas for the polymer system, the dimensions were $(0, 0)$ to $(200, 200)$. In each simulation, the domain was meshed with 128×128 second-order elements. The time step used for simulation for both monomer and polymer system was $\Delta t = 5 \times 10^{-3}$. The initial configuration of the fields $X(r)$, $Y(r)$, and $\Psi(r)$ was generated using Gaussian random numbers with mean values \bar{X} , \bar{Y} , and $\bar{\Psi}$ and the variances were in the order of 10^{-2} (Kawakatsu, 1994). Bi-periodic boundary conditions were applied for X , Y , Ψ and \mathbf{v} . The parameters $\bar{D}^Y = \bar{D}^\Psi = 1.0$, $\bar{X} = 0.0$ (symmetric composition of homopolymer), $\bar{Y} = 0.0$ (symmetric composition of block copolymer), $\bar{\Psi} = 0.2$ (20% block copolymer), $\eta = 1$, $\rho = 1$ and $Z = 6$ were used in all simulations.

7.6 Results and Discussion

7.6.1 Validation of the result

Before presenting the detailed results on the phase separation, first the model is validated and its dependency on the domain size, mesh size and time step is investigated. To do this, the average structure size (details of the calculation is given in Eq. (7.38), described later in this section) of the concentration field X was evaluated for different domain sizes, mesh sizes and time steps. Figure 7.3a shows the average structure size of X for different domain sizes varying from 4×4 to 128×128 . It is observed that the average structure size for X converges upon increasing the domain size from 4×4 to 128×128 . In our further studies, a domain size of 128×128 was chosen to be consistent with the system used by Kawakatsu (1994). Next, to check the mesh dependency of the results, different mesh sizes varying from 100×100 to 156×156 elements were used. The average structure size of X for different mesh sizes are shown in Figure 7.3b. It can be seen that all three meshes give the same average structure size of X showing that the results are mesh independent. Generally, at high resolution (smaller mesh size), the accuracy is very high but at the same time the computation time to solve the highly non-linear coupled equations is also very long. Thus as a compromise between accuracy and computation time, a mesh consisting of 128×128 elements was chosen for further calculations.

To check the time-step dependency, three different time steps were tried. A decrease in time step, on one hand, implies an increase in accuracy of the calculation of the unknown concentration fields, while on the other hand, it implies a non-linear increase in the computation time. Figure 7.3c shows the evolution of the average structure size of X . For further calculation, a time step $\Delta t = 5 \times 10^{-3}$ is chosen for convenience. Although for validation, only the average structure size of X has been shown, but the calculations for Y also yield the same results. However, the calculation on $\delta\Psi$ was not possible, because the concentration levels are one order of magnitude lower than for X and Y .

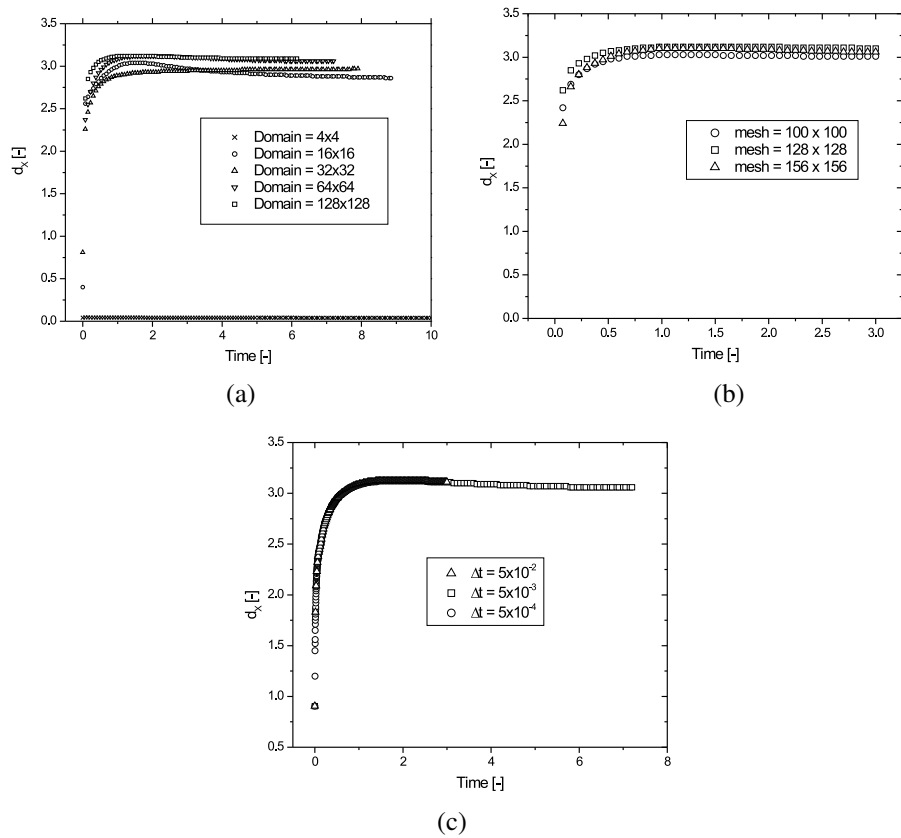


Figure 7.3: Average structure size of X for (a) different domain size and for (b) different mesh size and (c) different time steps.

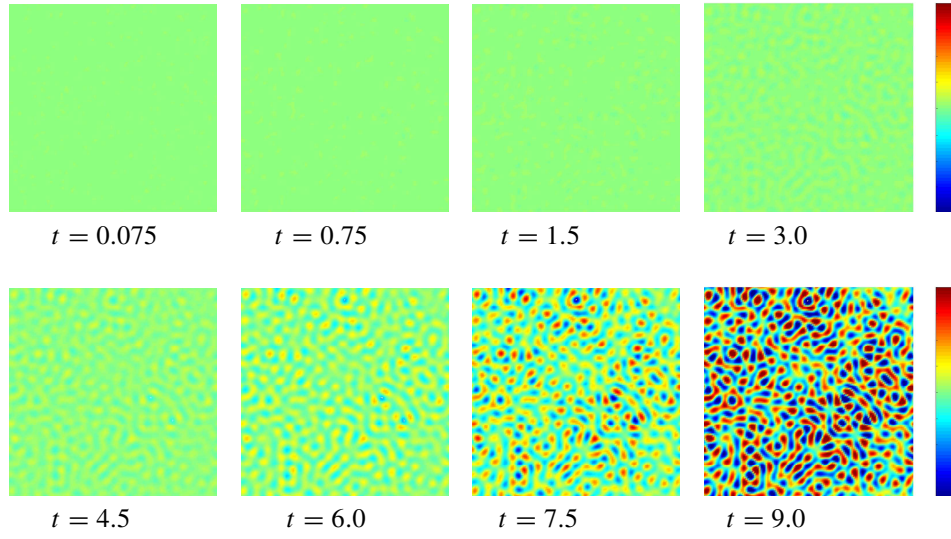


Figure 7.4: Structure development of X , color changes from blue (-0.4017) to red (0.4031).

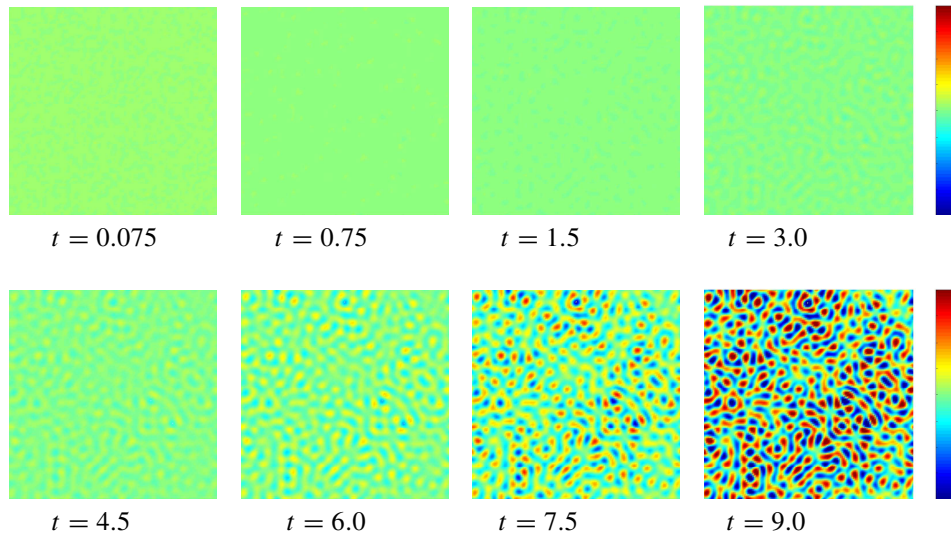


Figure 7.5: Structure development of Y , color changes from blue (-0.3821) to red (0.3917).

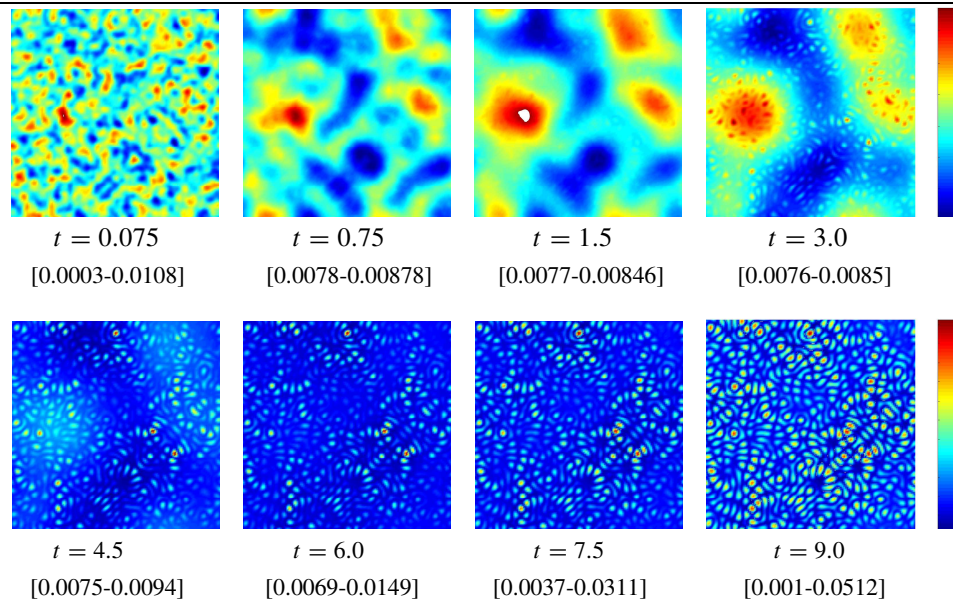


Figure 7.6: Structure development of $\delta\Psi$ ($\Psi - \bar{\Psi}$), color changes from blue (minimum) to red (maximum) with the maximum and minimum for each time is given in the bracket.

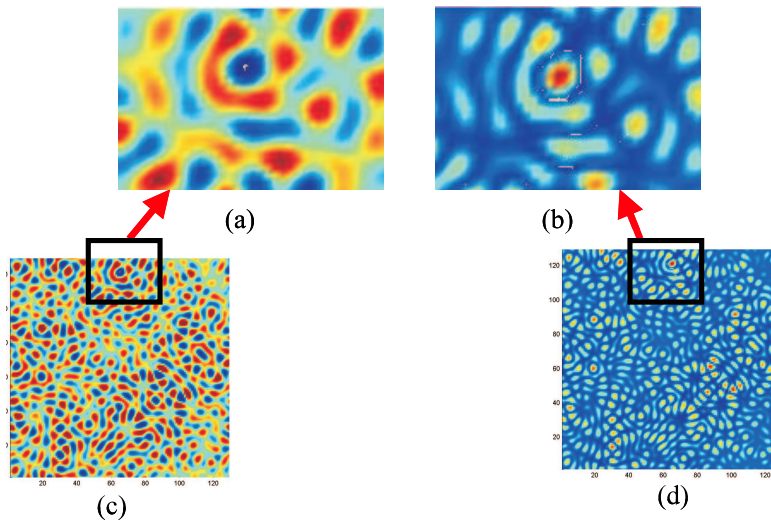


Figure 7.7: Enlarged picture of X and $\delta\Psi$ at $t = 9.0$.

7.6.2 Monomer system

First, the phase separation of the monomer system was studied for which the polymerization index was chosen one ($N=1$). The block copolymer contains two monomers with an overall polymerization index $2N$. Now, with the chosen domain size, mesh size and time step, the computation was done for the monomer system and the evolution of the concentration fields, $X(\mathbf{r}, t)$, $Y(\mathbf{r}, t)$ and $\delta\Psi(\mathbf{r}, t)$ ($\Psi(\mathbf{r}, t) - \bar{\Psi}$) at different times are shown in Figures 7.4 - 7.6. For X and Y (Figures 7.4 and 7.5), all the pictures were re-scaled with respect to the final concentration levels, whereas for $\delta\Psi$ (Figure 7.6), the re-scaling was not done because of low concentration level, which is one order lower than the concentration levels of X and Y . The changes in concentration were first observed at the dimensionless time $t = 1.5$ for both X and Y , and at $t = 3.0$ for $\delta\Psi$ and these changes are followed up to $t = 9.0$ for all X , Y and $\delta\Psi$ respectively.

Next, the concentration fields of X and $\delta\Psi$ at $t = 9.0$ (Figure 7.7c - 7.7d) are zoomed in and shown in Figure 7.7a and 7.7b. From Figures 7.7a, the two homopolymers could be seen in red (maximum) and blue (minimum) colors, whereas in Figure 7.7b the corresponding block copolymer is seen in blue, which is found to be at the interface between the two homopolymers.

The average structure size can be calculated using a correlation function defined as:

$$G(\mathbf{r}, t) = \frac{1}{N^d} \sum (c(\mathbf{x} + \mathbf{r}, t) - c_{av}) \cdot (c(\mathbf{x}, t) - c_{av}), \quad (7.38)$$

where \mathbf{r} and \mathbf{x} are the lattice vectors, $c(\mathbf{x}, t)$ is the concentration at any point at time t , c_{av} the average concentration, N is the number of grid points, and d the dimensionality, in our case $d = 2$. Radial averaging is carried out using a Brillouin zone function to eliminate any directional effects (Keestra, 2004):

$$g(r, t) = \frac{1}{N_r} \sum_{r-\Delta(r/2) \leq |x| < r+\Delta(r/2)} g(r, t). \quad (7.39)$$

Similar to Chapter 6, the average structure size is determined by the first intersection of the correlation function with the x -axis. The evolution of average structure size of concentration fields X and Y during phase separation are shown in Figures 7.8a and 7.8b. For times up to 1.5, the average structure size of X increases and remains the same thereafter. For Y , the average structure size first goes to a maxima at $t = 1.0$ and then decreases till $t = 2.0$ and then remains constant thereafter. Unfortunately, the average structure size for Ψ could not be obtained because of the low concentration levels, which is one order lower than the concentration level of X and Y .

From the above observations, it is clear that only the concentration level changes, whereas the average structure size remains constant. It can be concluded that only the initial stage of spinodal decomposition is observed. The intermediate and the late stage of spinodal decomposition could not be observed, which might be due to complexity of the coupled non-linear equation.

7.6.3 Polymer system

After studying the initial stage of phase separation for the monomer system, the phase separation of the polymer system was studied for which the polymerization index was chosen

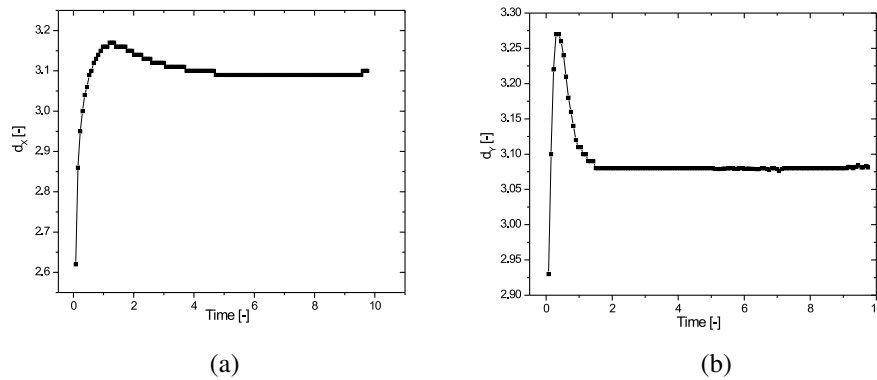


Figure 7.8: Average structure size versus time for (a) X and for (b) Y.

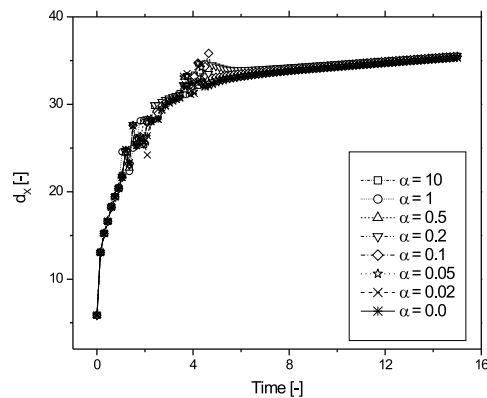


Figure 7.9: Average structure size of X for different α .

100, i.e. $N = 100$. In the polymer system, only the effect of block length of copolymer and the effect of hydrodynamics was studied.

Effect of block length

The effect of the length of the block copolymer on the phase separation of ternary system is studied by varying α . Figure 7.9 shows the average structure size of X for different α 's, i.e. for different block lengths. It is observed that there is no variation in average structure size of X with a variation in block length, whereas for Y, the domains change from macrophase separated to microphase separated structure (shown in Figure 7.10), when α varies from small to large values, i.e. from longer to shorter block length. The system is dominated by macrophase separated domains of the homopolymers, when α increases from 0 to 0.2. A further increase in α results in both macrophase and microphase separated structure. Similar results were obtained by Janert and Schick (1997) for the block copolymer/homopolymer mixture, where they observed expulsion of homopolymers, when it was longer than the diblock and lead to both microphase and macrophase separated domains. The corresponding time at which the

structure change from macrophase to microphase separated domains is shown in Table 7.1. The time of cross-over from macrophase to microphase separated domains varies proportional to the value of α .

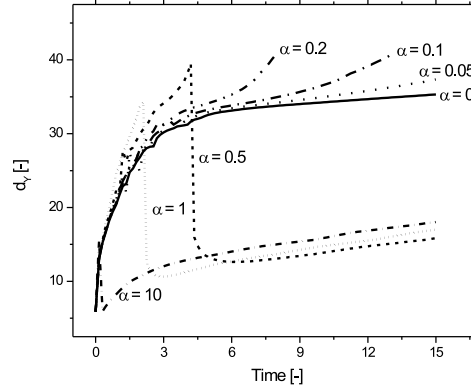


Figure 7.10: Average structure size of Y for different α .

Table 7.1: Transition time from macrophase to microphase for different α

α	0.5	1.0	10.0
Time	4.45	2.25	0.25

The results discussed above were obtained without including hydrodynamic interactions. Next the effect of hydrodynamic interaction is studied by combining the momentum balance equation (Eq. (7.36)) to the evolution equation (Eq. (7.29) - Eq. (7.31)).

Effect of hydrodynamics

Using the dimensionless variables defined earlier and $g^* = (ga\sqrt{\chi})/(\rho\eta v)$, with v as the characteristic velocity, the momentum balance equation in dimensionless form reads as:

$$\mathbf{0} = -\nabla g + \nabla \cdot (\nabla v + \nabla v^T) + \frac{1}{Ca}(\mu_X \nabla X + \mu_Y \nabla Y + \mu_\Psi \nabla \Psi), \quad (7.40)$$

where $Ca = (\eta v)/(\rho a^2 \chi)$ is the capillary number. Ca was varied from 10^{-3} to 10^3 and the corresponding effect on the average structure size of X is shown in Figure 7.11. It can be seen that the average structure size remained the same irrespective of the value of capillary number. This is due to the fact that the system is still in the initial stage of phase separation. Similar results were obtained for no hydrodynamic interaction on the initial stage phase separation of the homopolymer blends in Chapter 6. The hydrodynamic interaction is expected to enhance the intermediate and late stage of the phase separation, as is observed for the homopolymer blends (Chapter 6) with a variation in capillary number.

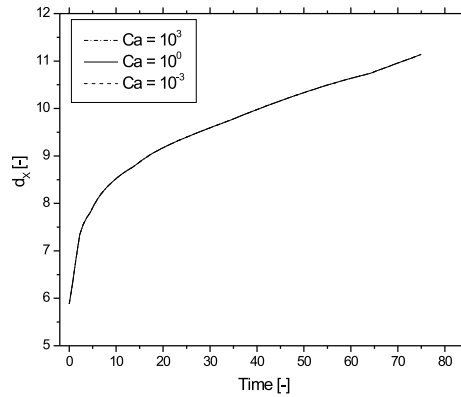


Figure 7.11: Average structure size of X for different hydrodynamic number.

7.7 Concluding remarks

Phase separation of the non-reactive homopolymers was first studied in Chapter 6, where macrophase separation was observed with three different stages of phase separation, i.e. initial, intermediate and late stage. Then lamellar structure was observed for the pure diblock copolymer. Next, instead of starting directly with the reactive system, where numerical limitations arise due to the logarithmic term at initial times, the phase separation of the ternary system of homopolymer and block copolymer containing 20 vol% block copolymer was studied with diffuse-interface modeling. Only the initial stage of phase separation was observed in both the monomer and polymer system for the ternary mixtures. The intermediate and late stage could not be studied, which might be due to the complex coupled non-linear equations and due to the evolution of two different length scales during the phase separation. For the monomer system, the block copolymer was found to be present at the interface between the two homopolymers. For the polymer system, both micro and macrophase separation were observed with smaller block length i.e. for larger α . The hydrodynamic interaction did not play any role at the initial stage of phase separation for the ternary system, which is also known from the homopolymer blends in Chapter 6. It is expected that the hydrodynamic interaction will play a role in the intermediate and late stages of phase separation, but unfortunately we could not simulate these stages because different length scales arise from both micro and macrophase separation. Multi-scale simulation would be an alternative to tackle these length scale issues. After simulating the ternary system containing 20 vol% block copolymer, the different structure described in the phase diagram (Figure 7.2) can be obtained by computing the dynamics of reactive system where block copolymers are formed with time.

Bibliography

- Abid, S. (1993). . Ph.D. thesis, Inst. Fluid Mech, Toulouse, France.
- Abid, S. and Chesters, A. K. (1994). The drainage and rupture of partially mobile films between colliding drops at constant approach velocity. *Int. J. Multiphase Flow*, **20**, 613–629.
- Amestoy, P. R. and Duff, I. S. (1989a). Memory management issues in sparse multifrontal methods on multiprocessors. *Int. J. Supercomput. Appl.*, **7**, 64–69.
- Amestoy, P. R. and Duff, I. S. (1989b). Vectorization of a multiprocessor multifrontal code. *Int. J. Supercomput. Appl.*, **3**, 41–43.
- Amestoy, P. R. and Puglisi, C. (2002). An unsymmetrized multifrontal LU factorization. *SIAM J. Matrix Anal. Appl.*, **24**, 553–557.
- Aref, H. (1991). Stochastic particle flow in laminar flow. *Phys. Fluids. A.*, **3**, 1009–1013.
- Badiang, J. G. and Aube, J. (1996). One-step conversion of aldehydes to oxazolines and 5,6-dihydro-4H-1,3-oxazines using 1,2- and 1,3-azido alcohols. *J. Org. Chem.*, **61**, 2484–2487.
- Baker, W. E. and Saleem, M. (1987a). Coupling of reactive polystyrene and polyethylene in melts. *Polymer*, **28**, 2057–2062.
- Baker, W. E. and Saleem, M. (1987b). Polystyrene-polyethylene melt blends obtained through reactive mixing process. *Polym. Eng. Sci.*, **27**, 1634–1641.
- Baker, W. E. and Saleem, M. (1988). Rubber toughening of polystyrene through reactive blending. *Polym. Eng. Sci.*, **28**, 1427–1433.
- Banaszak, M. and Whitmore, M. D. (1992). Mean field theory of phase behaviour of ternary blockcopolymer-homopolymer blends. *Macromolecules*, **25**, 249–260.
- Baumert, M., Zimmermann, J., Scheerble, J., and Mulhaupt, R. (1999). Synthesis of oxazoline-terminated polystyrene via controlled-radical polymerization. *Macromolecules*, **32**, 2503–2510.
- Binder, K. (1983). Collective diffusion, nucleation, and spinodal decomposition in polymer mixtures. *J. Chem. Phys.*, **79**(12), 6387–6409.

- Bird, R. B., Stewart, W. E., and Lightfoot, E. N. (1994). *Transport Phenomena*. Wiley, New York.
- Boere, R. T., Oakley, R. T., and Reed, R. W. (1987). Preparation of N,N,N'-tris(trimethylsilyl)amidines; a convenient route to unsubstituted amidines. *J. Org. Chem.*, **331**(2), 161–167.
- Borggreve, R. J. M. and Gaymans, R. J. (1989). Impact behaviour of nylon-rubber blends: 4. Effect of the coupling agent, maleic anhydride. *Polymer*, **30**, 63–70.
- Braun, D. and Saechtling, H. (1982). *Simple methods for identification of plastics*. Hanser, Munich.
- Broesta, D. and Fredrickson, G. H. (1990). Phase equilibria in copolymer/homopolymer ternary blends: molecular weight effects. *J. chem. Phys.*, **93**(4), 2927–2938.
- Brown, S. B. (1992). *Reactive extrusion: principles and practice*. Hanser, Munich.
- Cahn, J. W. (1964). Phase separation by spinodal decomposition in isotropic systems. *J. Chem. Phys.*, **42**(1), 93–99.
- Cahn, J. W. and Hilliard, J. E. (1958). Free energy of a nonuniform system. I. Interfacial energy. *J. Chem. Phys.*, **28**(2), 258–267.
- Cahn, J. W. and Hilliard, J. E. (1959). Free energy of a nonuniform system. III. Nucleation in a two-component incompressible fluid. *J. Chem. Phys.*, **31**, 688–699.
- Charoensirisomboon, P., Chiba, T., Solomko, S. I., Inoue, T., and Weber, M. (1999). Reactive blending of polysulfone with polyamide: a difference in interfacial behavior between in situ formed block and graft copolymers. *Polymer*, **40**(24), 6803–6810.
- Charoensirisomboon, P., Inoue, T., and Weber, M. (2000). Pull-out of copolymer in situ-formed durig reactive blending: effect of copolymer architecture. *Polymer*, **41**(14), 6907–6912.
- Chen, C. T., Rees, L. H., Cowley, A. R., and Green, M. L. H. (2001). Palladium(II) complexes with the bidentate iminophosphine ligand [Ph₂PCH₂C(Ph):N(2,6-Me₂C₆H₃)]. *J. Chem. Soc: Dalton Trans.*, **22**, 1761–1763.
- Chesters, A. K. (1991). The modelling of coalescence in fluid-liquid dispersions: a review of current understanding. *Trans. IChemE. Part A*, **69**, 259–270.
- Choi, Y. H., Choi, H. K., Looman, O., Lefeber, A. M. G., and Verpoorte, R. (2004). *Phytochemical analysis*, **15**, 325–331.
- Clarke, N. and McLeish, T. C. B. (1998). Shear flow effects on phase separation of entangled polymer blends. *Phy. Rev. E*, **57**(4), 3731–3734.
- Coleman, M. M., Graf, J. F., and Painter, P. C. (1991). *Specific interactions and miscibility of polymer blends*. Technomic publishing, Pennsylvania.
- Cook, H. E. (1970). Brownian motion in spinodal decomposition. *Acta Metall.*, **18**, 297–306.

- Corey, E. J. and Wang, Z. (1993). Enantioselective conversion of aldehydes to cyanohydrins by a catalytic system with separate chiral binding sites for aldehyde and cyanide components. *Tetrahedron Lett.*, **34**(25), 4001–4004.
- Cowie, J. M. G. and Lath, D. (1988). Miscibility mapping in some blends involving poly(styrene-*co*-acrylonitrile). *Makromol. Chem. Macro. Symp.*, **16**, 103–112.
- Culberston, B. M. (1989). *Contemporary topics in polymer science, Vol 6, multiphase macromolecules systems*. Plenum, New York.
- Culberston, B. M. (2002). Cyclic imino ethers in step-growth polymerizations. *Prog. Polym. Sci.*, **27**, 579–626.
- Cumming, A., Wiltzius, P., Bates, F. S., and Rosedale, J. H. (1992). Light-scattering experiments on phase-separation dynamics in fluid mixtures. *Phys. Rev. A*, **45**(2), 885–897.
- Datta, S. and Lohse, D. J. (1996). *Polymeric compatibilizers*. Hanser, New York.
- Davis, H. T. and Scriven, L. E. (1982). Stress and structure in fluid interfaces. *Adv. Chem. Phys.*, **49**, 357–454.
- De Gennes, P. G. (1980). Dynamics of fluctuations and spinodal decomposition in polymer blends. *J. Chem. Phys.*, **72**, 4756–4762.
- Debier, D., Devaux, J., and Legras, R. (1995). Blends of Bisphenol a PC and Acrylic polymers. 1. A chemical reaction mechanism. *J. Polym. Sci. Part A.*, **33**, 407–414.
- Dedecker, K., Groeninckx, G., and Inoue, T. (1998). Reactive compatibilization of A/(B/C) polymer blends. Part 3. Quantitative analysis of the interfacial thickness and the interfacial reaction. *Polymer*, **39**, 5001–5010.
- Donovan, A. R. and Moad, G. (2005). A novel method for determination of polyester end-groups by NMR spectroscopy. *Polymer*, **46**, 5005–5011.
- Earnest, T. R. and MacKnight, W. J. (1980). Infrared studies of hydrogen bonding in ethylenemethacrylic acid copolymers and ionomers. *Macromolecules*, **13**, 844–849.
- El Malbrouk, K. and Bousmina, M. (2005). Effect of hydrodynamics on dynamics of phase separation in polystyrene/poly(vinyl methyl ether) blend. *Polymer*, **46**, 9005–9014.
- Elmendorp, J. J. (1986). . Ph.D. thesis, Delft University of Technology, the Netherlands.
- Epstein, B. N. (1979). Toughened polyamide blends. *U.S. Patent*, (4,174,358).
- Fayt, R., Jerome, R., and Teyssie, P. (1981). Molecular design of multicomponent polymer systems. I. Emulsifying effect of poly(hydrogenated butadiene-*b*-styrene) copolymers in LDPE/PS blends. *J. Polym. Sci. Polym. Lett. Edn.*, **19**(2), 79–84.
- Fayt, R., Jerome, R., and Teyssie, P. (1986). Molecular design of multicomponent polymer systems. XII. Direct observation of the location of a block copolymer in low-density polyethylene-polystyrene blends. *J. Polym. Sci. Polym. Lett. Edn.*, **24**(1), 25–28.
- Fernandez, M. L., Higgins, J. S., Horst, R., and Wolf, B. A. (1995). Complex miscibility behaviour for polymer blends in flow. *Polymer*, **36**, 149–154.

- Fredrickson, G. H. (1996). Diffusion-controlled reactions at polymer-polymer interfaces. *Phys. Rev. Lett.*, **76**, 3440–3443.
- Fredrickson, G. H. and Milner, S. T. (1996). Time-dependent reactive coupling at polymer-polymer interfaces. *Macromolecules*, **29**, 7386–7391.
- Frumpp, J. A. (1971). Oxazolines. their preparation, reactions, and applications. *Chem. Rev.*, **71**, 483–505.
- Fujitsu, Y., Sezume, T., Kitano, K., Narakawa, K., Mikami, T., Kawamura, T., Sato, S., Nishio, T., and Yokai, T. (1989). Thermoplastic polyolefin-polycarbonate blends. *European Patent*, **3,081,79**.
- Glotzer, S. C., Stauffer, D., and Jan, N. (1994). Monte Carlo simulations of phase separation in chemically reactive binary mixtures. *Phys. Rev. Lett.*, **72**, 4109–4112.
- Glotzer, S. C., Marzio, E. A. D., and Muthukumar, M. (1995). Reaction-controlled morphology of phase-separating mixtures. *Phys. Rev. Lett.*, **74**, 2034–2037.
- Gunton, J. D., Miguel, M. S., and Sahni, P. S. (1983). *The dynamics of first-order phase transitions*, volume 8 of *Phase transitions and critical phenomena*. Academic Press, London.
- Hashimoto, T. and Izumitani, T. (1993). Effect of a block copolymer on the kinetics of spinodal decomposition of polymer blends. 1. Nonuniversality in scaled characteristic quantities versus reduced time. *Macromolecules*, **26**, 3631–3638.
- Hashimoto, T. and Izumitani, T. (1994). Effect of a Block Copolymer on the Kinetics of Spinodal Decomposition of Polymer Blends. 2. Scaled Structure Factor. *Macromolecules*, **27**, 1744–1750.
- Hashimoto, T., Takenaka, M., and Jinnai, H. (1991). Scattering studies of self-assembling processes of polymer blends in spinodal decomposition. *J. Appl. Crystal.*, **24**, 457–456.
- Helfand, E. and Tagami, Y. (1972). Theory of the interface between immiscible polymers. II. *J. Chem. Phys.*, **56**, 3592–3597.
- Hindawi, A., Higgins, J. S., and weiss, R. A. (1992). Flow-induced mixing and demixing in polymer blends. *Polymer*, **33**, 2522–2529.
- Hobbs, S. Y., Dekkers, M. E. J., and Watkins, V. H. (1989). The morphology and deformation behaviour of toughened poly(phenylene oxide)/polyamide blends. *J. Mater. Sci.*, **24**, 2025–2030.
- Hseih, D. T. and Pfeiffer, D. G. (1995). Chemical transformation of nitrile to reactive oxazoline functionality on a preformed polymer. *J. Appl. Polym. Sci.*, **56**(12), 1667–1672.
- Hseih, D. T., Pfeiffer, D. G., and Schulz, D. N. (1995). Synthesis of reactive oxazolyl styrene-acrylonitrile copolymers. *J. Appl. Polym. Sci.*, **56**(12), 1673–1677.
- Hu, G. H., Scaffaro, R., and Lamantia, F. (1998). Chemical modification of nitrile to oxazoline functionality on a SAN copolymer in the melt. *Pure Appl. & Chem.*, **A35**(3), 457–471.

- Huh, J. and Jo, W. H. (2002). Phase behaviour of ternary blends of diblock copolymer with homopolymer blends. *J. Chem. Phys.*, **117**(21), 9920–9926.
- Ide, F. and Hasegawa, A. (1974). Studies on polymer blend of nylon 6 and polypropylene or nylon 6 and polystyrene using the reaction of polymer. *J. Appl. Polym. Sci.*, **18**, 963–974.
- Janert, P. K. and Schick, M. (1997). , Phase behavior of ternary homopolymer/diblock blends: influence of relative chain lengths. *Macromolecules*, **30**, 137–144.
- Janssen, J. (1993). *Dynamics of Liquid-Liquid Mixing*. Ph.D. thesis, Eindhoven University of Technology, the Netherlands.
- Janssen, J. M. H. and Meijer, H. E. H. (1995). Dynamics of Liquid-Liquid Mixing: A 2-zone model. *Poly. Eng. Sci.*, **35**, 1766–1772.
- Jeon, H. K., Macosko, C. W., Moon, B., Hoyer, T. R., and Yin, Z. (2004). Coupling reactions of end- vs. mid-functional polymers. *Macromolecules*, **37**, 2563–2571.
- Jiao, J., Kramer, E. J., Vos, S., Moller, M., and Koning, C. (1999). Morphological changes of a molten polymer/polymer interface driven by grafting. *Macromolecules*, **32**, 6261–6269.
- Kambour, R. P., Bendler, J. T., and Bopp, R. C. (1983). Phase behaviour of polystyrene, poly(2,6-dimethyl-1,4-phenylene oxide), and their brominated derivatives. *Macromolecules*, **16**, 753–757.
- Kammer, H. W., Kummerloewe, C., Kressler, J., and Melior, J. P. (1991). Shear-induced phase changes in polymer blends. *Polymer*, **32**(8), 1488–1492.
- Kawakatsu, T. (1994). Computer simulation of self-assembling processes of a binary mixture containing a block copolymer. *Phys. Rev. E*, **50**(4), 2856–2862.
- Kawakatsu, T., Kawasaki, K., Furusaka, M., Okabayashi, H., and Kanaya, T. (1993). Late stage dynamics of phase separation processes of binary mixtures containing surfactants. *J. Chem. Phys.*, **99**(10), 8200–8217.
- Kawakatsu, T., Kawasaki, K., Furusaka, M., Okabayashi, H., and Kanaya, T. (1994). Theories and computer simulations of self-assembling surfactant solutions. *J. Phys. Condens. Matter.*, **6**(32), 6385–6408.
- Keestra, B., van Puyvelde, P. C. J., Anderson, P. D., and Meijer, H. E. H. (2003). Diffuse interface modeling of the morphology and rheology of immiscible polymer blends. *Phys. Fluids*, **15**, 2567–2575.
- Keestra, B. J. (2004). *Computational and experimental analysis of structure development in two phase polymer systems*. Ph.D. thesis, Eindhoven University of Technology, The Netherlands.
- Khandpur, A. K., Foerster, S., Bates, F. S., Hamley, I. W., Ryan, A. J., Bras, W., Almdal, K., and Mortensen, K. (1995). Polyisoprene-polystyrene diblock copolymer phase diagram near the order-disorder transition. *Macromolecules*, **28**, 8796 – 8806.
- Khatavkar, V. V., Anderson, P. D., and Meijer, H. E. H. (2006). On scaling of diffuse interface models. *Chem. Eng. Sci.*, **61**, 2364–2378.

- Kielhorn, L. and Muthukumar, M. (1999). Spinodal decomposition of symmetric diblock copolymer/homopolymer blends at the Lifshitz point. *J. Chem. Phys.*, **110**(8), 4079–4089.
- Kim, E., Kramer, E. J., Wu, W. C., and Garrett, P. D. (1994). Diffusion in blends of poly(methyl methacrylate) and poly(styrene-*co*-acrylonitrile). *Polymer*, **35**, 5706–5715.
- Kim, E., Kramer, E. J., Garrett, P. D., Mendelson, R., and Wu, W. C. (1995a). Diffusion of styrene-acrylonitrile copolymers. *J. Mat. Sci.*, **30**, 1709–1714.
- Kim, E., Kramer, E. J., Garrett, P. D., Mendelson, R., and Wu, W. C. (1995b). Surface segregation in blends of styrene-acrylonitrile copolymers. *Polymer*, **36**(12), 2427–2433.
- Kim, H. Y., Jeong, U., and Kim, J. K. (2003). Reaction kinetics and morphological changes of reactive polymer-polymer interface. *Macromolecules*, **36**, 1594–1602.
- Kim, H. Y., Ryu, D. Y., Jeong, U., Kho, D. H., and Kim, J. K. (2005). The effect of chain architecture of in-situ formed copolymers on interfacial morphology of reactive polymer blends. *Macromolecular Rapid Commu.*, **26**, 1428–1433.
- Ko, C. C., Kyu, T., and Smith, S. D. (1995). Dynamic aspects of phase decomposition in reactive blends of PC and s-PMMA. *J. Polym. Sci. Part B.*, **33**, 517–525.
- Koberstein, J. T. and Stein, R. S. (1983). Small-angle x-ray scattering measurements of diffuse phase boundary thicknesses in segmented polyurethane elastomers. *J. Pol. Sci.*, **21**, 2181–2200.
- Koning, C., van Duin, M., Pagnouille, C., and Jerome, R. (1998). Strategies for compatibilization of polymer blends. *Prog. Polym. Sci.*, **23**, 707–757.
- Kopylovich, M. N., Kukushkin, V. Y., Haukka, M., da Silva, J. J. R. F., and Pombeiro, A. J. L. (2002). Zinc(II)/ketoxime system as a simple and efficient catalyst for hydrolysis of organonitriles. *Inorg. Chem.*, **41**(18), 4798–4804.
- Kukushkin, V. Y. and Pombeiro, A. J. R. (2002). Additions to metal-activated organonitriles. *Chem. Rev.*, **102**(5), 1771–1802.
- Lai, J. T., Filla, D., and Shea, R. (2002). Functional Polymers from Novel Carboxyl-Terminated Trithiocarbonates as Highly Efficient RAFT Agents. *Macromolecules*, **35**, 6754–6756.
- Ledwith, A., Russo, S., and Sigwalt, P. (1989). *Comprehensive polymer science: The synthesis, characterization, reaction and application of polymers*. Eastmond.
- Lee, J. Y., Painter, P. C., and Coleman, M. M. (1988). Hydrogen bonding in polymer blends. 3. Blends involving polymers containing methacrylic acid and ether groups. *Macromolecules*, **21**, 346–35.
- Lee, M. H., Fleischer, C. A., Morales, A. N., Koberstein, J. T., and Koningsveld, R. (2001). The effect of end groups on thermodynamics of immiscible polymer blends 2. Cloud point curves. *Polymer*, **42**, 9163–9172.
- Leibler, L. (1980). Theory of microphase separation in block copolymers. *Macromolecules*, **13**, 1602–1617.

- Leibler, L. (1981). Theory of phase equilibria in mixtures of copolymers and homopolymers, 1. *Makromol. Chem. Rapid. Commun.*, **2**, 393–400.
- Leibler, L. (1991). Block copolymers at interfaces. *Physica A.*, **172**, 258–268.
- Levenspiel, O. (1972). *Chemical reaction engineering*. Wiley International, New York.
- Lin, C. C., Jeon, H. S., Balsara, N. P., and Hammouda, B. (1995). Spinodal decomposition in multicomponent polymer blends. *J. Chem. Phys.*, **103**(5), 1957–1971.
- Lowengrub, J. and Truskinovsky, L. (1998). Quasi-incompressible Cahn-Hilliard fluids. *Proc. R. Soc. London Ser. A.*, **454**, 2617–2654.
- Lowenthal, R. E., Abiko, A., and Masamune, S. (1990). Asymmetric catalytic cyclopropanation of olefins: bis-oxazoline copper complexes. *Tetrahedron Lett.*, **31**(42), 6005–6008.
- Lyatskaya, Y., Gersappe, D., Gross, A., and Balazs, A. C. (1996). Designing compatibilizers to reduce interfacial tension in polymer blends. *J. Phys. Chem.*, **100**, 1449–1458.
- Lyngaae-Jorgenson, J. and Sondergaard, K. (1987). Phase transitions during shear flow of two phase polymer blends ii. styrene-acrylonitrile/poly(methylmethacrylate) transitions to 'homogeneous' melt state. *Polym. Eng. Sci.*, **27**(5), 351–358.
- Lyu, S. P., Cernohous, J. J., Bates, F. S., and Macosko, C. W. (1999). Interfacial reaction induced roughening in polymer blends. *Macromolecules*, **32**, 106–110.
- Macosko, C. W., Guegan, P., Khandpur, A. K., Nakayama, A., Marechal, P., and Inoue, T. (1996). Compatibilizers for melt blending: Premade block copolymers. *Macromolecules*, **29**, 5590–5598.
- Macosko, C. W., Jeon, H. K., and Hoye, T. R. (2005). Reaction at polymer-polymer interfaces for blend compatibilization. *Prog. Polym. Sci.*, **30**, 939–947.
- Madbouly, S. A. (2003). Binary miscible blends of poly(methyl methacrylate)-poly(a-methyl styrene-co-acrylonitrile). IV. Relationship between shear flow and viscoelastic properties. *J. Macromol. Sci.*, **288**, 1209–1224.
- Madbouly, S. A., Chiba, T., Ougizawa, T., and Inoue, T. (1999). Shear effect on the phase behaviour and morphology in PMMA/SAN-29.5 blend. *J. Macromol. Sci.*, **38**, 79–92.
- Maurits, N. M., Sevink, G. J. A., Zvelindovsky, A. V., and Fraaije, J. G. E. M. (1999). Pathway controlled morphology formation in polymer systems: Reaction, Shear, and Microphase separation. *Macromolecules*, **32**, 7674–7681.
- Meakin, P. and Deutch, J. M. (1983). Monte Carlo simulation of diffusion controlled colloid growth rates in two and three dimensions. *J. Chem. Phys.*, **80**, 2115–2123.
- Meyers, A. I. and Mihelich, E. D. (1976). Die ntzlichkeit der 2-Ooazoline in der synthese. *Angew. Chem.*, **88**(10), 321–324.
- Milner, S. T. (1997). How do copolymer compatibilizers really work? *Mat. Res. Sci. Bull.*, **22**(1), 38–42.

- Milner, S. T. and Xi, H. (1996). How copolymers promote mixing of immiscible homopolymers. *J. Rheol.*, **40**(4), 663–687.
- Mori, E., Pukanszky, B., Kelen, T., and Tudos, F. (1984). Lewis acid initiated melt reactions of polystyrene and EPDM rubber. *Polym. Bull.*, **12**, 157–163.
- Motoyama, M. (1996). Morphology of binary mixtures which undergo phase separation during chemical reaction. *J. Phys. Soc. Jpn.*, **65**, 1894–1897.
- Mruzik, M. R., Abraham, F. F., and Pound, G. M. (1978). Phase separation in fluid systems by spinodal decomposition. II. A molecular dynamics computer simulation. *J. Chem. Phys.*, **69**(8), 3462–3467.
- Myers, R. H. and Montgomery, D. C. (2001). *Response surface methodology: Process and product Optimization using designed experiments*. John Wiley, New York.
- Nakayama, A., Inoue, T., Guegan, P., and Macosko, C. W. (1993). Compatibilizers for melt blending: premade vs. reactively formed block copolymers. *Polym. Preprints*, **34**, 840–841.
- Noolandi, J. and Hong, K. M. (1984). Effect of block copolymers at a demixed homopolymer interface. *Macromolecules*, **17**, 1531–1537.
- Odian, G. (1994). *Principle of polymerization*. Academic Press, New York.
- Ohta, T. and Kawasaki, K. (1986). Equilibrium morphology of block copolymer melts. *Macromolecules*, **19**, 2621–2632.
- Olabisi, O., Robeson, L. M., and Shaw, M. T. (1979). *Polymer-polymer miscibility*. Academic Press, New York.
- Olivier, E. J. (1986). Polyamide grafted EPM blend. *U.S. Patent*, (4,594,386).
- Orr, C. A., Adediji, A., Hirao, A., Bates, F. S., and Macosko, C. W. (1997). Flow-induced reactive self-assembly. *Macromolecules*, **30**, 1243–1246.
- Orr, C. A., Cernohous, J. J., Guegan, P., Hirao, A., Jeon, H. K., and Macosko, C. W. (2001). Homogeneous reactive coupling of terminally functional polymers. *Polymer*, **42**, 8171–8178.
- O'Shaughnessy, B. and Sawhney, B. (1996). Polymer reaction kinetics at interfaces. *Phys. Rev. Lett.*, **76**, 3444–3447.
- O'Shaughnessy, B. and Vavylnois, D. (1999). Reactive polymer interfaces: how reaction kinetics depend on reactivity and density of chemical groups. *Macromolecules*, **32**, 1785–1796.
- Pagnoulle, C. (2000). *Reactive compatibilization of SAN/EPR blends*. Ph.D. thesis, University of Liege, Belgium.
- Papathanasiou, T. D., Higgins, J. S., and Soontaranun, W. (1999). An investigation of shear induced mixing in the PSAN/PMMA blends. *Polym. Eng. Sci.*, **39**(12), 2461–2474.

- Park, D. W. and Roe, R. J. (1991). Effect of added block copolymer on the phase-separation kinetics of a polymer blend. 2. Optical microscopic observations. *Macromolecules*, **24**, 5324–5329.
- Paul, D. R. (1978). *Polymer blends*. Academic Press, New York.
- Paul, D. R. and Newman, S. (1997). *Polymer blends I and II*. Academic Press, New York.
- Pernot, H., Baumert, M., Court, F., and Leibler, L. (2002). Design and properties of co-continuous nanostructured polymers by reactive blending. *Nat. Materials*, **1**, 54–58.
- Petschek, R. and Metiu, H. (1983). A computer simulation of the time-dependent Ginzburg-Landau model for spinodal decomposition. *J. Chem. Phys.*, **79**, 3443–3449.
- Piglowski, J., Gancarz, I., and Wlazlak, M. (2000). Oxazoline-functionalized hydrogenated nitrile rubber as impact modifier for polyamide-6. *Polymer*, **41**(10), 3671–3681.
- Pillion, L. Z. and Utracki, L. A. (1984). Compatibilization of polyester/polyamide blends via catalytic ester-amide interchange reaction. *Polym. Eng. Sci.*, **24**, 1300–1305.
- Pillion, L. Z., Utracki, L. A., and Pillion, D. W. (1987). Crystallinity as a selection criterion for engineering properties of high density polyethylene. *Polym. Eng. Sci.*, **27**, 562–569.
- Pincus, P. (1981). Dynamics of fluctuations and spinodal decomposition in polymer blends. II. *J. Chem. Phys.*, **75**(4), 1996–2000.
- Porod, G. (1951). The x-ray small-angle scattering of close-packed colloid systems. I. *Kolloid-Zeitschrift*, **124**, 83–114.
- Postma, A., Davis, T. P., Donovan, A. R., Li, G., Moad, G., Mulder, R., and Shea, R. (2006). A simple method for determining protic end-groups of synthetic polymers by ^1H NMR spectroscopy. *Polymer*, **47**, 1899–1911.
- Pratt, C. F., Phadke, S. V., and Olivier, E. J. (1986). Olefinic impact modifiers for thermoplastic polyester resins. *WO*, (88/05452).
- Puri, S. and Frisch, H. L. (1994). Segregation dynamics of binary mixtures with simple chemical reaction. *J. Phys. A*, **27**, 6027–6030.
- Rabeony, M., Hseish, D. T., and Peiffer, D. G. (1992). Nearly monodisperse spherical domain morphology in PC/PMMA blends following decomposition coupled with an interchange reaction. *J. Chem. Phys.*, **97**(6), 4505–4511.
- Roe, R. J. and Kuo, C. M. (1990). Effect of added block copolymer on phase-separation kinetics of a polymer blend. 1. A light-scattering study. *Macromolecules*, **23**, 4635–4640.
- Saleem, M. and Baker, W. E. (1990). In situ reactive compatibilization in polymer blends: Effects of functional group concentrations. *J. Appl. Polym. Sci.*, **39**, 655–678.
- Sano, Y. (1989). Polymerization of bis(2-oxazoline) compounds with dicarboxylic acids. *J. Polym. Sci. Part A*, **27**, 2749–2753.

- Scaffaro, R., Carianni, G., Mantia, F. P. L., Zerroukhi, A., Mignard, N., and Granger, R. (2000). On the modification of the nitrile groups of acrylonitrile/butadiene/styrene into oxazoline in the melt. *J. Polym. Sci. Part. A.*, **38**(10), 1795–1802.
- Schacht, P. A. and Koberstein, J. T. (2002). The effect of end groups on thermodynamics of polymer blends III LCST phase diagram. *Polymer*, **43**, 6527–6534.
- Schafer, R., Kressler, J., and Mulhaupt, R. (1996). FTIR spectroscopic studies on the interfacial reactions of oxazoline-functionalized polymers. *Acta Polymerica*, **47**, 170–179.
- Schulz, M. and Frisch, H. L. (1994). Microphase and macrophase separation in irreversible reacting chemical binary mixtures. *J. Chem. Phys.*, **101**(6), 5013–5016.
- Schulz, M. and Paul, B. (1998). Freezing of spinodal decomposition by irreversible chemical growth reaction. *Phys. Rev. B*, **58**, 11096–11098.
- Scott, C. and Macosko, C. W. (1991). Model experiments concerning morphology development during the initial stages of polymer blending. *Polym. Bull.*, **26**, 341–348.
- Scott, C. and Macosko, C. W. (1994). Model experiments for the interfacial reaction between polymers during reactive polymer blending. *J. Polym. Sci., Part B*, **32**, 205–213.
- Siggia, E. D. (1979). Late stages of spinodal decomposition in binary mixtures. *Phys. Rev. A*, **20**, 595–605.
- Staal, B. B. P. (2005). *Characterization of co-polymers by MALDI-TOF-MS*. Ph.D. thesis, Eindhoven University of Technology, the Netherlands.
- Suess, M., Kressler, J., and Kammer, H. W. (1987). The miscibility window of poly(methyl methacrylate)/poly(styrene-co-acrylonitrile) blends. *Polymer*, **28**, 957–960.
- Sundararaj, U. and Macosko, C. W. (1995). Drop breakup and coalescence in polymer blends: The effects of concentration and compatibilization. *Macromolecules*, **28**, 2647–2657.
- Sung, L. and Han, C. C. (1995). Light scattering studies on phase separation in binary blends with addition of di-block copolymers. *J. Polym. Sci., Part B*, **33**, 2405–2412.
- Tan, N. C., Tai, S. K., and Briber, R. M. (1996). Morphology control and interfacial reinforcement in reactive polystyrene/amorphous polyamide blends. *Polymer*, **37**, 3509–3519.
- Taylor, G. I. (1934). The formation of emulsions in definable fields of flow. *Proc. R. Soc. London Ser. A.*, **146**, 501–523.
- Ten Brinke, G., Karsaz, F. E., and MacKnight, W. J. (1983). Phase behaviour in copolymer blends: poly(2,6-dimethyl-1,4-phenylene oxide) and halogen-substituted styrene copolymers. *Macromolecules*, **16**, 1827–1832.
- Tran, T. L., Chan, P. K., and Rousseau, D. (2005). Morphology control in symmetric polymer blends using spinodal decomposition. *Chem. Eng. Sci.*, **60**(24), 7153–7159.
- Utracki, L. A. (1989). *Polymer alloys and blends: thermodynamics and rheology*. Hanser, Munich.

- Utracki, L. A. (1998). *Commercial polymer blends*. Chapman & Hall, London.
- Utracki, L. A. (2002). *Polymer blends handbook*. Academic Publisher, Dordrecht.
- Vainio, T., Hu, G.-H., Lambla, M., and Seppala, J. (1996). Functionalized polypropylene prepared by melt free radical grafting of low volatile oxazoline and its potential in compatibilization of PP/PBT blends. *J. Appl. Polym. Sci.*, **61**(5), 843–852.
- Van Durme, K., van Mele, B., Bernaerts, K. V., Verdonck, B., and Du Prez, F. E. (2006). End-group modified PVME characterization and LCST demixing behavior in water. *J. Polym. Sci. Part B.*, **44**, 461–469.
- Vasishtha, N. and Nauman, E. B. (1994). Hydrodynamics effects in the phase separation of binary polymer mixtures. *Chem. Eng. Comm.*, **129**, 29–39.
- Vaughn, H. L. and Robbins, M. D. (1975). Rapid procedure for the hydrolysis of amides to acids. *J. Org. Chem.*, **40**(8), 1187–1190.
- Verschueren, M. (1999). *A diffuse-interface model for structure development in flow*. Ph.D. thesis, Eindhoven University of Technology, The Netherlands.
- Vien, D., Colthup, N. B., Fateley, W. G., and Grasselli, J. G. (1991). *Infrared and raman characteristic frequencies of organic molecules*. Academic Press, New York.
- Vliet, R. E. V., Hoefsloot, H. C. J., Hamersma, P. J., and Iedema, P. D. (2000). Pressure-induced phase separation of polymer-solvent systems with dissipative particle dynamics. *Macromolecular Theory and Simulations.*, **9**, 698–702.
- Vrij, A. (1966). Possible mechanism for the spontaneous rupture of thin, free liquid films. *Discussion Faraday Soc.*, **42**, 23–25.
- Vrij, A. and Overbeek, J. T. G. (1968). Rupture of thin liquid films due to spontaneous fluctuations in thickness. *J. Am. Chem. Soc.*, **90**, 3074–3076.
- Warzelhan, V. (2004). Forum Discussion. July 04-09, Paris, France. IUPAC MACRO.
- Wenker, H. (1935). The synthesis of 2-oxazolines and 2-thiazolines from N-acyl-2-aminoethanols. *J. Am. Chem. Soc.*, **57**, 1079–1080.
- Willemse, R. X. E. (2005). *New insights into free-radical polymerization kinetics*. Ph.D. thesis, Eindhoven University of Technology, The Netherlands.
- Willemse, R. X. E., Staal, B. B. P., Donkers, E. H. D., and van Herk, A. M. (2004). Copolymer fingerprints of polystyrene-block-polyisoprene by MALDI-ToF-MS. *Macromolecules*, **37**, 5717–5723.
- Witte, H. and Seelinger, W. (1974). Cyclische imidsaureester aus nitrilen und aminoalkoholen. *Leibniz An. Chem.*, pages 996–1009.
- Wolf, B. A. (1984). Thermodynamic theory of flowing polymer solutions and its application to phase separation. *Macromolecules*, **17**, 615–618.
- Wu, S. (1985). Phase structure and adhesion in polymer blends: A criterion for rubber toughening. *Polymer*, **26**, 1855–1863.

- Yuan, X. F. and Jupp, L. (2002). Interplay of flow-induced phase separations and rheological behavior of complex fluids in shearbanding flow. *Europhys. Lett.*, **60**(5), 691–697.
- Yukioka, S. and Inoue, T. (1991). Ellipsometric analysis of polymer-polymer interface. *Polym. Comm.*, **32**, 17–19.
- Yukioka, S. and Inoue, T. (1994). Ellipsometric analysis on the in situ reactive compatibilization of immiscible polymer blends. *Polymer*, **35**, 1182–1186.
- Yukioka, S., Nagato, S., and Inoue, T. (1992). Ellipsometric studies on mutual diffusion and adhesion development at polymer-polymer interface. *Polymer*, **33**, 1171–1176.
- Zhao, R. and Macosko, C. W. (2002). Slip at polymer-polymer interfaces: rheological measurements on coextruded multilayers. *J. Rheo.*, **46**, 145–167.
- Zheng, Q., Peng, M., Song, Y., and Zhao, T. (2001). Use of WLF-like function for describing the nonlinear phase separation behavior of binary polymer blends. *Macromolecules*, **34**, 8483–8489.

Technology Assessment

The area of synthetic polymers is seemingly mature in view of the fact that no novel polymers are expected with substantial market potential (conclusion from discussion IUPAC meeting, July 2004, Paris). This statement holds in particular for polymers used in engineering applications, whereas expectations are still running high for new functional polymers in special applications, e.g. polymers in medicine, electronics (display technologies), although in small quantities.

The vast majority of polymers for engineering applications used today were developed in the 1960s and 1970s. Consequently, the focus in the coming decades will be on exploiting the ultimate properties of existing polymers. One of the ways of improving the balance between the properties, processing and cost of existing polymers is blending. The most effective way of overcoming problems related to blend incompatibility, both from a technological and economic point of view, is in-situ compatibilization, i.e. reactive blending. A traditional method of compatibilization of polyamides is the use of maleic anhydride-containing polymers, which has found commercial application. For polyesters, epoxide-containing polymers have been used, which however are quite expensive.

In the thesis, a direct/straightforward procedure for producing oxazoline-containing polymers from the modification of low-cost commercial polymers, such as styrene acrylonitrile (SAN), is described. Similar procedures could be used to get oxazoline-modified polymers containing acrylonitrile, such as acrylonitrile butadiene styrene (ABS) and nitrile butadiene rubber (NBR) (Hu *et al.*, 1998; Piglowski *et al.*, 2000). The main advantage of oxazoline-containing polymers over the earlier mentioned compatibilizers is the universal applicability, since oxazolines are reactive towards carboxylic acid, amine, hydroxide and anhydride. Apart from polyamides and polyesters, oxazoline-containing polymers can also be blended with hydroxyl-containing polymers, such as polycarbonate (PC) and polyphenylene ether (PPO).

Next, reactive blending was studied with the model system containing oxazoline/acid functional pairs to understand the fundamental processes, i.e. diffusion of reactive chains to the interface and reaction between the functional groups during blending. This was studied first with the static bilayer films followed by the dynamic films with superimposed extensional flow. It was observed that only extensional flow, i.e. stretching is sufficient to enhance the further reaction during blending. The efficiency of mixing is generally enhanced by a combination of stretching and folding, the so-called 'bakers transformation' (Aref, 1991), which is realized in most static mixers such as multi-flux. Thus, multi-flux can be used as a versatile tool for reactive blending instead of the dynamic mixers such as extruders.

Furthermore, two-types of reactive compatibilizers were investigated: one gives graft copolymer (random-random system) and the other gives cross-linked copolymer (random-end system). The random-end system reacted for longer times as compared to the random-random

system without undergoing the diffusion limitation. Again, Extensional flow enhanced the diffusion of reactive chains in case of random-random system. Thus, both random-random and random-end system can be used in the multi-flux where only extensional flow is imposed, to get higher reaction conversion, which will result in nano-sized dispersed phase in the continuous matrix during reactive blending and hence will have improved mechanical properties (Pernot *et al.*, 2002).

For partially miscible system, reaction between oxazoline and acid groups enhanced the compatibility between PMMA/SAN blends with the formation of graft copolymer. Generally, in partially miscible system, only spinodal decomposition mechanism is used to get micro-structured morphology. If the spinodal decomposition is used along with the reaction between the reactive chains as shown in the thesis, then the nano-structured morphology can be obtained for the partial miscible system with enhanced mechanical properties.

Finally, reactive blending was also studied computationally starting from the simple non-reactive homopolymer blends followed by addition of complexity in steps. The homopolymers showed macrophase separation, whereas block copolymer showed only microphase separated structure. The mixtures of homo- and block copolymer showed both micro- and macrophase separated structures. Further, the model described in the thesis can be extended to add both reaction term and external shear boundary condition into the set of equations to simulate the industrial reactive blending process. Thus by following the procedure depicted above, different morphologies can be obtained with time for the reactive blending, which will be helpful in designing the reactive system for specific applications. This procedure of doing the computer simulation before actually going into the experimental details will be cost-effective in most of the polymer industry dealing with reactive blends.

Samenvatting

Polymeren worden vaak met elkaar gemengd om de uiteindelijke eigenschappen te optimaliseren. Vanwege het lange keten karakter is het mengen van polymeren op moleculaire schaal erg moeilijk en zijn als gevolg de meeste combinaties van polymeren niet mengbaar en hebben dientengevolge na mengen ook inferieure eigenschappen, dankzij de hoge oppervlaktespanning en daarmee samenhangende instabiele morfologie. Dit kan worden ondervangen door het toevoegen van compatibilisatoren, m.n. blokcopolymeren, die oppervlakreactief zijn, de oppervlaktespanning reduceren en de morfologie stabiliseren door het onderdrukken van coalescentie. In het algemeen worden blokcopolymeren van het A-B type gebruikt voor het stabiliseren van A/B mengsels, maar deze kunnen ook in-situ gemaakt worden, ook bekend als reactief mengen. Dit proces kan worden beschouwd als een 'zwarte doos' proces waarin tegelijkertijd diffusie van reactieve ketens naar het grensvlak en snelle reacties tussen reactieve groepen optreden onder invloed van een complex stromingsveld, m.n. afschuiving en rekstroming.

De doelstelling van het onderzoek beschreven in dit proefschrift was om meer inzicht te krijgen in de fundamentele processen die tijdens reactief mengen van niet-mengbare en gedeeltelijk mengbare polymeren optreden door het combineren van zowel experimenten als berekeningen. Experimenteel werd gebruik gemaakt van een model systeem van polymeren met een oxazoline en een zuur functionaliteit, dat relatief langzaam reageert in vergelijking met de vaak gebruikte anhydride/amine systemen. De berekeningen van het complexe reactief mengen proces werden uitgevoerd met een diffuus-grensvlak model en was opgedeeld in een aantal stappen met toenemende complexiteit. Er werd uitgegaan van het fasescheidingsproces van een mengsel van twee homopolymeren zonder reactie, waarna dit werd uitgebreid via een systeem van alleen blokcopolymeren naar een ternair mengsel van twee homopolymeren en daarmee samenhangende blokcopolymeer.

Voor de experimentele studie werd oxazoline-gemodificeerde polymeren gemaakt met een willekeurige verdeling van oxazoline groepen uitgaande van poly(styreen-*co*-acrylonitril) (SAN) door een reactie met 2-aminoethanol, zowel in oplossing als in de smelt. De omzetting van de nitril-functionaliteit tot oxazoline werd gevolgd met FTIR en NMR spectroscopie. De smelt modificatie liet een hogere omzetting zien dan de oplossingsmodificatie. Het reactie mechanisme werd bestudeerd met een model systeem bestaande uit 2-isopropyl-1,3-oxazoline, dat geprepareerd was door de reactie van 2-aminoethanol met isobutyronitril in aanwezigheid van Lewis-zuur katalysatoren. De reactieproducten werden geanalyseerd met ¹H NMR spectroscopie en GC-MS. Tevens werden de reactie kinetiek en het effect van de verschillende katalysatoren bestudeerd en lieten zien dat zink- en cadmium-gebaseerde systemen het meest actief en selectief waren.

In de meeste gevallen reactief mengen op grote-schaal extruders uitgevoerd, waarin een com-

plex stromingsveld wordt opgelegd op de componenten die aan het grensvlak reageren. Om het complicerende effect van stroming op de grensvlakreactie te vermijden werden alle in dit proefschrift beschreven experimenten uitgevoerd met twee-laags systemen. Voor het niet-mengbare systeem met de oxazoline en zuur functionaliteiten werd het effect van de positie van de oxazoline functionele groep in de SAN copolymeer keten op de grensvlakreactie kinetiek en de grensvlakt dikte onderzocht met respectievelijk FTIR spectroscopie en ellipsometrie. Als eerste werd een willekeurig oxazoline-gefunctionaliseerde SAN gebruikt met een willekeurig zuur-gefunctionaliseerde poly(etheen) (*random-random systeem*). De grensvlakreactie is een eerste-orde reactie met betrekking tot de beginconcentratie van de oxazoline. In het beginstadium gedraagt de reactie volgens een Arrhenius-verband, wat aangeeft dat we te maken hebben met een reactiegecontroleerd gebied. De tijdschaal van de reactie is vergelijkbaar met de tijdschaal van de diffusie van de reactieve ketens wat bepaald werd door gebruik te maken van een drielaagssysteem met een niet-reactieve SAN-tussenlaag. De tijdschaal voor diffusie was veel sneller dan de tijdschaal voor reactie. Daarnaast werd waargenomen dat de grensvlakt dikte als functie van tijd, zoals gemeten met ellipsometrie, sterk toeneemt in het begin van de reactie, waarna een plateau wordt bereikt, terwijl de reactie nog verder doorgaat. Verversing van het grensvlak werd bewerkstelligd door het opleggen van een rekstroming, waardoor de migratie van nieuwe reactieve ketens van de bulk naar het grensvlak optreedt. Hierdoor werd de grensvlakreactie opnieuw geïnitieerd. Gebaseerd op deze resultaten kon een model voor de grensvlakreactie worden ontwikkeld met drie stadia. In het beginstadium nemen zowel de grensvlakreactie als ook de grensvlakt dikte toe vanwege de migratie van reactieve ketendelen vanuit de bulk naar het grensvlak, hetgeen leidt tot de vorming van H-vormige graft copolymeren aan het grensvlak. In het tussenstadium vertraagt de migratie van reactieve ketendelen door de aanwezigheid van vertakte graft copolymeren aan het grensvlak. In het laatste stadium treedt geen migratie van reactieve ketendelen vanuit de bulk naar het grensvlak meer op, omdat het grensvlak verzadigd is met vertakte copolymeren en alleen intraketen copolymerisatie reacties kunnen optreden. Als tweede systeem werd de grensvlakreactie bekeken voor een systeem bestaande uit een oxazoline-gefunctionaliseerde SAN bekeken met de functionele groep aan het einde van de keten in plaats van willekeurig verdeeld over de keten, dat werd gereageerd met een zuur-gefunctionaliseerde poly(etheen) (*end-random systeem*). Het beginstadium is vergelijkbaar met het random-random systeem behalve dat Y-vormige copolymeren werden gevormd voor de end-random systemen. De grensvlakspanning is lager voor Y-vormige dan voor H-vormige copolymeren, hetgeen leidt tot de spontane vorming van een ruw grensvlak in het tussenstadium van de reactie. In het eindstadium nemen de modulaties van het grensvlak toe en worden micellen gevormd in de poly(etheen) fase, wat weer verdere migratie van nieuwe reactieve ketendelen faciliteert vanuit de bulk naar het grensvlak en de grensvlakreactie verder toe kan nemen en verversing van het grensvlak overbodig maakt.

Het fasescheidingsproces voor reactief mengen van gedeeltelijk-mengbare systemen werd experimenteel bestudeerd met kleine-hoek licht verstrooiing (SALS) en de resultaten werden vergeleken met de berekeningen met het diffuus-grensvlak model. Om het effect van de reactie tussen de oxazoline- en zuurgroepen op de fasescheiding van gedeeltelijk-mengbare systemen werd een systematische studie opgezet. Allereerst werd de fasescheiding van een model-systeem van twee niet-reactieve polymeren onderzocht, bestaande uit poly(methyl methacrylaat) (PMMA) en SAN. De SALS-studie liet een lower critical solution temperature (LCST) van 203 °C zien voor een mengsel met een gewichtsverhouding van 70/30 PMMA/SAN28 (28 gew% AN). Als tweede werd het effect van de zuur eind-groepen bekeken op de fas-

escheiding met het SAN/eind-PMMA-zuur systeem, waarvoor een kritische temperatuur van 250 °C werd gevonden als gevolg van de toegenomen interactie tussen de nitril- en zuurgroepen. Daarna werd het effect van oxazoline functionaliteiten op de fasescheiding bestudeerd met ran-SAN-oxaz/PMMA systemen en waargenomen werd dat de LCST naar nog hogere temperaturen verschoof dan voor het SAN/eind-PMMA-zuur systeem, als gevolg van de extra afstoting tussen styreen, acrylonitril en oxazoline segmenten in het ran-SAN-oxaz copolymeer. De kritische temperatuur kon niet worden waargenomen in het experimenteel toegankelijke temperatuurgebied (max. 300 °C) voor het reactieve systeem van ran-SAN-oxaz/eind-PMMA-zuur, vanwege de vorming van copolymeren.

Als laatste werd het fasescheidingsproces van reactieve systemen numeriek bestudeerd door eerst uit te gaan van mengsels van homopolymeren. De vergroevingsdynamiek liet alleen macrofasescheiding zien met drie verschillende stadia, namelijk begin-, tussen- en eindstadium. De power-law schalingscoëfficiënt (α) kan variëren tussen 0.33 (diffusie gecontroleerd) en 1.0 (hydrodynamica gecontroleerd). In het onderzochte PMMA/SAN28 systeem varieerde deze coëfficiënt van 0.55 in het tussenstadium tot 0.86 in het eindstadium, wat aangeeft dat het systeem meer gedomineerd wordt door de hydrodynamica in het eindstadium van de fasescheiding. De numerieke analyse liet zien dat de power-law coëfficiënt veranderde van 0.38 tot 0.69, wanneer het capillair getal (Ca) werd verlaagd van 10 tot 0.5. In het vervolg werden enkele kritische parameters, zoals de dikte van het grensvlak en de diffusie constanten, verkregen uit de SALS-metingen gebruikt in de berekeningen om de kinetiek van fasescheiding te voorspellen met het Cahn-Hilliard model. De experimentele tijdschaal voor het begin van de fasescheiding was trager dan de numeriek bepaalde tijdschaal, hetgeen veroorzaakt kan worden door het lagere initiale ruisniveau voor de simulaties. Voor de diblokcopolymeeren werd gevonden dat de vergroevingsdynamiek alleen gerelateerd was aan microfasescheiding. Vervolgens werd de fasescheiding van het ternaire systeem bestaande uit twee homopolymeren en een blokcopolymeer met een volume fractie van 20 % blokcopolymeer bestudeerd. Alleen het beginstadium kon worden waargenomen, wat misschien verklaard kan worden door het feit dat twee lengteschalen kunnen optreden tijdens de fasescheiding. Zowel micro- als macrofasescheiding werden waargenomen wanneer de lengte van blokcopolymeer kleiner was dan de lengte van het homopolymeer. Na de simulatie van het ternaire systeem met een vast percentage blokcopolymeer kan het model worden uitgebreid om reactieve systemen te beschrijven waarin het blokcopolymeer wordt gevormd als functie van tijd door de reactie tussen reactieve groepen aanwezig in de homopolymeren.

Acknowledgements

I believe that the completion of the thesis was only possible through direct and otherwise help extended by many people within and outside SKT group. It has been great working at SKT and I enjoyed the last 4 years here. First of all, I would like to thank prof. P.J. Lemstra for giving me an opportunity and complete freedom to work on this project. I would like to thank my supervisor dr. Han Goossens for his interest and scientific input in the project. I am grateful to you for giving freedom to work, especially allowing me to work on the computational part of the thesis. His contribution towards structuring the thesis is also highly acknowledged. I would like to thank my second co-promoter dr. Patrick Anderson for all his support and encouragement specially relating to the numerical part of the work. His ready to attitude for correcting the manuscripts and chapters is highly appreciated. I express my gratitude to Martin van Duin for his interesting remarks and discussions though out the work. Gert de Wit is highly acknowledged for all the discussions and specially structuring the quadrant system study of the work.

I would like to extend my gratitude to prof. Ludwik Leibler from ESPCI, Paris for his kind acceptance to be in my reading committee, despite his busy schedule and providing critical comments to improve the thesis. I am also thankful to dr. Bert Klumperman and prof. Erik Nies for their valuable comments in the experimental and computational part of the thesis respectively.

Free energy formulation is one of the difficult propositions with respect to modeling of polymers, but it looked easy to me with the help of dr. Paul van der Varst. Thank you Paul for all the never-ending discussions related to mathematics, maple and latex software. I am very thankful to Mr. Otto van Asselen for all his help relating to the infrared measurements. I am grateful to Peter Lipman for helping me with the GC-MS measurements. I would like to thank dr. J.A.J. Jansen from Philips, Eindhoven for introducing me to the world of ellipsometry and Toon de Win and Mr. Roy for helping me with the measurements and interpreting the results.

I thank Vinayak for his help in computational matter and critical comments to some of the chapters. I appreciate help from Bert Keestra during the initial stage of my research particularly dealing with the Sepran program. Lots of e-mail discussions and few informal discussions with Maru were very helpful. I am also thankful to Li Juan from Fudan University, who was working here on the ASIA-LINK project. She did some magnificent work, which is also a part of my thesis.

I enjoyed my time in office with Francesco, Dennis, Carmen, Ankur, Luigi and Dirk. Thank you Luigi (Maestro) for all the scientific and mostly non-scientific discussions. Mark, Roy and Jules were very helpful all the time. I am also thankful to Vid, Edgar, Vini, Joost, Cees, Jules, Chris, Carmen, Irina, Merina, Morris, Richard, Roel, Jan-willem, Nilesh, Sachin, Ruchi, Soney, Mark who made Friday trips to Utrecht, to attend RPK lectures, nice and enjoyable.

I would like to thank all my past and present colleagues from the SKT group for their help throughout my research time. Colleagues from SPC namely Jelena, Baas, Bert and Marteen are also thanked for their valuable discussions throughout. Colleagues from MaTe: Fredrico, Mrutyunjay and Vini are appreciated for their discussions as well. I am also indebted to Elly and Inneke for their support. Special thanks to Elly for looking into many matters like residence permit and housing.

Apart from my professional life, I am greatly indebted to the Desi-Junta for having nice time in Eindhoven. My special thanks to Sachin, Nilesh, Rajan, Sreepad, Ankur, Rajesh, Sreejit, Vidya, Mani, Viny, Keshav, Sai, Girish, Kirti, Vinit, Chaitanya, Vishal, Mrutyunjay, Rahul, Amol and Chattarbir, all of whose presence felt myself being at home. Later on the Gang was strengthened by the addition of Gayatri (1), Gayatri (2), Radha, Rupali, Manju, Lipi and Sudha. I would also like to thank Ananta and Jayashree for their support at many times.

Finally, I am deeply indebted to my parents and family members who have always provided me with the moral support and encouragement. I would like to thank all of my teachers and past professors, who educated me and instilled in me the art of learning.

Curriculum Vitae

Manoranjan Prusty was born on September 4th 1977 at Cuttack, India. He did his primary school education at Cuttack. After finishing higher secondary school from Ravenshaw college at Cuttack in 1995, he studied Chemical Engineering at the Indira Gandhi Institute of Technology, Utkal University, Bhubaneswar, India. After completion of his Bachelor's degree, he joined Chemical Engineering department at Indian Institute of Science, Bangalore and completed his Master's degree in January 2001 after completion of his Master's thesis entitled 'Reactive blending of Nylon-6 and LDPE using an Epoxy based compatibilizer' under the supervision of Prof. Manas Chanda. He continued working as a Research Associate at the same department, where he was working on the Rheological characterization of polymer gels and studying flow instabilities through flexible tubes.

In October 2001, he started working as a Design Engineer at Larsen and Turbo, Mumbai, India. He spent eight months working on the design of refinery equipments.

In July 2002, he started his PhD-study at the Eindhoven University of Technology, Eindhoven, The Netherlands, in the group "Polymer Technology (SKT)", under supervision of Prof. P. J. Lemstra. During his PhD-study, he completed all five modules of the course 'Registered Polymer Technologist' (RPK, Register Polymeerkundige), organized by the 'National Dutch Graduate School of Polymer Science and Technology' (PTN, 'Polymeertechnologie Nederland'). As of the 1st of August 2006, he will be working as an R&D scientist for BASF AG at Ludwigshafen, in the Polymer Division.